University of Southern Queensland

Faculty of Engineering and Surveying

Use of Near-infrared Photogrammetry to Determine Crack and Surface Deformation in Small Structures

A dissertation submitted by

Paul David Lenton

In fulfilment of the requirements of

Courses ENG4111 and 4112 Research Project

Towards the degree of

Bachelor of Spatial Science (Survey)

Submitted: October, 2011

Abstract

The purpose of this Research Project was to compare conventional (colour) photogrammetry with near-infrared photogrammetry to determine whether the use of near-infrared photogrammetry is a suitable method for measuring structural deformation. To undertake this, laboratory testing was conducted by Mr. Daniel Pratt (as part of his undergraduate thesis) under controlled circumstances on a number of structural materials to gauge whether there was a significant difference between the two methods of photogrammetry. Anecdotal evidence provided by Mr. Pratt suggested there were no significant differences in method and that near-infrared photogrammetry was a suitable method.

This Research Project then examined the two photogrammetric methods on the Hodgson Creek bridge, located at Eton Vale, approximately 16km southwest of Toowoomba on the New England Highway. Both diffuse and retro-reflective targets were used for this project, with the targets placed upon Pier 4 of this structure. A control traverse, using conventional total station equipment was used to place control station under the structure and locate targets on the pier headstock to within ±0.002m. Image capture was conducted at night with the resulting stereo images imported into the *Australis v6.0* photogrammetric software package for processing.

The *Australis* bundle adjustment results agreed with the findings of the laboratory studies, and suggest at face value that there is no significant difference between the two methods, and suggests that near-infrared methods are indeed suitable for conducting deformation studies. However a number of issues occurred in the field that have the potential to influence the results of photogrammetric work undertaken on built structures. It is recommended that further investigation, combined with a tightening of error sources, should be undertaken to ensure best possible conditions for field photogrammetric studies, and allow for accurate comparisons be made between photogrammetric methods.

University of Southern Queensland

Faculty of Engineering and Surveying

ENG4111 and 4112 *Research Project*

Limitations of Use

The Council of the University of Southern Queensland, its Faculty of Engineering and Surveying, and the staff of the University of Southern Queensland, do not accept any responsibility for the truth, accuracy or completeness of material contained within or associated with this dissertation.

Persons using all or any part of this material do so at their own risk, and not the risk of the Council of the University of Southern Queensland, its Faculty of Engineering and Surveying or the staff of the University of Southern Queensland.

This dissertation reports an educational exercise and has no purpose or validity beyond this exercise. The sole purpose of the course pair entitled "Research Project" is to contribute to the overall education within the student's chosen degree program. This document, the associated hardware, software, drawings, and other material set out in the associated appendices should not be used for any other purpose: if they are so used, it is entirely at the risk of the user.

Prof Frank Bullen
Dean
Faculty of Engineering and Surveying

Certification

I certify that the ideas, designs and experimental work, results, analyses and conclusions set out in this dissertation are entirely my own effort, except where otherwise indicated and acknowledged.

I further certify that the work is original and has not been previously submitted for assessment in any other course or institution, except where specifically stated.

Paul David Lenton

Student Number: 0050078460

_____
Signature

_____
Date

Acknowledgements

First, I would like to acknowledge my project supervisor, Dr. Albert Chong for his help and guidance throughout this year. His knowledge and willingness to provide assistance when required has proved to be invaluable.

I would also like to thank my friend and manager, Mr. Eric Brown of the Department of Transport and Main Roads for the use of Departmental equipment and vehicles to undertake the fieldwork component of this project, as well as any time off to undertake these studies, when required.

Last, but by no means least, I would like to thanks my wife Susan and our children Samantha and Corey, for their love, patience and understanding not only for this last year, but throughout the entire degree program. I promise I won't do it again…

Table of contents

List of figures

List of tables

List of appendices

1 Introduction

1.1 Outline of the study

Structural deformation measurement and monitoring is of importance to those wishing to construct or utilise constructed objects, as structural failure has the potential to lead to death or serious injury to persons and/or property should a failure occur. To avoid such a consequence, photogrammetry is but one method of measurement used to determine whether deformation is, or has occurred, and the extent to which it is likely to affect the built structure.

Conventional photogrammetry uses colour photographs to determine deformation measurements. It has proven to be an effective method of determining structural deformation. However, recent evidence in other fields of study suggest that near-infrared photogrammetry may be a more accurate and precise method of determining structural deformation in small scale structures. The aim of this research project is to determine whether the hypothesis that *"near-infrared photogrammetry is a suitable method for determining structural deformation"* holds true.

1.2 Introduction

Small structures, such as bridge members, are subjected to both static and dynamic stresses from the moment they are constructed. Static stresses in this instance would include the weight of the structure itself, as well as the weight placed upon the structure from adjoining members. Dynamic stresses would include the placement of the structure into position (and any harmonic or other vibrations generated in the placement of the member into position), and in the case of bridges, traffic flows across the completed structure.

Such stresses can cause deformations in the structure that have the potential to shorten the lifespan of the structure or in the worst case scenario, lead to the ultimate failure of the structure. For the most part, the early indicators for deformation include cracking, increased flexion, and/or surface bulging that may

not be readily seen by the naked eye. In the past, structures thought to be undergoing deformation were monitored through the use of conventional survey instruments (theodolites and steel bands, total stations, accelerometers, etc.), but the accuracy and precision of such monitoring may be questionable due to the extent and location of the deformation, errors in station setup, and so on. However in recent years, photogrammetry has been able to more accurately determine the presence, extent and measurement repeatability of any deformation process.

In essence, conventional photogrammetry as indicated above uses one or more (calibrated) cameras to obtain a series of images over a given time period to gauge the extent of the deformation process. This process utilises the visible wavelengths of the electromagnetic spectrum (0.4-0.7μm) in the same way that a person would use a camera to take an ordinary photograph. The image is then imported into a suitable software package and then examined for the presence of any deformation features. Because conventional photogrammetry uses the visible potion of the electromagnetic spectrum, a suitable light source is required for image exposure; solar radiation provides such a suitable light source, as does external light sources such as a flash or electric-powered light.

The reliance on a particular light source is a major drawback to conventional photogrammetry in that the capture of images must be undertaken in daylight, or at night/low-light periods when the object of interest is illuminated by artificial light sources. This in itself can pose safety issues, particularly where there is a risk of drivers becoming distracted or blinded by flashes or extremely bright light sources. This potentially serious safety issue is thought to be overcome using near-infrared photogrammetric techniques.

Used for many years on airborne platforms (high-altitude aircraft and satellite systems), near-infrared photogrammetry utilises the portion of the electromagnetic spectrum in the region of 0.7-1.3μm. As this is beyond the visible light spectrum, it does not require a light source (natural or artificial) to capture an image. Instead, this technique captures the emitted radiation of an object through the use of special infrared film (panchromatic or colour), or through the use of infrared camera filters.

An added benefit that has evolved from using the infrared portion of the electromagnetic spectrum is the increased detail available for examination within an image. Infrared film can be used to distinguish objects of similar colours but different wavelength emission characteristics. Since World War II when photogrammetrists used infrared film to distinguish between camouflaged objects and vegetation, the infrared wavelength has been used to characterise different vegetation types, map differing geological and morphological characteristics of the earth, differentiate between varying land use patterns, and more recently, utilised in various biomedical applications. It is hypothesised that, due to the nature of the infrared portion of the electromagnetic spectrum, deformation progression within small structures may be more accurately defined and the extent of deformation characterised with greater precision, when compared to conventional photogrammetry techniques.

1.3 Reason for study

Conventional photogrammetry is a well research and respected method of measuring or monitoring deformation in built structures. Traditionally, this method uses natural or external light sources to illuminate the structure and associated target systems sufficiently so as to measure the deformation that is, or may be, occurring in the structure. However, should measurement activities take place at night, then external lighting systems have the potential to cause light nuisance to a variety of stakeholders.

Many structures that undergo photogrammetric measurement are bridge structures on local or main road systems. Not only do the external light sources impinge on the aesthetic quality of nearby residences, but of more importance is the impact that these lighting systems may have of the drivers that are utilising the structure during the measurement period. Drivers have the ability to become blinded or disorientated by the light systems, with an increase in the risk or potential of an accident occurring as a result of driver distraction.

As general-purpose near-infrared photography has shown, there is no requirement for additional flash or lighting systems to acquire a suitable photographic image in low light or night conditions. This in turn presents the opportunity to lower the

risk of an accident occurring at a bridge site, as more often than not, the photogrammetrist will be out of sight and not requiring illumination during the period of the study. However, there is little data on the use of near-infrared photogrammetry for structural deformation measurements; near-infrared photogrammetric studies have been mostly restricted to medical applications, as outlined in studies by Chong & Matheau (2006), for example. It is hoped that this study will expand the knowledge based of near-infrared photogrammetric applications.

1.4 Research aim and objectives

1.4.1 Aim

The aim of this research project is to determine whether *near-infrared photogrammetry is a suitable method to determine structural deformation in small structures*. This aim will be achieved by conducting a number of laboratory and field-based testing on typical construction materials and a 'live' structure to test the hypothesis that near-infrared photogrammetry is suitable to undertake structural deformation monitoring.

1.4.2 Objectives

There are a number of specific objectives that will be examined to determine whether near-infrared photogrammetry is a suitable method of measuring structural deformation, and include:

- *Examination of existing literature*: the literature review will review a number of studies in which structural deformation has been captured by a variety of survey methods (including photogrammetry), and those results compared against each of the different survey methods. From this review, the suitability of photogrammetry as a method of structural deformation monitoring will be determined.
- *Deformation testing on typical construction materials in the laboratory:* a number of deformation tests will be conducted within the laboratory environment upon steel, wood and reinforced concrete test beams. These tests will capture any deformation using both conventional (colour

photography) and near-infrared photogrammetric techniques. These tests will be conducted under dark, low light and normal lighting conditions

- *Assessment of photogrammetric images:* to adequately assess the ability of near infrared photogrammetry to identify and measure accurately any significant differences between the two photogrammetric methods under certain pressure applications to measure beam deformation (target movement and direction, crack length, width, number, and so on, should they occur). Because of the size of this research project, the laboratory research will be conducted by Mr. Daniel Pratt and presented as part of his Research Project. A brief discussion will occur on his results to determine the relevance of his results to this Research Project..
- *Verification of laboratory results in the field:* making the assumption that there is some difference between the two methods, it is anticipated that the discussion will focus on not only the results, but whether it is beneficial to use near-infrared photogrammetry to measure or monitor structural deformation in real-life structures. To do this, a comparison between retro reflective and paper targets under bright and night conditions will be undertaken. Any differences in methods can also be thought of in terms of any additional costs associated with conventional photogrammetry (lighting, manpower, time, personnel, safety aspects, and so on).

2 Literature review

2.1 Introduction

This chapter will review some of the relevant literature associated with this project. It has been designed such that the reader will gain an understanding on the electromagnetic spectrum and the influence that it has on photogrammetry. It will also outline structural deformation and the some of the current methods that are used in measuring structural deformation. Finally, it will explain what is, and some important concepts behind photogrammetry, including a section on the mathematics used in photogrammetric processing.

2.2 The electromagnetic spectrum

2.2.1 Concept of electromagnetic wavelengths

To understand the concept of electromagnetic wavelengths, it is first necessary to define what a wave is. The Oxford Dictionary describes a wave as '*…a periodic disturbance of the particles of a substance which may be propagated without net movement of the particles, such as in the passage of undulating motion, heat, or sound….*'. This periodic disturbance produces peaks and troughs as it travels along through a medium, with wavelength defined as the measurement of distance between successive peaks or troughs, or the distance in which the disturbance repeats itself (Knight, 2004). Figure 1 below shows a typical sinusoidal wave diagram showing the wavelength and amplitude of a given wave. For the purposes of this description, the amplitude is the magnitude of change in a wave from its baseline (represented in Figure 1 by the dashed line) to the peak (or trough) of the wave.

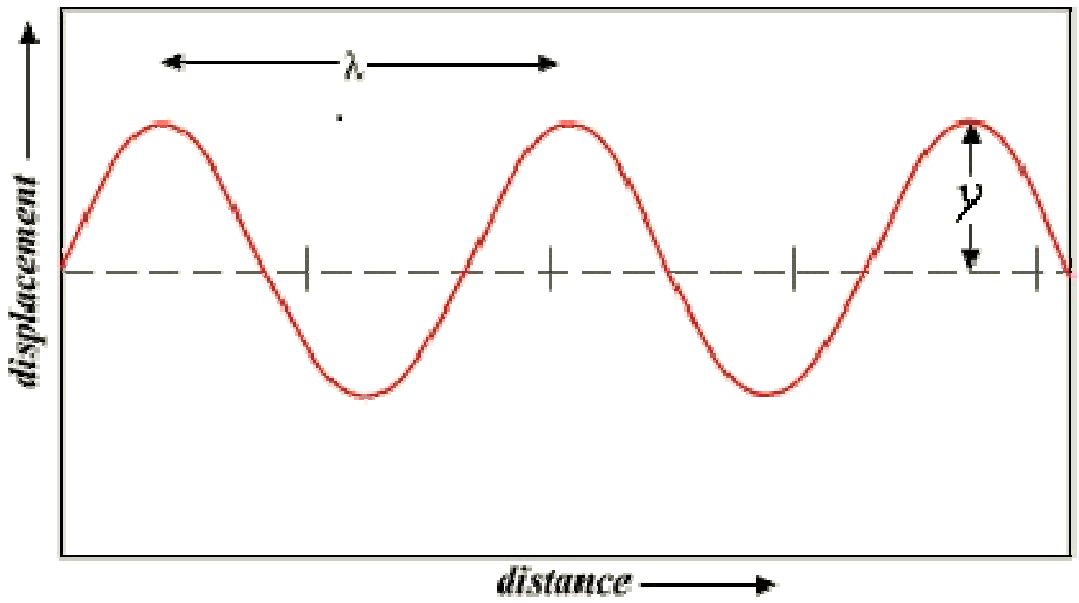

Figure 1. A typical sinusoidal wave, showing the wavelength (λ) and amplitude (γ) of a given wave.

(source: Wikibooks, 2011).

Electromagnetic waves (refer to Figure 2), although having the characteristics of the typical sinusoidal wave are in fact waves of fields, and not of matter; Giancoli (2005) states that it is because of this property that electromagnetic waves can propagate in space. Further, Giancoli (2005) suggests that both these wave fields at any point are perpendicular to each other, and to the direction of wave travel. These wave fields consist of a mass of photons, travelling at the same velocity. A characteristic of these fields are that while the photons may have the same electromagnetic composition, yet can have a wide variance in frequency.

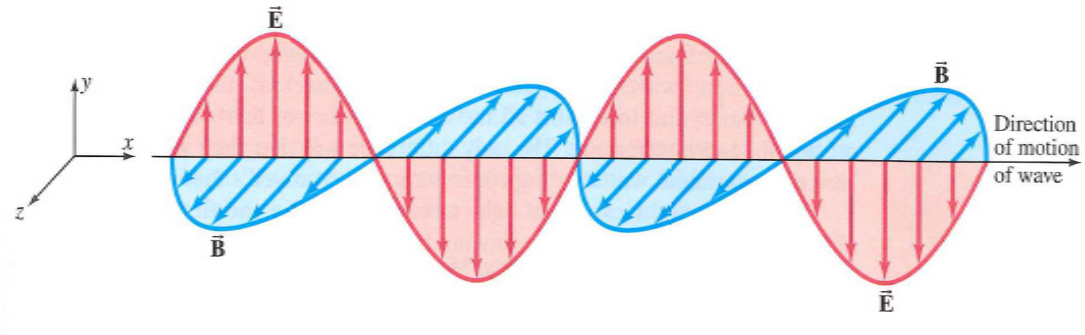

Figure 2. A typical electromagnetic wave, showing the vertical displacement of the electric wave (in red) and the horizontal displacement of the magnetic field (in blue).

(source: Giancoli, 2005)

Electromagnetic waves are not treated in isolation as can be inferred from the above 'simple' diagrams, but form part of the electromagnetic spectrum. This spectrum contains radiation that range from gamma rays at one end of the spectrum, through to radio waves at the other. The electromagnetic spectrum can be seen diagrammatically in Figure 3; Knight (2004) reports these wavelengths of the spectrum have the most influence over today's technologies, ranging in wavelength from $3x10^{-10}$nm (gamma rays) to $3x10^{4}$m (radio waves). Lillesand, *et al.* (2004) point out that it should also be remembered that there is no clear cut dividing line between the differing portions of the electromagnetic spectrum, yet suggest some overlap may occur dependent on the remote sensing methods used to divide the various portion of the spectrum.

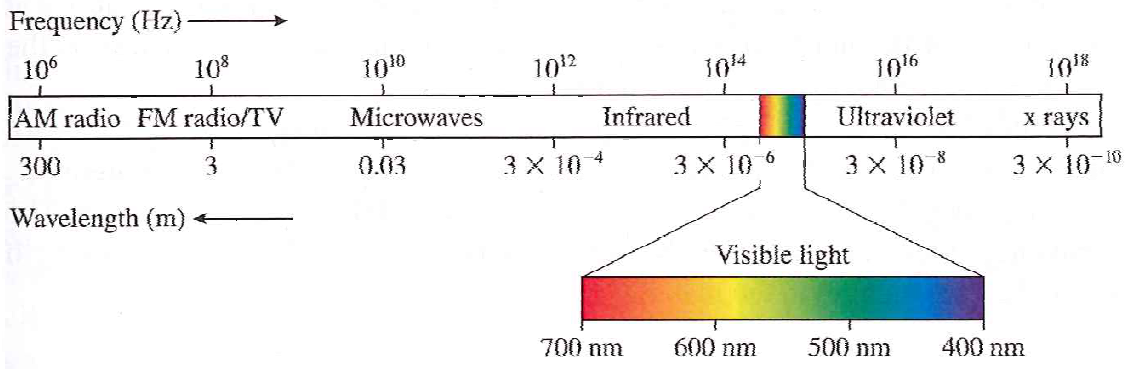

Figure 3. The electromagnetic spectrum.

(source: Knight, 2004).

From Figure 3, it can be seen that the section entitled visible light has been highlighted. Immediately to the left of the visible light range (longer wavelength, lower frequency) is the near-infrared portion of the electromagnetic spectrum. It is these two portions of the spectrum that are of the most importance within close-range photogrammetric studies.

2.2.2 The visible light spectrum

Figure 3 outlines the portion of the electromagnetic spectrum termed visible light. Located between the wavelengths of 400-700nm, it is commonly broken into three main sub-portions – 400-500nm (blue), 500-600nm (green) and 600-700nm (red).

Schlessinger (1995) states that the apparent colour(s) of an object is due to the energy reflected by that object, and the physiological and psychological response of the brain once that reflected energy strikes the retina. Making the assumption that all the wavelengths of the visible light portion of the electromagnetic spectrum could be viewed at the same time, white light is all that would be viewed. However, through the process of dispersion, the different wavelengths can be separated from each other for us to interpr*et a*s different colours. The best and most obvious form that the process of dispersion can be explained as the passing of white light through a prism; white light is split into the different wavelengths to view the myriad of colours that these wavelengths are comprised of. Alternatively, light passing through rain, forming a rainbow, achieves the same outcome as that of the prism – separation of wavelengths by apparent colour.

If the ambient light is low or non-existent, such as in a dark room, the apparent 'blackness' would indicate that there are no wavelengths of the visible light spectrum reaching the eye. The only way that objects could be viewed in this situation is through the use of an artificial light source such as a torch or lamp, or through a device that operates at wavelengths beyond that of visible light and into the infrared.

2.2.3 The infrared spectrum

The infrared portion of the electromagnetic spectrum occurs above that of the visible light spectrum, and in a similar way, is broken into three sub-portions – 700-1300nm (near infrared), 1300nm-3000nm (mid infrared) and 3000nm – 1mm (far infrared). Yet, unlike that of the visible light spectrum, objects viewed in the infrared portion of the electromagnetic spectrum are identified by the energy they emit rather than reflect (Schlessinger, 1995).

There are many applications of infrared technologies, such as communications, astronomy, night vision, plant and soil health, and thermal imaging. However, one of the rapidly developing areas is infrared digital photography. Ruscello (2010) states that infrared capable cameras are better able to penetrate haze and fog due to the longer wavelengths of infrared radiation. This capability is

becoming more important on a global scale with increasing levels of airborne pollution, and allows for a cleaner, crisper picture to be produced. However, infrared spectrum imaging produces the false colour images (due to characteristics of the photographed objects' emissions) that give a slightly different perspective on an object than humans would normally be used to identifying with that object.

Ruscelllo (2010) suggests that in the absence of special infrared film (of standard manual cameras), digital cameras capture infrared photographs through the use of an appropriate filter located at the front of the lens which blocks the visible wavelengths. Alternatively, a digital sensor can be placed in front of a special filter (infrared cut-off filter) internal to the camera. While either method is effective, these two methods used in combination ensure complete blockage of visible radiation from a captured image.

2.3 Structural deformation

2.3.1 What is structural deformation?

Structural deformation can be described as changes that occur in a structure from normal wear and tear over time, or from rapid changes that occur due to external factors applied to the structure. Indeed, Maas and Hampel (2006) loosely define structural deformation as a change in the 3-dimensional shape of an object; this assumes that there is a pre-existing knowledge of the original shape prior to change.

However, in some cases the pre-existing knowledge may not be available. Suspicion as to a deformation events' occurrence may be present due to the appearance of small cracks or perhaps a slight bulging in the structure. In this case, the commencement of monitoring should occur as soon as practical, to provide a baseline of the integrity of the structure, such that any further monitoring will indicate the presence (or otherwise) of a deformation event.

Many scientists and engineers over a long period of time have suggested that deformation actually occurs upon the appearance of cracks in a structure. Barazzetti and Scaioni (2009) suggest that even as far back as 1920, research into

fracture mechanics was occurring, although it was not until the 1950's that this field of study was started to be taken seriously. The field of fracture mechanics therefore could define structural deformation as the appearance of (or the continuing of existing) cracking in a structure where the fracture magnitude, defined by the width and linear extension, significantly increases (Barazzetti & Scaioni, 2009).

2.3.2 Current methods for measuring structural deformation

Photogrammetry is but one method that is used to undertake structural monitoring tasks. However, as stated previously, most photogrammetric applications to date have used conventional (colour) photogrammetry, with little work or data currently available on infrared photogrammetric applications outside of medical applications.

Barazzetti and Scaioni (2009) and Mass and Hampel (2006) state that current methods of measuring displacement and deformation in structures is primarily through the use of wire strain gauges and inductive displacement transducers. It is recognised that these methods tend to produce one-dimensional data; to produce two- or three-dimensional data, considerable instrumental effort is required. Because of the complexity of multi-dimensional data collection, these gauges and transducers are generally ineffective in providing sufficient and conclusive data to determine structural deformation. Further, Whiteman, *et al*. (2002) state that they can be heavily influenced by external electromagnetic fields, and degraded results can occur once the gauges operate outside of their (narrow) linear range.

Barazzetti and Scaioni (2009) and Maas and Hampel (2006) suggest that conventional geodetic techniques involve the use of a combination of total station and inductive transducer techniques to measure (static) deformation in small structures, such as bridges. However, because of the accuracy of the total station, and the relatively small deflections expected in short span structures, such slight deformation will not be identified through conventional instrument acquisition.

Ronnholm, *et al.* (2009) reports that current terrestrial laser scanning technology is at a stage where acceptable results can be achieved for exacting tasks, though it

is not widely used for structural deformation measurements. However, total station control measurements must be put in place for the laser scanner to be effective in measuring such fine measurements. Much of the accuracy of the laser scanner is reliant on the fact that a large point cloud is produced. It is also recognised that laser scanning cannot yet be used in isolation, but is more effective as a complementary method of deformation surveying.

Mills & Barber (2004) suggest that tape measurements and hand recording are still commonplace, though reflectorless EDM and time of flight laser scanning systems is also becoming more prevalent. Laser systems are still at a relative disadvantage with current technologies, as over lager distances the laser angle becomes more acute, therefore less precise. Further, lasers may give a false impression of the wall, particularly where the surface is disjointed or uneven, such as a brick wall. Multipath issues are a problem with laser scanners, as they rely on a clear path in order to obtain the best accuracies. At the current development stage, Mills & Barber (2004) recommend that laser scanning can be used as a complementary method.

While little work has been conducted in this area, Roberts, *et al.* (2010) suggests that survey-grade global positioning system (GPS) receivers may be used to undertake deformation monitoring. Studies conducted by Roberts *et al.*, (2010) report that sub-centimetre deflections and deformations (in bridges) can be achieved with GPS; however it recognised that these studies were conducted on bridges with large span lengths, and given the (current) vertical accuracies able to be achieved with GPS, this method may not yet be suitable for the fine and precise measurements required on many structures.

2.4 Photogrammetry

2.4.1 What is photogrammetry?

Comprised of a combination of two Greek words, 'photogrammetry' can be loosely translated as 'light drawn to measure' (Fryer, 2001). Further, Fryer (2001) suggests that photogrammetry is the science and art of determining the size

and shape of objects as a consequence of analysing images that have been recorded on film or some other form of electronic media.

There are many who have attempted to define the term 'photogrammetry'. For instance, Mikhail, *et al.* (2001) suggests that photogrammetry is a process of deriving metric information about an object through measurements made on photographs of that object. Mitchell (2007) continues on this definition to state that from these photographs accurate sets of coordinates can be obtained for an unlimited number of points on an object.

Broadly speaking, Jiang, *et al.* (2008) defines photogrammetry as a technique for determining the three-dimensional geometry of an object by analysing a series of two-dimensional photographs. These photographs are taken from at least two different camera positions (Jáuregui, *et al.*, 2003) such that the line of sight from each point of concern on an object runs through the perspective centre of the camera.

Photogrammetry can be broken into two distinct fields – aerial and terrestrial photogrammetry. Aerial photogrammetry, as the name implies, requires photographs to be captured by means whereby the camera is not in contact with the surface of the Earth. The principle methods of aerial photograph capture is by airborne or satellite systems. Terrestrial photogrammetry then implies that the camera has some form of contact with the ground, whether hand held, tripod or even some sort of elevated platform. Terrestrial photogrammetry can be further broken down into two distinct areas – (general) terrestrial photogrammetry and close-range photogrammetry, where the distance from camera to object, and object size is less than 100m (Jiang, *et al.*, (2008). Jáuregui, *et al.* (2003) suggests that the distance of close-range photogrammetry has limits of between 100mm to 100m; presumably because the closer distance cannot provide sufficient control points to produce accurate three-dimension coordinates.

Once restricted to the domain of calibrated metric cameras, the low cost, high quality digital cameras now available mean that the science and art of photogrammetry is open to anyone interested in the subject.

2.4.2 Brief history on photogrammetry

Much of the content of this section is covered in greater detail by Mikhail *et al.* (2001), Luhmann, *et al.* (2006) Jiang, *et al.* (2008).

The theory behind photogrammetry can be traced back to the late 1400's where painters, such as a Vinci, undertook geometric studies of (and subsequently painted) objects to imply three-dimension images (Mikhail *et al.*, 2001). Further developments continued; though cameras were not available until a number of centuries later (becoming widely used in the 1800's), the mathematical principles behind photogrammetry were developed in other fields of study in the 1600's and 1700's.

In the mid-1800's the Frenchman, Nadir, captured photographs of the countryside from balloons, and cityscapes were taken from rooftops for the purposes of constructing citywide maps. This last point was expanded on by the person who went on to become regarded as the father of photogrammetry, Laussedat, who, in 1895 developed the first suitable camera and procedure for making accurate photographic measurements (Mikhail *et al.*, 2001; Luhmann, *et al.*, 2006; Jiang, *et al.*, 2008). At a similar time to Laussedat, a Prussian named Meydenbauer began recording historical monuments and buildings in photographs, later establishing a State Institute to record and house these images (Jiang, *et al.*, 2008).

A major development in photogrammetry occurred in 1910, with the formation of the International Society of Photogrammetrists. One of the technical commissions of this society was established in 1926 which examined the specific areas of aerial, terrestrial and engineering photogrammetry (Jiang, *et al.*, 2008), though this field of endeavour was largely ignored until the development of cheaper and faster processing systems, and affordable and accurate off-the-shelf non-metric cameras in the 1960's and 1970's.

Other such as Gruen (in Jiang, *et al.*, 2008) suggest that there are four clear developmental stages of photogrammetry, being:

> *Era 1:* Technological foundation of photogrammetry (1850 – 1984) where processes, procedures and technologies were developed and enhanced;

Era2: The period between 1984 to 1988, where the development of prototype systems, calibration mechanisms and the expansion of charged coupled devices (CCD's), used primarily in digital camera systems significantly reduced the time and cost of photogrammetric processes;

Era 3: Expanded on the development of Era 2, the period between 1988 to 1992 saw increased research and development in the field of close-range photogrammetry and expanded on the potential uses of photogrammetry in the measurement of complex three-dimensional objects from easily acquired two-dimensional images; and

Era 4: the period since 1994 has seen the cost of high quality, non-metric cameras significantly decrease, automation processes in the off-the-shelf programs increase, and has seen the increased used of photogrammetry in the engineering field of study.

2.4.3 Advantages and disadvantages of photogrammetry

Photogrammetry is a method of surveying structural deformation that is gaining acceptance from a variety of professionals interested in measuring and monitoring deformation in built structures. Jiang, *et al.* (2008) and Whiteman *et al.*, (2002) state that the main advantages include photogrammetry being a non-contact method of data acquisition that can be used to gather data in difficult-to-access areas, it is not as labour-intensive as other methods of survey commonly used in deformation measurement, it has the ability to record a large amount of data during a short period of time, and store acquired data easily in both hardcopy and electronic forms, and it is a convenient method to undertake routine monitoring tasks.

Woodhouse, *et al.* (1999) expands further on the above advantages to include the stability and optimal resolution of the sensor is superior to that of other systems, and has the ability to allow both static and dynamic monitoring and measurement of structures undergoing deformation processes. This is extremely important where a high rate of data capture is required, such as in the case of undertaking stress testing to induce failure in test structures. Barazzetti and Scaioni (2009) suggest that advantages of photogrammetry include compactness, lightweight,

good geometric stability and provide simple interfacing at low cost. Photogrammetry also is moving toward the use of inexpensive, off the shelf cameras that are freely available to the novice user (Jiang, *et al.*, 2008).

Because of the size of the camera unit, there are generally no restrictions regarding visibility as can be expected with GPS or even conventional survey instruments in confined spaces or in areas of cover. Jiang, *et al.* (2008) state that examination of results obtained in comparative tests conducted between photogrammetric systems and strain gauges, photogrammetric methods are as capable as strain and induction transducer gauges in measuring fine structural deformations with expected accuracies of between 0.1-0.2mm. In other comparative testing between convention instruments and photogrammetry, Jiang, *et al.* (2008) suggests that photogrammetric methods were more efficient, easier and cost-effective than instrumental methods.

There appears to be little disadvantage in using photogrammetry to undertake deformation monitoring. Comparative tests between photogrammetry and other conventional and emergent survey techniques (i.e. laser scanners) suggest that similar (or better) results are obtained. However, in the case where any structural deformation has produce fine cracking, photogrammetry can state that separation of targets has occurred, but is unable to exactly pinpoint where the crack is until it has become visually obvious (Maas and Hampel, 2009).

2.5 Important mathematical concepts behind photogrammetry

There is a considerable amount of complex mathematical modelling within the field of photogrammetry. Many of these are matrices, and systems of linear equations, relating to the transformation or determination of sets of unknowns related to camera parameters. Thankfully, with today's technologies and photogrammetric software programs, the majority of the calculations involved with photogrammetry are undertaken automatically, thereby allowing the user to concentrate on other aspects of a photogrammetric experiment. For detailed mathematical explanations, readers are directed to Luhmann, *et al.* (2006) and Cooper & Robson (2001).

2.5.1 Determining three-dimensional measurements from photographs

In order to acquire three dimension properties of an object of concern, it is necessary to understand an important concept, that of the principle of triangulation. Mitchell (2007) suggests that in terms of photogrammetry, it best understood by imaging a camera with a single ray projecting out of the lens of the camera toward a point on the object of concern (refer to Figure 4). This ray will have an unknown distance between the lens of the camera, but will be fixed for position and orientation by the camera.

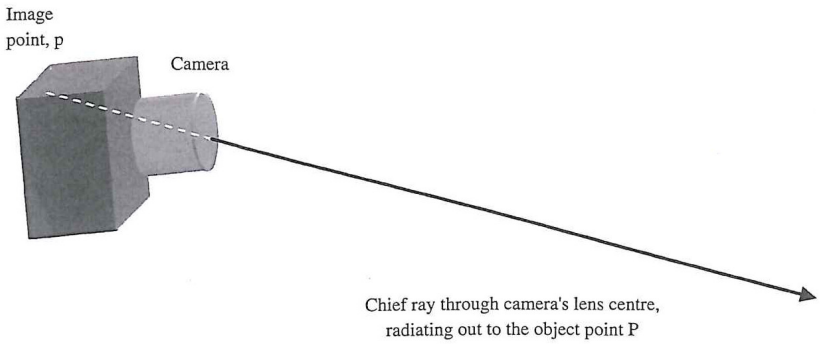

Figure 4. Projection of the single ray to determine direction in space.

(source: Mitchell, 2007)

If it then assumed that two separate cameras (or a single camera acquiring the same object from another position) each have a single ray projecting to the same point on the object, the three dimensional coordinates of the position on the object can be attained (refer to Figure 5). The capture of additional images with that particular point located on the image will further strengthen the positional coordinates.

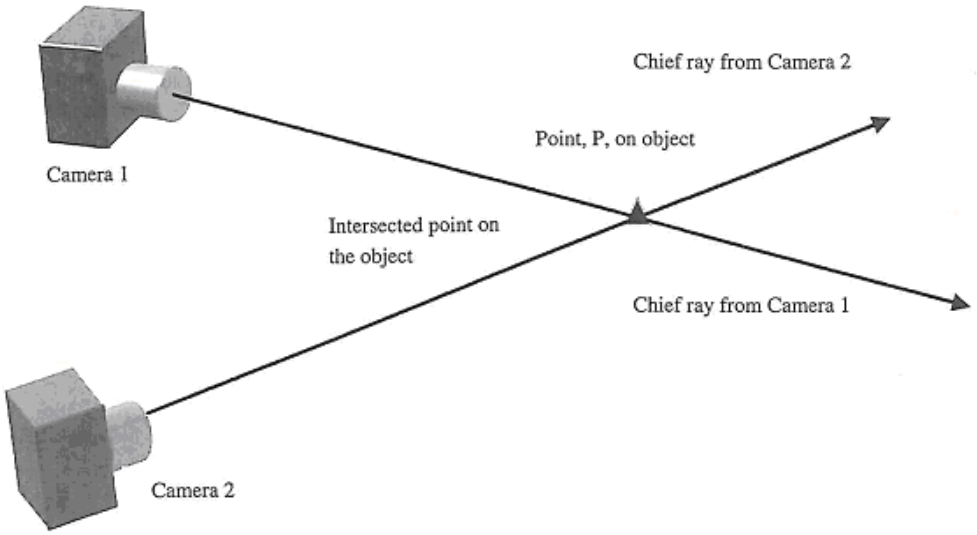

Figure 5. Using the intersection of two single rays to determine object position.

(source: Mitchell, 2007)

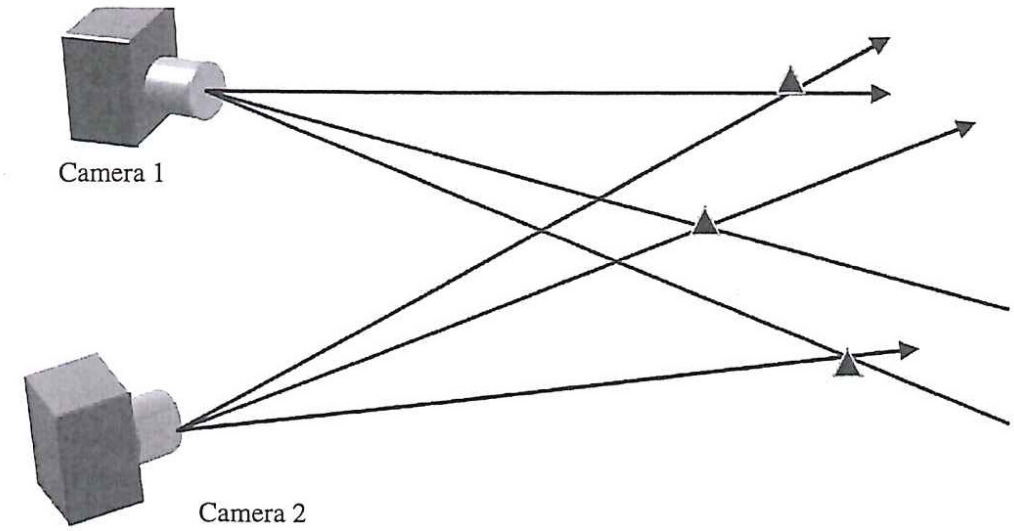

Figure 6. Using multiple rays to determine the position of a number of objects within a single image.

(source: Mitchell, 2007)

The above discussion focussed on a single ray being emitted from the lens of the camera to the object of concern. However, multiple rays are projected from the camera when capturing an image, hence the capture not only of the object of

concern, but much peripheral information that surrounds the object. Expanding on the two single ray concept above, if multiple points on the object are captured in a number of images from a number of independent stations (refer to Figure 6), then a true three dimension image of the object can be attained.

The above discussion is very simplistic. The actual coordinates will be determined in freeware or commercial photogrammetric software packages, such as *Australis* once the images are imported and processed through bundle adjustment. Three dimensional measurements (and the associated accuracies of those points captured within a series of images) will also be heavily influenced by the method of photogrammetric capture – single, stereo or multistation convergent methods.

2.5.2 Concept of coordinates

Mitchell (2007) suggests that the mathematical modelling behind photogrammetry adopts a number of different sets of coordinates. These are arguably the most important part of photogrammetry, as the aim of photogrammetry is to measure the difference between a set of coordinates, or to measure those differences following deformation to determine the displacement that has occurred. To this end, it is necessary to define the types of coordinates used in photogrammetry; Mitchell (2007) suggests the following definitions

- *image coordinate system:* the image itself has a set of coordinates based on the Cartesian coordinate systems with its origin at the centre of the image. These coordinates are generally denoted in lowercase italic *x, y, z.*
- *object coordinate system:* the structure has a set of coordinates which are often referred to as a ground coordinate system, and is also a three dimensional Cartesian coordinate system. For permanent structures, this object coordinate system is based on a State or National geodetic network, but in the case of mobile objects, takes on an arbitrary coordinates. It is usually denoted by the uppercase letters *X, Y, Z.*
- *camera coordinates:* are similar to the object coordinate system and are denoted by the letters X_i, Y_i, Z_i. It is the camera that relates the object and

image coordinates to produce the measurements obtained by photogrammetry.

However, because the object and image coordinates will often not be in parallel with each other, the cameras image coordinate system must be rotated to be parallel with the object coordinate system. Assuming rotation will occur (within the software package), then Mitchell (2007) states that the chief ray projecting from an image point *p* with image coordinates of x_p, y_p will travel through the lens with object coordinates of X_i, Y_i, Z_i, to intersect point P on the object of concern with coordinates X_p, Y_P, Z_P giving rise to the collinearity equations that represent the chief ray:

$$x_p = c_i \frac{r_{11i}(X_P - X_i) + r_{12i}(Y_P - Y_i) + r_{13i}(Z_P - Z_i)}{r_{31i}(X_P - X_i) + r_{32i}(Y_P - Y_i) + r_{33i}(Z_P - Z_i)}$$

$$y_p = c_i \frac{r_{21i}(X_P - X_i) + r_{22i}(Y_P - Y_i) + r_{23i}(Z_P - Z_i)}{r_{31i}(X_P - X_i) + r_{32i}(Y_P - Y_i) + r_{33i}(Z_P - Z_i)}$$

where:

r = the elements of the 3x3 rotation matrix (Mikhail, *et al*. (2001), utilising the three angles of rotation between the object and image coordinate system, and

c_i = the principal distance of the camera, determined from the camera calibration.

Mikhail *et al*. (2001) report that the above collinearity equations form the basis of the bundle adjustment used in photogrammetric software. However, Mikhail *et al*. (2001) suggests that a direct linear transformation, based on the collinearity equations, may be a more efficient process to calculate the physical position of the camera, hence the coordinates of the object of concern.

2.6 Camera properties and image acquisition

2.6.1 Camera calibration

Cameras with a fixed focus and focal length are beneficial to the photogrammetric process. Traditionally the realm of metric cameras, photogrammetric processes

are now adopting the use of readily available off-the shelf-cameras to undertake photogrammetric work. A primary driver behind the shift to off-the shelf-cameras in photogrammetry has been the large costs and inflexibility associated with metric cameras. However Fraser & Al-Ajlouni (2006) state that one on the largest impediments to utilising off-the-shelf digital cameras for photogrammetric purposes is the requirement to acquire images with fixed zoom and focal settings.

Determination of lens distortion parameters is critical for measurement quality. Thomas & Cantré (2009) state that many off-the-shelf digital cameras have a short distance between the lens and the sensor which achieves a large depth of field. This is advantageous because the distance between measuring points and perspective centre has no significant influence on measurement accuracy. However, digital cameras can change their optical properties easily, and often without the conscience knowledge of the user. Because of this, Jiang & Jáuregui (2010) report that the principal reason of calibration is to determine and fix the focal length, principal point and lens distortion parameters of the camera, thereby removing or minimising any systemic errors from the photogrammetric process. Mikhail *et a*l (2001) also adds that the calibration will also determine the rotation and translation between the object space and the camera coordinate systems. Further, Thomas & Cantré (2009) suggest that every camera (metric or non-metric) not only needs to be calibrated prior to a photogrammetric exercise, but also needs to be recalibrated after each change to optical system.

Measurements using digital photos require exact information about sensor pixel size and sensor resolution in both the horizontal and vertical direction (Thomas & Cantré, 2009) and to obtain these data, camera settings need to be determined before starting the photography (Jiang & Jáuregui, 2010). It may be the case that considerable pre-planning of the photogrammetric work, in terms of location, conditions and camera parameters needs to be undertaken prior to the commencement of the precise works. This is in agreement with Chong and Matheau (2006), who suggest that the conditions involved with the calibration of a camera (in terms of object distance) should be similar to the photogrammetric exercise, being conducted prior to image capture.

Jiang & Jáuregui (2010) report that there are two main methods for camera calibration – a stand alone calibration method that utilises some form of known control, such as an Anhui dissection control plate, with or without additional scale bars, or self-calibration methods, where sufficient good quality targets acquired in a series of images from actual measurements form the basis of the calibration process. Jiang & Jáuregui (2010) suggest that self calibrating methods often yield greater accuracy as environmental variables are applied to both the calibration and the actual measurements. Additionally, the self-calibration technique does not require a set of known object-space coordinates of photographed targets (Chong & Matheau, 2006) and as such, self-calibration methods are becoming the norm for digital camera calibrations in multi-image, close-range photogrammetry (Fraser & Al-Ajlouni, 2006). While it is recognised that self calibration saves time and simplifies measurement, Woodhouse *et al.*, (1999) warn that self-calibration techniques should be avoided where single camera stations are used, as they achieve unreliable calibration results. Interestingly Mitchell (2007) suggests another reason for calibration – correct calibration can compensate for lower optical and sensor properties of off-the-shelf digital cameras, which allow them to be used to acquire precise and accurate measurements, expected from photogrammetric studies

For the self-calibration method of camera calibrations, the images are acquired and passed into a photogrammetric software package (such as *Australis*) for digitising and further processing. From this, a bundle adjustment report is obtained that outlines resultant values for the interior orientation parameters of the camera, such as the principal distance, principal point offs*et a*nd a number of additional parameters that correct various lens distortion qualities. Whiteman, *et al.* (2002) provides a brief set or formulae that the calibration software resolves in order to determine the interior orientation of the camera:

$$\Delta x = \bar{x}\left(k_1 r^2 + k_2 r^4 + k_3 r^6\right) + p_1\left(r^2 + 2\bar{x}^2\right) + 2p_2\,\overline{xy} + a_1\,\bar{x}$$

$$\Delta x = \bar{y}\left(k_1 r^2 + k_2 r^4 + k_3 r^6\right) + p_2\left(r^2 + 2\bar{y}^2\right) + 2p_1\,\overline{xy}$$

where:

$\Delta x, \Delta y$	are corrections to the image point coordinates
$\bar{x}, \bar{y}$	are the image point coordinates reduced to the principal point
r	the radial distance given by the equation $r = \sqrt{\bar{x}^2 + \bar{y}^2}$
k_1, k_2, k_3	are the coefficients of radial lens distortion
p_1, p_2	are the coefficients of decentering lens distortion
a_1	is the x-axis scale factor that arises due to electronic digitising bias.

For a detailed description of camera parameters adjusted during the calibration process, and the mathematics associated with calibration, it is advised to consult Cooper & Robson (2001) or Luhmann *et al.* (2006).

2.6.2 Camera geometry and network

Planning issues and network control

Prior to conducting a photogrammetric experiment several planning issues need to be addressed, including the definition of datum, and optimization of the camera system for position and illumination (Woodhouse *et al*., 1999). To aid in datum definition, Jáuregui *et al*. (2003) states that a network of control points or a coordinate reference system should consider the location and placement of targets and/or calibrated scale bars, thereby establishing a scale between the acquired images and the structure under investigation. This target establishment is usually undertaken with a total station which places stationary control points around the object and surveyed to determine their 3D coordinates. The positioning of the actual targets is of importance as the positions must optimise the geometry of the photogrammetric measurements (Woodhouse *et al.*, 1999). Once established, Woodhouse *et al*. (1999) and Jiang & Jáuregui (2010) recommends that an initial round of images be acquired to check the interior and exterior orientation parameters of the camera, and to check that lighting conditions provide sufficient illumination of the targets.

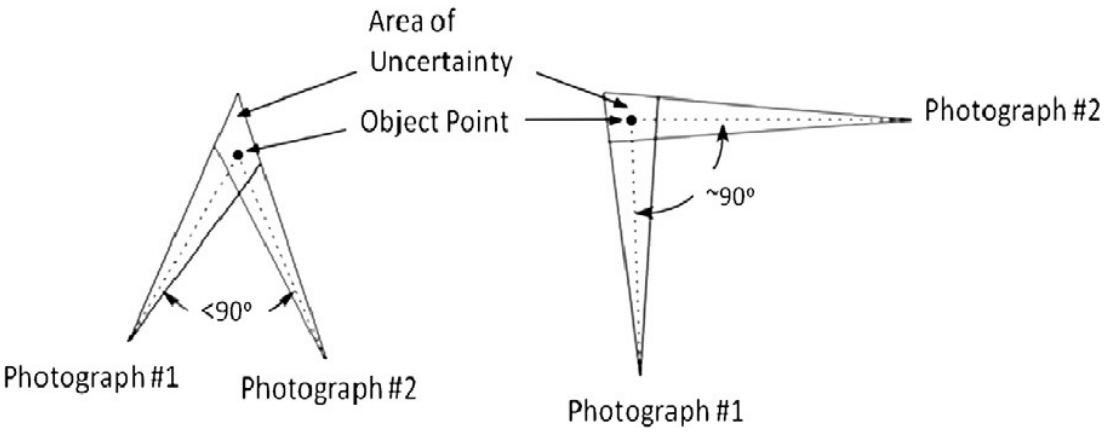

Figure 7. Minimising the area of uncertainty

(source: Jiang & Jáuregui, 2010)

Jiang & Jáuregui (2010) also state that another basic principle governing camera placement and orientation is to ensure that the angle between the optical axes of the cameras is close to a right angle. Conducted either using a single camera from two different stations, or two camera capturing the image at the same time from the two different station, the area of uncertainty around the point of interest is minimised (refer to Figure 7 above). It would be advantageous to attain a third shot from another plane perpendicular to the first two, further reducing this area of uncertainty (Jiang & Jáuregui, 2010).

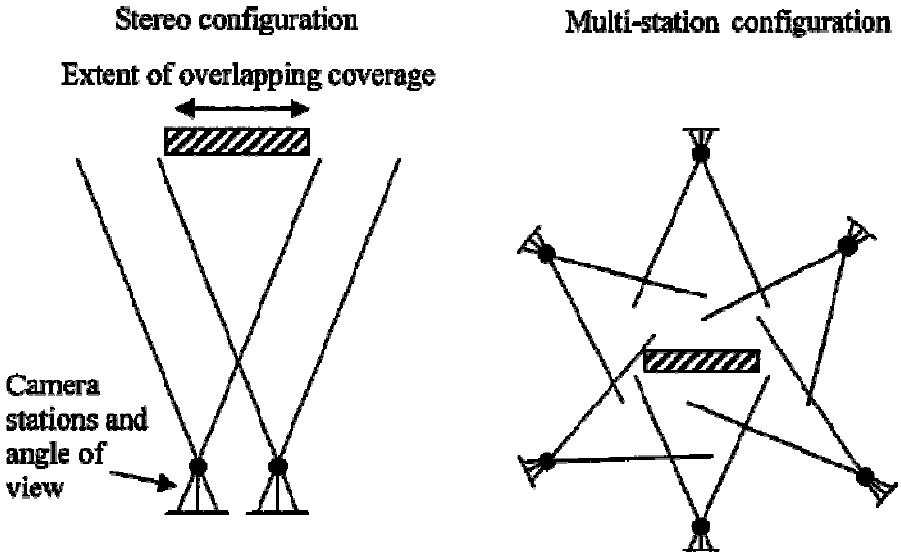

Figure 8. Principal photogrammetric network configurations.

(source: Mills and Barber, 2004)

Mills & Barber (2004) suggest that two principle network configurations can be used to determine three dimensional coordinates from photogrammetric images. Figure 8 outlines these two configurations. The first network is that of a stereo network, commonly used to interpr*et a*erial photography, but can be used to determine the three dimensional coordinates on an object of interest. The second configuration is that of the multistation convergent network, where an object is surrounded by a number of stations and images acquired and processed to produce a three dimensional image of the object.

Because more than two images are used, there are greater observational redundancies, improving accuracy, precision and reliability (Mills & Barber, 2004), and is therefore the primary configuration used to undertake the self-calibration technique and associated bundle adjustment for the calibration of non-metric cameras.

Single camera measurement

The primary purpose of photogrammetry is to determine the three dimensional coordinates of objects for the purposes of measurement. Because single camera measurements use a single camera, the reconstruction of three dimensions objects utilising single camera measurements requires significant additional geometric information (Luhmann *et al.* (2006). Typically applied for rectifications (Luhmann *et al.* (2006), Jiang *et al.* (2008) and Thomas & Cantré (2009) report that single camera setup uses the principle that if the camera image and object planes are parallel the actual dimension of an object will be directly proportional to that measured in the image.

In terms of mathematics, Cooper & Robson (2001) note that a single image will give rise to two collinearity equations that will have six unknown parameters three rotation unknowns and three perspective centre coordinate unknowns; these unknowns are termed exterior orientation parameters of the camera. These will be solved in the bundle adjustment by iterative least squares estimation. However, Thomas & Cantré (2009) state that single capture methods are used infrequently, with algorithms for single capture analysis often missing from photogrammetric

software packages and would therefore require significant additional manual work in order to achieve sufficient adjustment resolution.

Stereophotogrammetric measurements

Stereo imagery is acquired where an automated stereoscopic image compilation process is used (Luhmann *et al.*, 2006) to process the images, such as the *Australis* software package. The process of stereoscopy provides that a point of interest on an object can be seen from another image taken from another camera located at a different station. To ensure that this can be achieved, Luhmann *et al.* (2006) suggests that there are three camera positions that stereoscopy can be achieved (refer to Figure 9); the normal configuration (Figure 9a) where the two camera stations are located parallel and equidistant from the object of interest, and able to locate the same target from two different camera station images; shifted configuration (Figure 9c) where the cameras, while parallel to the object are at different offset, thereby requiring different scales to be applied to the image during the software processing; and convergent configurations (Figure 9b) where a greater angle of convergence than that of the human vision can be used to obtain the stereoscopic images.

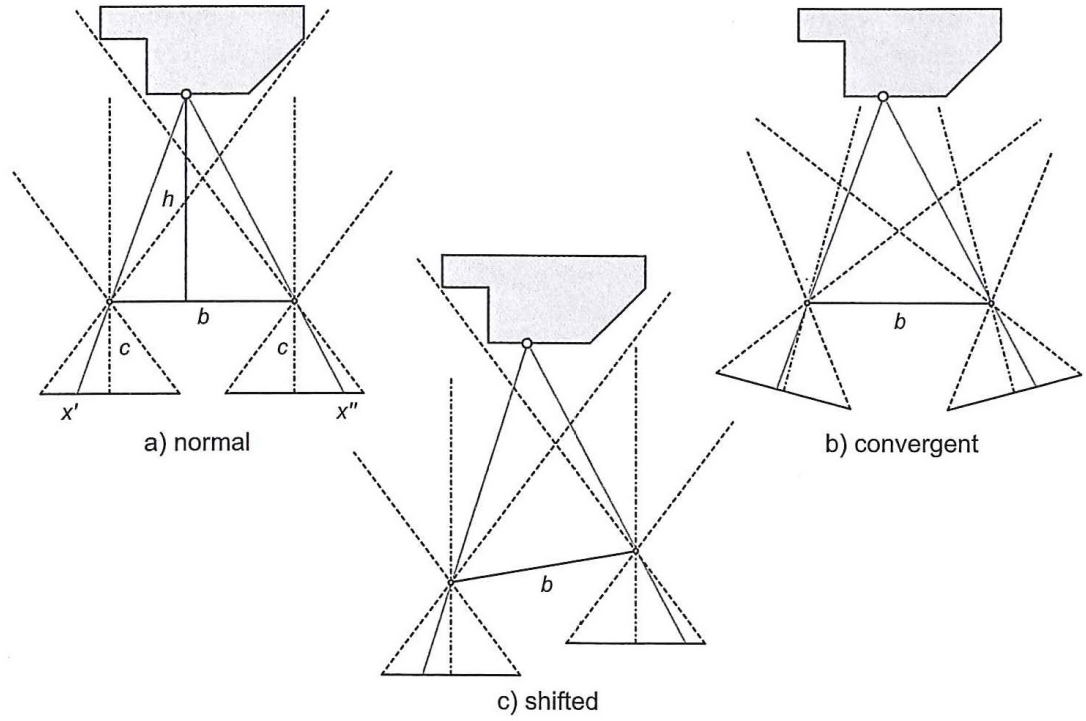

Figure 9. Stereoscopic image configurations.

(source: Luhmann *et al.*, 2006)

Fraser (2001) and Mills & Barber (2004) warn that stereoscopic geometry can produce an inhomogeneous precision in the z axes (poor depth precision) and is largely dependent on the height to base ratio (Luhmann *et al.*, 2006). This will require pre-planning to determine the exact requirements and tolerances of the photogrammetric project to account for this potential problem.

Multistation convergent networks

The number of camera stations and viewing directions are not restricted when using a multistation convergent network, with an object being acquired by an unlimited number of images to enable sufficient intersecting angles of bundles of rays in object space (Luhmann *et al.*, 2006). Mills & Barber (2004) and Jiang *et al.* (2008) state that because of the amount of images that can potentially be used in the multistation configuration, the superior network design offered has a larger observation redundancy which improves accuracy, precision and reliability. This reliability ensures that uniform object accuracies in all coordinate directions can be attained (Luhmann *et al.*, 2006).

Figure 8 indicates the basic multistation convergent network layout; the majority of close-range photogrammetric application utilise this configuration. This is especially so where a number of different viewing locations are required to capture areas otherwise occluded by the structure/shape of the object, or to meet the specified project requirements (Luhmann *et al.*, 2006). Further, it is the multistation convergent network that best allows for the simultaneous calibration of cameras by self-calibrating bundle adjustment procedures (Luhmann *et al.*, 2006) within an accepted photogrammetric software program.

2.6.3 Camera sensors

There are two main types of image sensors that cameras use in order to acquire an image. While completely different, in terms of size, operation and functionality, they both end up achieving the same end goal: conversion of light into an electrical charge to produce an image (Teledyne Dalsa, 2011).

The first of the sensors is a charged coupled device, or CCD. This sensor consists of an array of photosensitive pixels that capture the light coming into the camera through the lens and then stores that information of the array as an electric charge Litwiller, 2001). Teledyne Dalsa (2011) reports that this charge is then converted to voltage before being passed on as an analog signal. This signal then gets converted into a digital image outside of the sensor.

The second sensor, the complementary metal oxide semiconductor (CMOS) sensor works similarly, except that each pixel (as opposed to the array of pixels) processes the light within each pixel (Litwiller, 2001) before the signal is output as a digital signal. This chip has numerous other components attached that allow this process to occur, but requires less off-chip processes to achieve the same operation as the CCD.

Both sensor types were developed in the late 1960's and early 1970's. Teledyne Dalsa (2011) report that the CCD technologies were preferred in photographic applications due to their lower costs, simpler operation, smaller size and greater image quality, however, as the silicon chip matured and technologies surrounding production improved, there is now little difference between them. However, the performance comparison provided by Teledyne Dalsa (2011) suggest interestingly that while the CCD sensors have low signal to noise ratio (as there is less additional circuitry attached to the sensor to function), CMOS sensors have a greater capacity to reduce the blooming effect that may occur in the image acquisition process.

3 Research design and methodology

3.1 Laboratory testing

The laboratory testing and results is the subject of a research project conducted by Mr. Daniel Pratt for his undergraduate thesis. Specific testing and results will not be discussed, however a broad overview of his methods and results will be commented on.

3.1.1 Materials and equipment

To undertake the laboratory testing, consideration was given to the types of structures likely to be monitored and the materials that those structures may be constructed with. However, due to the size of the test area and the testing machine used in the laboratory photogrammetric work, test materials could only be representative of those used in structure construction. As such the materials tested consisted of timber railway sleeper, steel square-section, concrete, and fibre composite beams. In addition, a C-section guardrail post was included in the testing regime.

Targets used during the laboratory testing comprised of retro-reflective targets and non-reflective (diffuse) paper targets. The retro-reflective targets consisted of a black, commercially produced adhesive tape cut into a number of 10mm squares. Central to these squares was a retro-reflective circle, approximately 1.6mm in diameter. The diffuse targets consisted of a white, 10mm paper square, with a 3.2mm diameter black circle located centrally in the white square. These targets were glued to the beams in semi-random positions, as well as upon the universal testing machine.

The loading of the beams was conducted using a Shimadzu Universal Testing Machine. This machine is capable of varying the load applied to objects; as each of the beams were constructed of different materials, it was recognised that uniform pressures could not be placed on each beam and as such the Shimadzu machine was considered suitable to undertake the laboratory testing of the beams.

Pre-testing pressure was applied to the beams to determine likely pressures that may indicate beam deformation. To this end, it was determined that the test pressures applied to the beams were:

- Timber: 0kN, 25kN, and 45kN.
- Concrete: 0kN, 7kN, and 13kN.
- Glass polymer resin: 0kN, 5kN, and 9.5kN.
- Steel square section: 0kN, 25kN, and 42.5kN.
- Steel C-section: 0kN, 25kN, and 45kN.

The cameras used to undertake the laboratory (and subsequent field) testing were Sony HDR-SR10 video cameras with CMOS image sensor and night vision capability. With a still picture resolution of 4 megapixels, photographs are produced in *.jpeg format. For night vision images, a Sony HVL-HIRL video infrared light was attached to the interface shoe located at the top rear of the camera unit. The IR emitter had a variable intensity switch to allow for an intensity to be matched to the conditions in which the camera and IR emitter is being used.

3.1.2 Control points and camera calibration

To ensure that any deformation to the beams can be quantified, a calibration board was included in each of the photographs. This board, black with white retro-reflective targets at varying heights had been pre-calibrated such that the distance between each of the targets, and the height of each target, was precisely known. The retro-reflective targets on this board are the same as those used on the test beams (black adhesive tape with a 1.8mm diameter retro-reflective circle). This board also allowed for the calibration of the cameras (conducted separately to the beam photogrammetry); as the interior and exterior orientation of the cameras will vary from camera to camera, and determination of these values is essential in measuring deformation with photogrammetric techniques.

To ensure that the calibration board used for the camera calibration and additional control in the photogrammetric work has precise horizontal and vertical coordinates, an Anhui dissection control plate was employed. Further, a calibration scale bar with a known and precise length between the retro-reflective targets either end of the control rod. The calibration process for the large calibration board was processed in a similar manner to that of the photogrammetric images.

3.1.3 Image capture and processing of acquired images

Following calibration, a series of single images of each of the beams, under various load pressures, were captured. Sufficient overlap of the images ensured that stereoscopic photos could be produced. Images, once captured, were imported into the *Australis v.6* software program for processing. Camera parameters used in the software processing can be found in Table 2 (refer to Section 3.2.3).

The laboratory processing and subsequent results, form part of the Research Project conducted by Mr Daniel Pratt. As such, little further discussion will occur within this Research Project, and will thus be saved for his discussions.

3.2 Field testing

3.2.1 Structure selection

A number of structures in the Darling Downs region of Queensland were examined for suitability in conducting field testing of conventional and infrared photogrammetry. Structural and positional aspects considered desirable were primarily the location with respect to Toowoomba, size of the structure, traffic volume, access to the structure, and site safety. The structure considered to meet these criteria was the Eton Vale Bridge, approximately 16.5km southwest of Toowoomba.

The Eton Vale Bridge (Figure 10) crosses Hodgson Creek, a slow flowing stream approximately 6m wide and 2m deep at the bridge location during normal flow.

Constructed in 1969, the Eton Vale Bridge is described on the construction plans as a prestressed slab deck concrete bridge. With dimensions of 188'4" (36.088m) long and 28' wide (8.534m), the overall deck unit consist of 70 prestressed girders and 10 prestressed kerb units. Supporting these girders and kerb units are four piers, each pier containing 5 x 16" (0.406m) hollow-spun piles driven to refusal. The pier headstock is nominally 2'6" (0.792m) in height; the targets used in the field testing are fixed to pier headstock number 4, and the associated piles.

Figure 10. The Hodgson Ck bridge at Eton Vale.

3.2.2 Establishment of control

Control traverse

In order to establish 3-dimensional co-ordinates for the retro-reflective and plain targets attached to the pile cap and piers of the Hodgson Creek bridge, a control traverse was undertaken at the bridge site. Datum was established between the survey marks MR16K and QT17K, two co-ordinated and levelled benchmarks established by the Department of Transport and Main Roads. Co-ordinate values attached to these marks are considered to be accurate, having been coordinated

during a recent traverse prior to construction works in the vicinity of the bridge site.

Between the datum marks, a number of secondary survey stations were established as part of the traverse. These stations were observed using the Leica TCRP1203+ 'Sets of Angles' program. Parameters used in the program allowed for a round of six face left/face right reciprocal readings to each of the stations to obtain horizontal and vertical coordinates for each station. Of importance to the bridge target location, two stations (Stations 3 and 4) were established approximately 3.5m adjacent to the piles and pile headstock to which the targets were attached.

The survey program *12d (ver. 9.1)* was used to process the traverse data. Utilising this program, reduction of the field data was conducted using the parameters contained in Table 1. The 12d report file for the control traverse, and the coordinates of the stations, can be found in Appendix B.

Table 1. Main parameters used in the 12d data reduction process.

Projection:	MGA94 Zone 56
N–values:	winter_nvalues
Adjustment method:	Bowditch adjustment

For the purposes of this research project, the reduced levels (RL's) of the secondary survey stations have remained with trigonometric heighting only; it was considered that as the two datum marks have spirit-levelled values, and that the traverse is relatively short in length with few stations contained on the traverse line, trigonometric heights will be sufficient to calculate target RL's.

Target construction, placement and co-ordination

Similar to that of the laboratory testing, two types of targets were constructed for use in the field photogrammetric work. The first type of target is that of a paper target, constructed of a 40x40mm white cardboard square with a ¾" (19.05mm) hollow-punched black cardboard circle glued centrally to the white square. The

second type of target is a retro-reflective target, constructed of a ¾" (19.05mm) hollow-punched retro-reflective tape (3M™ Scotch® Reflective Tape 198DCNA, 25mm x 1m, 12/cs) glued to a 40x40mm black cardboard square.

Consideration of target placement was undertaken to ensure sufficient coverage of the structure given its size and constructed material. For vertical positioning, it was decided that the pier headstock would contain three rows (A-C) of targets and that the piers would contain four rows (D-G) of targets. Horizontally (left-to-right) and based on the dimensions of the structure, it was decided that there would be 21 columns of targets; the total number of targets are 106. Figure 11 (below) is an example of the location of the targets on the structure.

Figure 11. An example of the target placement and location on the Hodgson Creek bridge pier headstock.

Prior to target placement, a plumb bob was used to define a central line from the base of the bridge girders through the centreline of the piers. Following this, the piers and pier headstock were measured such that rows A and C were positioned approximately 100mm from the upper and lower surface of the headstock, with row B central to rows A and C. Separation is therefore approximately 250mm vertically between the targets on the headstock. To ensure uniformity, the pier

targets were measured similar to that of the headstock, with row D approximately 100mm below the pier/headstock intersection and spaced at approximately 250mm intervals. The total vertical height from row A to G is approximately 1.5m.

Horizontally, a mark was made approximately 750mm offset left and right of the pier centreline on the headstock, and a plumb line drawn from this mark. Where there are two types of targets (diffuse black circle and retro-reflective circle; refer to Figure 11) a mark 50mm offset left and right offset of the centreline was made for the location of the target. Once markout was completed, the concrete was cleaned of debris and the targets were secured to the piers and pier headstock using *Selleys Liquid Nails* construction adhesive.

Following target placement, the targets were located using the Leica TCRP1203+ instrument, and the onboard 'Survey' program. The instrument was set up on Station 3, and using the reflectorless EDM measurement mode, targets A100 through to G109 were manually sighted and measured. The instrument Station was moved to Station 4 and targets A110 through to G121 were measured as before. This data was then downloaded and processed in the *12d* survey package where a report file indicating the coordinates of the targets was generated. This file can be found in Appendix C.

Additional photographs were required of the bridge targets sometime after the original photographs were taken. This necessitated in the targets being replaced, as the targets nearer to the outer extents of the headstock had become faded, and the targets under the structure had become damaged as a result of the expansion joint above the headstock leaking following rainfall events. The new targets were constructed in the same manner as previously, and were glued to the targets that had become damaged. These targets were again located using the Leica TCRP1203+ instrument in reflectorless EDM measurement mode, and a new control file produced. Additional control targets were added to the headstock either side of the pile location, and between rows E and F on each pile to improve control network.

3.2.3 Image capture and processing of acquired images

The cameras used to undertake the targ*et a*cquisition were the same as those used to undertake the laboratory testing (refer to Section 3.1.1). Given the width of the structure, it was considered that four different camera locations were required to provide sufficient coverage and overlap between photographs and ensure stereoscopy for processing. These locations were approximately 6m to the front of the pier and headstock, and approximately 4m apart – 2 locations at either side of the bridge, and 2 locations equidistant apart underneath the structure.

Figure 12. Targ*et a*cquisition under bright light conditions.

From each location, four photographs were taken. The photographs were alternated between bright light (supplied by external floodlights powered by a portable generator) and total darkness. An example of this can be seen in Figure 12 and Figure 13, where the differences in illumination method (for the same photograph) are apparent. The photographs were captured in the following order – bright light (first direction), near infrared (first direction), bright light (second direction), near infrared (second direction), change of location. This process was repeated until all four locations had all four series of photographs captured.

Once the photography was complete, the photographs were downloaded and separated into illumination type for input into the *Australis v.6* software program

for processing. The camera parameters (Interior Orientation parameters), required to process the photographs, are contained in Table 2. These parameters were established as part of the camera calibration conducted prior to the laboratory testing.

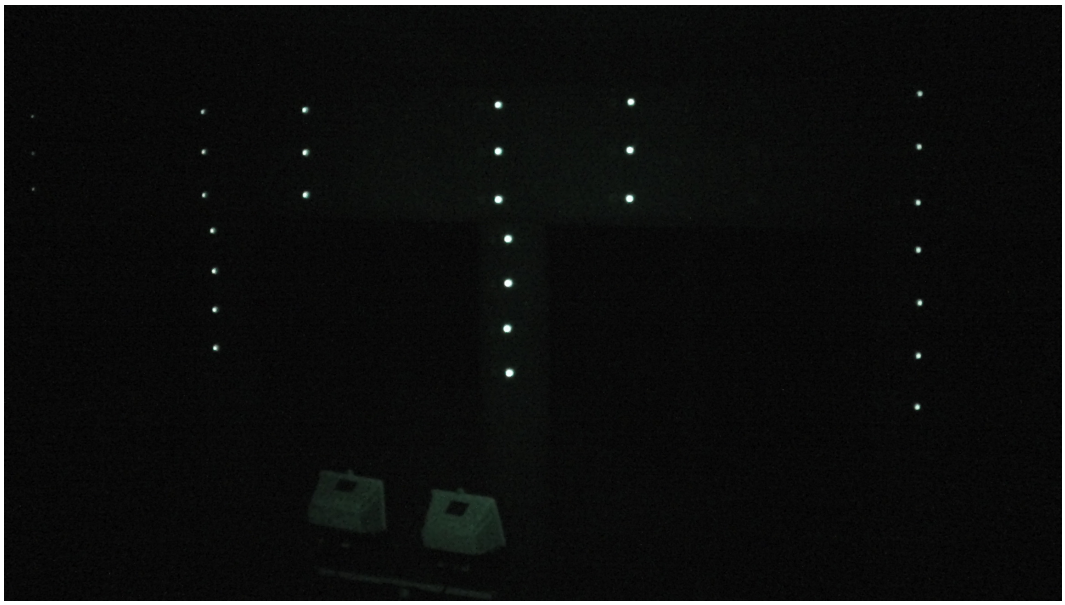

Figure 13. Targ*et a*cquisition under total darkness utilising the infrared emitter attached to the camera.

Table 2. Camera parameters used in the *Australis* software processing.

	Camera 1 (Light)	**Camera 2 (Light)**	**Camera 1 (NIR)**	**Camera 2 (NIR)**
Sensor size (mm)	2304 x 1296	2304 x 1296	2304 x 1296	2304 x 1296
Pixel size (mm)	0.00118	0.00118	0.00118	0.00118
Focal length(c)	3.041450	3.037979	3.040440	3.046335
(X_p)	0.002411	0.004786	0.001563	0.004673
(Y_p)	0.002904	-0.001954	-0.007710	-0.003862
(K_1)	-3.0268×10^{-3}	-1.1555×10^{-3}	-2.2043×10^{-3}	1.0704×10^{-3}
(K_2)	3.3475×10^{-3}	1.5128×10^{-3}	2.6412×10^{-3}	-1.1954×10^{-3}
(K_3)	-1.8291×10^{-3}	-1.2679×10^{-3}	-1.7789×10^{-4}	8.6875×10^{-4}
(P_1)	-1.6641×10^{-27}	-3.66208×10^{-27}	-1.0474×10^{-27}	-1.6979×10^{-27}
(P_2)	-2.2309×10^{-27}	-3.9374×10^{-27}	-1.9807×10^{-27}	-1.7375×10^{-27}
(B_1)	-1.4199×10^{-28}	-1.5735×10^{-28}	3.5849×10^{-28}	-1.4821×10^{-28}
(B_2)	3.4252×10^{-29}	4.1154×10^{-30}	6.6675×10^{-29}	-1.0567×10^{-29}

Referring to Table 2 and Table 3:

X_p, Y_p: Principal point offsets

K_1, K_2, K_3: Radial lens distortion

P_1, P_2: Decentering distortion

B_1, B_2: Affinity and shear parameters

Additional photographs were taken at the bridge site using a Sony Cybershot DSC-F828 digital still camera, capable off taking photographs with a CCD-type sensor and an 8MP resolution. For this series (of photographs), the number of photograph stations was increased from four to five (corresponding with the number of pier piles), with up to eight colour and eight near-infrared photographs taken at each station. Assuming eight photographs were taken at each station, four were captured at a different height to the other four, separated by a minimum of 0.5m. Sufficient overlap to obtain stereophotographs at each station occurred, similar to the original photogrammetric process described previously.

Table 3. Camera parameters used in the *Australis* software processing for the additional photographs.

	Camera 1 (Light)
Sensor size (mm)	3264 x 2448
Pixel size (mm)	0.0027
Focal length(c)	7.376340
(X_p)	-.0.028995
(Y_p)	-0.077898
(K_1)	2.9806×10^{-3}
(K_2)	-1.5919×10^{-5}
(K_3)	-8.8082×10^{-7}
(P_1)	-2.3624×10^{-27}
(P_2)	-5.6781×10^{-28}
(B_1)	3.7057×10^{-28}
(B_2)	5.8255×10^{-28}

The commencement of the *Australis* project required the input of the camera parameters, and the import of the target control file. This file, *.xyz file, necessitated in the (normal) Northing and Reduced Level columns exchanged due to the 3D nature of the program. As real-world coordinates were also used, the first three number of the Eastings, and first four numbers of the Northings, were removed, as the program is (apparently) unable to handle such large numbers in its coordinate system file.

Once the control and driveback files (the same control file but with a different function during the processing) had been imported to the project, the photographs were imported and the digitised. This digitising process allowed for each individual target to have a unique identification number attached to it; this number is directly related to the number assigned to the target during the total station observations as outlined in Section 3.2.2. The correct assignment of the target number during the digitisation process is essential so that overlapping photographs with corresponding target numbers are recognised during the adjustment process of the software.

Following digitisation, the Adjustment Control Variables (Rejection Limits, method of adjustment, etc.) were s*et a*nd then all the images underwent resection. This process involves the computation of coordinates based on the overlap of photographs with the unique target identifiers being located in each image. A check of the RMS values obtained from the resection gave an indication of any errors in the resection (in terms of misidentification of targets, clarity of photographs, etc.) before the Bundle Adjustment of the photographs was undertaken. It is this Bundle Adjustment that outlines the Exterior Orientation Parameters for each image, summarises the image coordinate residuals, provides standard errors for each target, and produces the coordinates for each target. The Bundle Adjustment reports can be found in Appendix D.

4 Results

Discussions with Mr. Daniel Pratt, and examination of the results obtained from the laboratory testing, suggest that there is no significant difference between conventional (colour) photogrammetry and near-infrared photogrammetry in the laboratory setting. The results suggested that there is between 0.1mm-0.3mm difference between the two photogrammetric methods (conventional v near-infrared). These laboratory results would then suggest that the expected accuracies of near-infrared photogrammetry are the same as, or at accuracies that can be described as the same, as that of conventional photogrammetry.

4.1 Background relating to the results

So that comparisons can be made and any differences between target types and photogrammetric methods can be identified, it was necessary to reduce the data into a single, simple measurement value. To do this, it was considered that the 3D distance was the best way to represent such data. Equation 1 (below) outlines the formula used to undertake the distance reduction used in the comparison between photogrammetric methods.

$$d_{3D} = \sqrt{(X_1 - X_2)^2 + (Y_1 - Y_2)^2 + (Z_1 - Z_2)^2} \qquad (1)$$

where:

X_1, X_2 = Easting value for the control and target type respectively

Y_1, Y_2 = Northing value for the control and target type respectively

Z_1, Z_2 = Northing value for the control and target type respectively

To determine the distances between targets, the 3D distance was used to firstly reduce the targets' coordinate data to a single value, and then calculate the distance between two randomly selected targets. For the purposes of this Research Project, nineteen target differences were determined. These differences

had the mean value of all distances reported. The method of calculation for the mean value is outlined in Equation (2).

$$\overline{X} = \frac{x_1 + x_2 + ...x_n}{n} \quad (2)$$

where:

$\overline{X}$ = mean value

x_n = observed difference between the two identical target type

n = number of observations

4.2 Issues associated with the reporting of results

There were two main issues that affected the reporting of the results, as follows:

1. Target acquisition of the diffuse targets was unable to be achieved under dark conditions, as there was no reflectance properties associated with these targets when illuminated by the near-infrared emitter, and
2. Target acquisition of the retro-reflective targets was unable to be achieved during daylight conditions, as the infrared camera was flooded with light, affecting the ability of the camera to acquire near-infrared daylight images.

In addition, the supplementary photogrammetry undertaken with the higher resolution camera is not presented in this section; the images were unable to be resected to produce a bundle adjustment within the *Australis* software program.

4.3 Target acquisition

4.3.1 Diffuse targets

The diffuse targets used during this Research Project were constructed of cardboard, as outlined in Section 3.2.2. There were no issues with illumination under normal daylight conditions, or with external lighting of the structure that prevented identification with colour photogrammetric images. However, as these

targets were unable to be identified under low light/dark near-infrared conditions, comparisons were unable to be made between diffuse light and diffuse dark conditions.

Table 4. Test-point comparison between the control and diffuse colour targets.

Target ID	EDM minus Paper Colour	Target ID	EDM minus Paper Colour
D100	0.00023	F100	0.00024
D105	0.00016	F105	0.00017
D110	0.00021	F110	0.00023
D115	0.00018	F115	0.00018
D120	0.00019	F120	0.00019
E100	0.00024	G100	0.00024
E105	0.00017	G105	0.00018
E110	0.00022	G110	0.00022
E115	0.00018	G115	0.00018
E120	0.00019	G120	0.00020

Comparisons were able to be made between the diffuse targets and the control targets under the provided external light. Compared data are restricted to the test-point data, or that data not associated with the control points. These are presented in Table 4. The positional differences between the reflectorless EDM control location and the diffuse targets used as photogrammetric control are negligible (in the order of 1/100 of a millimetre) and as such have not been included in Table 4.

Note that the resulting values for the difference in 3D distance between the reflectorless EDM control measurements and that of the paper colour measurements range between 0.16mm-0.24mm. The Research Project was attempting to achieve differences no greater than 1mm.

4.3.2 Retro-reflective targets

Similar to that of the diffuse targets, the retro-reflective targets used in this Research Project were constructed of easily obtained materials, as outlined in Section 3.2.2. Again, there were no adverse illumination issues with these targets, and were easily identifiable during the photogrammetric processing of the images in the *Australis* software package.

Table 5 outlines the test-point comparison between the reflectorless EDM control measurements and the colour retro-reflective targets under external illumination; the resultant differences in 3D distance are between 0.18mm-0.24mm. These results are well within the 1mm tolerances attempted as part of the Research Project. Note that the target identification differs between the diffuse and retro-reflective targets; as the targets are constructed of different materials, they are located in differences. In stating this, they are only separated by approximately 100mm (i.e. D100 is separated from D101 horizontally by 100mm).

Table 5. Test-point comparison between the control and retro-reflective colour targets.

Target ID	EDM minus Retro Colour	Target ID	EDM minus Retro Colour
D101	0.00022	F101	0.00023
D106	0.00016	F106	0.00019
D111	0.00024	F111	0.00024
D116	0.00019	F116	0.00020
D121	0.00019	F121	0.00020
E101	0.00022	G101	0.00024
E106	0.00018	G106	0.00019
E111	0.00024	G111	0.00024
E116	0.00020	G116	0.00019
E121	0.00020	G121	0.00021

Table 6 outlines the comparison between the reflectorless EDM control measurements and the near-infrared measurements of the test-points. As the photogrammetric method was near-infrared, no external illumination of the targets

was used. The resultant differences in 3D distance was between 0.16mm-0.24mm, and are within the attempted maximum tolerance of 1mm.

Comparisons were made between the colour retro-reflective and near-infrared retro-reflective targets for all placed retro-reflective targets. The results of this comparison are found in Table 7; as can be seen there is negligible difference between the two methods to acquire the retro-reflective targets (in the order of between 1/100 and 5/100 of a millimetre).

Table 6. Test-point comparison between the control and near-infrared retro-reflective targets.

Target ID	EDM minus Retro NIR	Target ID	EDM minus Retro NIR
D101	0.00022	F101	0.00023
D106	0.00016	F106	0.00019
D111	0.00023	F111	0.00023
D116	0.00019	F116	0.00019
D121	0.00019	F121	0.00020
E101	0.00023	G101	0.00024
E106	0.00018	G106	0.00019
E111	0.00023	G111	0.00024
E116	0.00019	G116	0.00019
E121	0.00020	G121	0.00021

Table 7. Comparison between the retro-reflective colour and retro-reflective near-infrared targets.

Target ID	Retro NIR minus Retro Colour	Target ID	Retro NIR minus Retro Colour
A101	0.00003	C116	0.00003
A103	0.00003	C118	0.00002
A106	0.00001	C121	0.00003
A108	0.00002	D101	0.00003
A111	0.00003	D106	0.00002
A113	0.00004	D111	0.00003
A116	0.00003	D116	0.00002
A118	0.00002	D121	0.00004
A121	0.00004	E101	0.00004
B101	0.00003	E106	0.00002
B103	0.00002	E111	0.00004
B106	0.00001	E116	0.00003
B108	0.00001	E121	0.00005
B111	0.00003	F101	0.00005
B113	0.00004	F106	0.00004
B116	0.00003	F111	0.00004
B118	0.00003	F116	0.00004
B121	0.00003	F121	0.00005
C101	0.00003	G101	0.00005
C103	0.00001	G106	0.00004
C106	0.00001	G111	0.00005
C108	0.00002	G116	0.00003
C111	0.00003	G121	0.00005
C113	0.00003		

4.3.3 Distance comparisons

A distance comparison was made between the reflectorless EDM control and the photogrammetric methods of 19 randomly selected targets. The 3D distance

differences had a mean value determined; these mean values are found in Table 8 below.

From Table 8, it can be seen that if it is accepted that the EDM-Paper Colour comparison is held fixed as a baseline, then the retro-reflective targets differ from the baseline value by between 0.28mm-0.51mm. These are well within the 1mm tolerance that was being attempted as part of this Research Project. The 3D distance difference between the retro-reflective targets (colour v near-infrared) is 0.1mm.

Table 8. Comparison of reduced distances between selected target points for all image types

	Distance (m)*
EDM – Paper Colour	-0.00035
EDM – Retro Colour	-0.00086
EDM – Retro NIR	-0.00063
Retro NIR –Retro Colour	-0.00013

* refer to Section 5.1 for further information

5 Analysis and Discussion

5.1 Commentary on results

It is unfortunate that there could be no direct comparison between diffuse targets during daylight/bright light conditions, and dark conditions. This would seem to be an expected observation. It is also unfortunate that the diffuse targets could not be distinguished in the near-infrared photography of the lower resolution video camera images, as comparisons between night and day diffuse targets would have been ideal to fully test the hypothesis that there is no significant difference between conventional and infrared photogrammetric methods for that target type.

However, the comparison between colour and near-infrared retro-reflective targets under light and dark conditions does allow for the comparison, as the same target type was able to be measured under both conditions. The results provided for in Table 7 would suggest that the hypothesis that no significant difference occurs between conventional and near-infrared would hold true.

Examination of Figure 16 would indicate that there may be potential to repeat this study using the higher resolution camera and measure the diffuse targets in infrared, as Figure 16 suggests that the diffuse targets may seen clearly in the near-infrared image. Similarly, it would have been preferential to acquire daytime near-infrared images to compare the diffuse and retro-reflective targets with those of the night. However, the aspect of the bridge allowed to much light into the CCD-sensor, completely obscuring any image that would be acquired. Were this to have been fully considered during the planning phase, additional results may have been generated that may or may not have supported the ‘no difference’ hypothesis.

In terms of comparison between target types, it is considered that there is no significant to negligible difference between the targets with almost identical 3D distance results between the test point targets. This would then indicate that the type of target does not particularly influence the capture and digitisation of the target, and would also infer that simply-constructed targets are as useful for

undertaking photogrammetric studies when compared to that of pre-manufactured targets.

The variations in distance outlined in Table 8 are above those in the previous three tables. However, they are all sub-millimetre and should be considered suitable for many photogrammetric applications. Note that the values are all minus values; stereophotographs (refer to Section 2.6.2) are reported as having precision errors in the z axes, or errors associated with depth precision. Whilst the results are within this projects' tolerances, the increase in z-axis error (almost 3 times in the worst case scenario) will need to be considered in the station configuration if tight accuracies are required.

It was noticed that a difference occurred between those still images captured using the video camera and those captured by the higher resolution camera. The clarity is much better in the higher resolution photographs, as was to be expected. However, the increase in resolution also meant that slight movements in camera station allowed for positional errors to occur in the image. It is suggested that, even though the images appeared clear to the naked eye, that the depression of the camera button or traffic over the structure contributed to the failure of the images in the bundle adjustment process. Because the examination of photogrammetric images involves points of millimetre accuracies, any slight movements will exacerbate any inherent positional errors or positional differences in the photogrammetric control.

5.2 Potential benefits between photogrammetric methods, and over traditional survey methods

There are many benefits that photogrammetry has over traditional survey methods; many of these were outlined in Section 2.4.3. However, advantages not described previously would include cost and time savings, and with particular reference to near-infrared photogrammetry, the ability to acquire images in restricted spaces with minimal equipment.

Given that observations from the laboratory testing suggest that there is no significant difference between the conventional and infrared photogrammetry in

terms of target acquisition and deviation measurement, then there is no reason to suggest that photogrammetry cannot become the basis to undertake deformation monitoring in small scale structures. For instance, the establishment times can be considerably reduced over that of conventional (survey instrument) monitoring, as additional time would be required to install geodetic control for target location, whereas photogrammetry can utilise plane or arbitrary coordinates. Equipment costs are substantially less than that of other instrumentation and are easily accessible to the ordinary user. Further, the targets used for photogrammetry can be constructed of materials that are easily accessible and simple to construct; pre-manufactured or specialised target systems are not necessary.

In terms of a comparison between photogrammetric methods in the field on 'live' structures, the results of this Research Project support those obtained from the laboratory testing. However, assuming that potential error sources are corrected or accounted for in the field (refer to Section 5.3) then is suggested that infrared photogrammetric monitoring has a significant advantage over that of conventional monitoring for the reasons outlined above. Other advantages include:

- Less equipment has to be deployed to undertake the same task.
- To undertake conventional photogrammetry at night, in low light conditions, or in restricted spaces, an artificial light source is required.
- When monitoring small scale structures, such as bridges, this artificial light source has the potential to cause light nuisance to residences surrounding the structure under observation, and has the potential to distract drivers utilising the structure as part of their travel. The only equipment that the infrared camera requires to undertake monitoring is the infrared emitter, attached to the top of the camera unit.

Further, the small size of the required infrared equipment allows for monitoring in confined spaces where it may not be possible to install artificial lighting. Artificial lighting is bulky, requires exact placement to ensure sufficient light coverage of the targ*et a*rea, and may cause increase heating of the confined space, or may increase the risk of ignition in spaces with combustible atmospheres. This may have been particularly relevant in the recent monitoring events of the Riverside Expressway in Brisbane (2009-10), where monitoring activities were

being conducted within the confined spaces between the deck and headstocks of the expressway on/off ramp. Infrared photogrammetry could have been effectively utilised in this scenario as the area of concern was confined, low in natural light and in hindsight, required a monitoring method that was quick, effective and needed precise measurements.

5.3 Problems and issues encountered during the field testing and processing activities

There were a number of issues that arose from the photogrammetric field testing, and mainly related to the infrared photogrammetry. However with respect to the colour photogrammetry, the primary issue was that the targets are not able to be captured in the absence of natural or artificial light sources at night. Because of this, and as would be expected, colour photogrammetric methods of data acquisition would normally be restricted to daylight hours where sufficient ambient light exists, or under daylight/night-time conditions where an external light source can be deployed to enhance ambient light and assist with the capture of colour photographs.

With respect to the near-infrared photogrammetry, an issue that became apparent early on in photograph acquisition was the blooming effect on the retro-reflective targets. Blooming occurs when the light hits the retro-reflective material and increases the apparent size of the target. Figure 14 gives an indication of the effect of blooming in one of the near-infrared photographs. In this Figure, note that the retro-reflective targets in the centre of the photograph are brighter and larger than those toward the edge of the photograph. This is the blooming that is apparent in many of the near-infrared photos.

A number of factors are involved in blooming. These include:

1. *The material used to construct the retro-reflective target:* there are different classes of retro-reflectivity, each with a different strength of return from the light shone upon the material. The higher the strength, the greater reflective return from the material. The material itself can differ; the targets used to undertake the laboratory work utilised the pre-

manufactured target that appeared to be constructed of very fine, almost granular, material, whereas the fieldwork used targets constructed of material similar to that found on guardrail, guideposts, traffic cones, etc. These two material may have different retro-reflective properties;

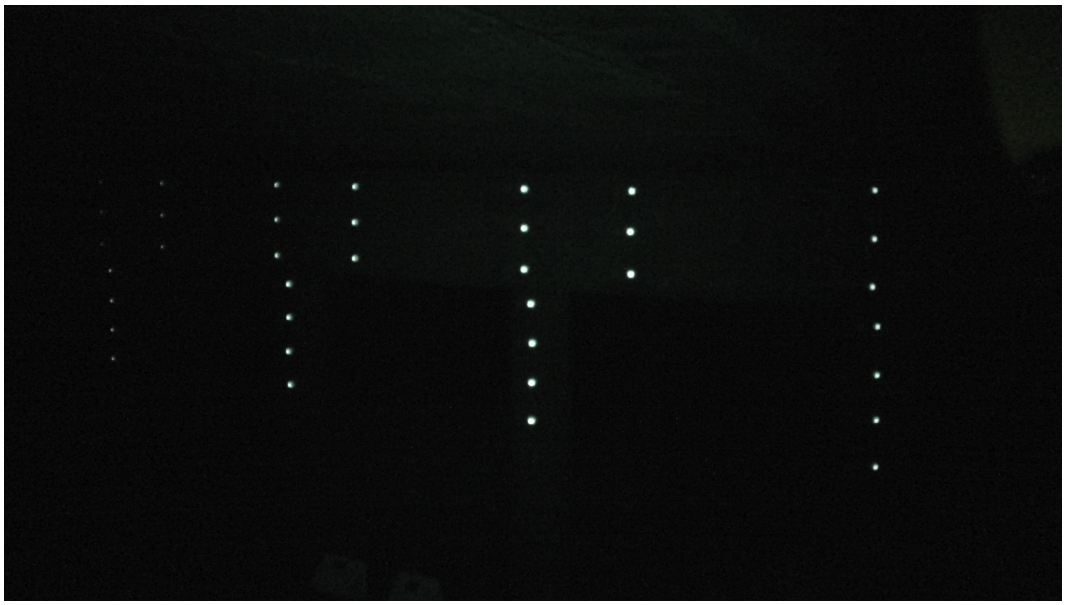

Figure 14. The effect of blooming on retro-reflective targets.

2. *Size of the target:* Target size is a function of the distance from the camera to the object of interest; the further the structure is from the camera, then the larger the target must be in order to acquire and digitise the target within software program, in this case, *Australis v.6*. However, there is a fine balance between target size and retro-reflectivity; larger targets have the ability to generate a greater return signal, therefore potential increasing the probability of blooming occurring. The target size of 20mm was selected on the basis of experience by the supervisor of this Research Project (Dr Albert Kon-Fook Chong) for an approximate distance of 6m from headstock to camera position;

3. *External near-infrared emitter:* all cameras used to undertake the fieldwork had an in-built near-infrared emitter. However, due to the availability, only one external near-infrared emitter was able to be obtained to enhance the infrared emission from these cameras. However, hindsight may suggest that either a second external emitter should have

been sourced, or omitted completely, as there was a significant visual difference in photographs between cameras.

Figure 15 outlines two images from the same camera station, where the cameras were separated on a supporting rod by around 0.5m. Figure 15(a) is the image from the camera without the external emitter attached, whereas Figure 15(b) had the external emitter attached. Note the difference in return emissions from the retro-reflective targets attached to the headstock; as can be seen, Figure 15(b) has a greater return signal from the targets. Further, blooming is apparent in Figure 15(b), which may have influenced any results from the bundle adjustment conducted within the *Australis* software program.

4. *Strength of the emitter:* associated with the blooming effect as described above is the strength of the external near-infrared emitter on one of the cameras. The particular emitter used has adjustable emission strength (low/medium/high); for the purposes of the nightwork, it was considered that the emitter should be on high to emit greater light, given that only one emitter was available for the project. However, it appears as though the emitter may be contributing to the blooming effect of the retro-reflective targets, thereby (negatively) influencing the resulting coordinate adjustment.

5. *Near-infrared emission beam:* It would appear that both the internal and external near-infrared emitters used during the fieldwork had a narrow emission beam. This was especially evident in the higher quality photographs taken during the second round of photography (as can be seen in Figure 16); while not as evident in the lower quality images of the video still photographs, it is suspected that the blooming may be a result of the narrow beam. If an emitter was available that had the ability to diffuse the beam and therefore spread the emission over a wider angle, perhaps an even spread of light would occur allowing for equal strength returns from the retro-reflective targets.

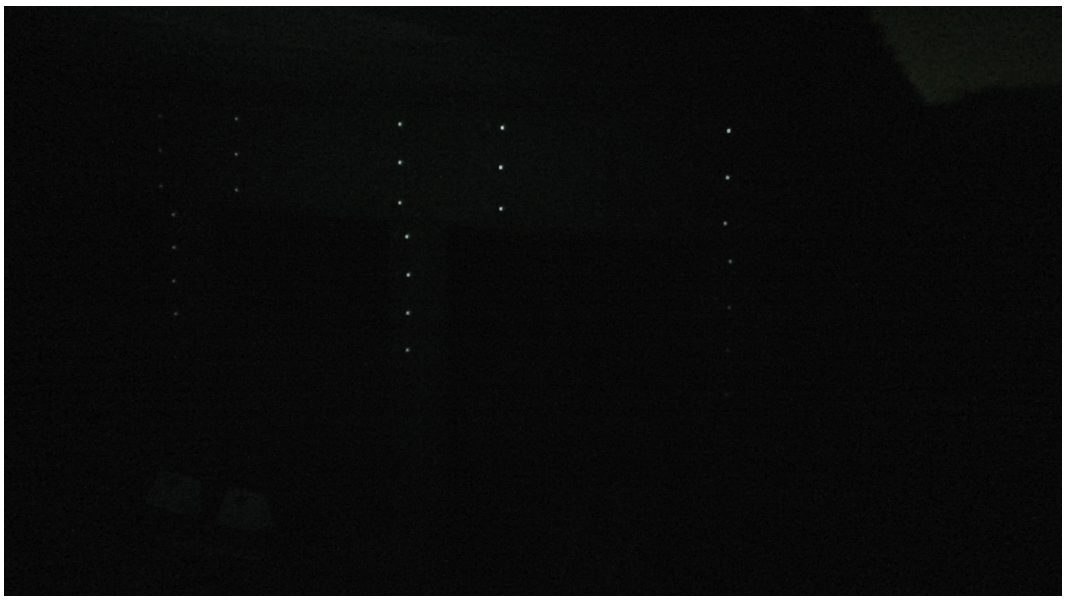

(a)

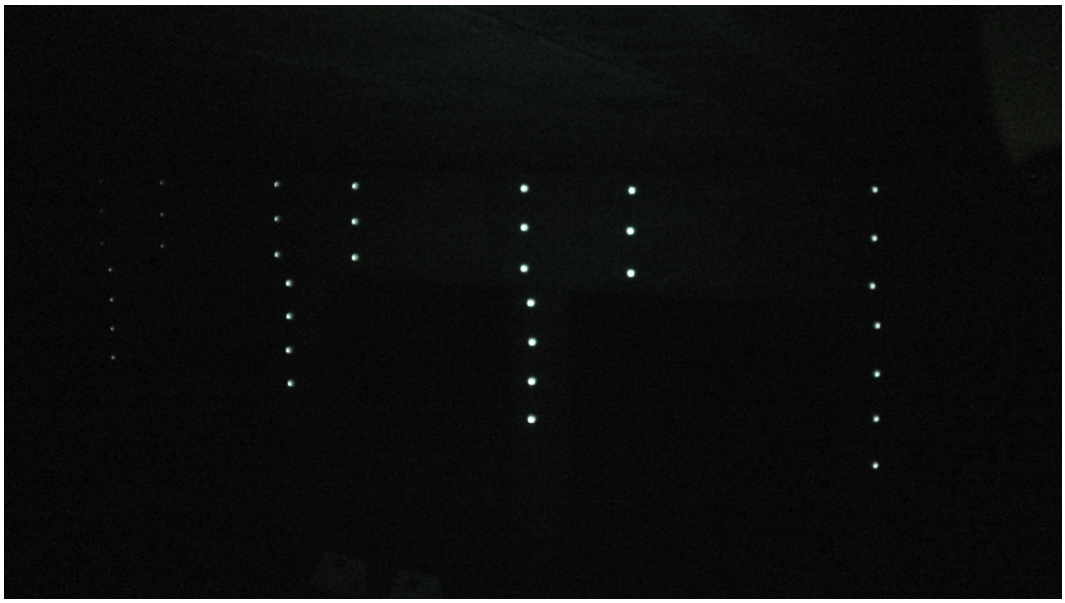

(b)

Figure 15. Differences in near-infrared emitter.

Other issues that arose during the near-infrared photogrammetry, and may also be applied to the colour photogrammetry, include:

1. *Aspect of the structure:* It was considered that the best time to conduct daylight photogrammetry was in the middle of the day, where the sun was overhead, and an equal amount of shadow was cast underneath the bridge structure, removing any shadow bias from the results. However, this

objective of this Research Project that was unable to be carried out. While colour photography was achieved during daylight, the near-infrared was not, primarily due to the aspect of the targets on the headstock structure. It was found that the light, although overhead, was still too bright for the near-infrared sensor, and produced a blank screen and image due to the light flooding the sensor surface.

Figure 16. Example of the narrow field of view of the emitted near-infrared light.

2. *Previously unknown structural issues:* Discussions with structural engineers of the Department of Transport and Main Roads suggest that there are a number of problems with the bearing pad of Pier 4 and expansion joint directly above the pier. This joint has suffered significant damage and is on a waiting list for replacement. As such, movement of the bridge deck at this joint occurs when traffic passes over the joint. Vehicles passing over Pier 4 while images are being acquired have the potential to influence the accuracy of those images with respect to target movement.

3. *Camera type:* The initial round of photogrammetry conducted used the low quality, 4MP digital *video* camera, whereas the second round of photogrammetry utilised the higher quality 8MP *still* digital camera. The quality of photographs produced show a significant difference in quality and clarity. It was expected that the higher quality camera would produce better result; however it was found that the 8MP camera was unable to resect the photographs to a sufficient accuracy to produce a reasonable bundle adjustment.

4. *Use of real-time coordinates:* Initially, it was suspected that because new target coordination was required (due to damage of existing targets), the new control file used in the resection was the reason for the poor adjustment of the second round of photogrammetry. However, comparison between the original reflectorless coordinates and the new reflectorless coordinates showed negligible differences in X, Y and Z coordinates.

   Consideration may need to be given to the use of an arbitrary control system using plane coordinates, and the use of one or more scale bars (or similar precisely measured control mechanism) to provide sufficient control to produce an acceptable resection and subsequent bundle adjustment.

5. *Densification:* The target base for this research Project is essentially a 9m x 3m area that contained between 106 (first round photogrammetry) and 132 (second round photogrammetry) targets. To ensure sufficient targets were acquired in each photograph, and to ensure sufficient overlap, the camera stations were between 4m and 6.5m distant from the headstock/pile surface.

   The laboratory results, which report good correlation between colour and near-infrared photogrammetry, were shot at distances generally not exceeding 1m, utilised smaller targets and had more targets per photograph that that of the fieldwork photographs. It may be that the increased densification in the laboratory produced the better bundle

adjustment, combined with the use of a scale bar and Anhui dissection control plate. Consideration may need to be given in future field studies to the inclusion of an increased target density combined with the scale bars.

6. *Stability of the camera station:* The first round fieldwork photogrammetry utilised two video cameras mounted on a horizontal bar attached to a general purpose camera tripod, whereas the second round utilised the camera mounted on the tripod only.

   As precise shots of the structure are required to produce an accurate bundle adjustment, the stability of the camera station is a high priority. Though not obvious in the first round of photography (possible due to the lower quality images produced), the slightest movement in the station produced errors in the captured image. This was particularly evident in the near-infrared photographs, where even the slight depression involved with pressing the button sometimes caused the camera to blur the retro-reflective targets, necessitating in the reacquisition of that image.

   To avoid this in future studies, consideration should be given to a more robust tripod setup, such as that of a survey instruments' tripod, coupled with a camera that has remote control capabilities.

7. *Centroid size:* In order to digitise the images with the correct and unique target identification in the *Australis* program, parameters need to be configured in the *Centroid Info* window. The two parameters that are of main concern are the window size (area in which the target must lie when selecting the location of the target on the image) and the Grey Range (specifies the minimum range of intensity of the target in the centroid window).

   When digitising, it may not be possible for these values to remain constant for all targets, and will require some manipulation for the program to recognise the target being digitised. However, the manipulation may be such that the target may require considerable degradation of the centroid in order for that point to be digitised. This effect was particularly noticeable

toward the extremities of the image where there was a large angle of incidence to those points from the camera station or, in the case of the near infrared images, the return from the retro-reflective targets was not as great ass those returns nearer to the near-infrared light emission from the camera or external emitter. Conversely, the blooming effect seen in some of the images also contributed to a degradation of the centroid size; the brighter returns required a larger window to determine the centre of the centroid in the digitisation.

8. *Aesthetics:* While a densification of (smaller) targets may improve the resection results and therefore produce a better bundle adjustment, tan increase in targets to a structure may decrease the visual amenity of that structure. For the purpose of this Research Project, aesthetic appeal was not a consideration, as the fieldwork occurred on the underside of a bridge structure in a rural setting. However, if this study was conducted in an urban setting, on the top side of a structure with a large amount of pedestrian and/or vehicular traffic, consideration would need to be given to the aesthetic appeal of that structure, especially if those targets need to be left *in situ* for some time.

9. *Temperature:* Concrete structures, such as the bridge structure used in the Research Project, are often constructed of materials that allow expansion and contraction. In this case, the construction material was concrete which is known to have expansion and contraction properties, dependent on the thermal load applied to the structure. Concrete has another property of importance – that of heat retention and loss over extended periods of time. This property, and using the case of the Hodgson Ck bridge, allows for the structure to heat up (and therefore expand) during daylight hours, and then slowly emit heat during the night hours (and therefore contracting). Assuming significant temperature differences at night, it would be expected that heat retained during the day would be completely removed from the structure by dawn the next day.

   At the time of target coordination and image capture, daytime temperatures at the site would vary from around 10°C to 24°C; and

temperature variation of 14°C. For reasons of safety and practicality, the target coordination was conducted in the middle of the daytime period, when the solar energy absorbed by the concrete would be at its greatest. The first round of image acquisition took place at around 1830hrs when the structure would be expected to cool and subsequently contract, although not appreciably so (for this time of day). The second round of image acquisition took place at 0400hrs at a time when the structure would be at its coolest.

It may be (although perhaps would be difficult to substantiate) that values obtained from the resection and bundle adjustment of the first-round images were similar to those of the target coordination values, as the temperatures of the structure had allowed for little contraction to occur, unlike that of the early morning images, where differences appear to be significant enough not to allow for the correct resection of the images.

5.4 Recommendations and further research

Recommendations flowing on from this Research Project concentrate on issues raised in Section 5.3 above. Specifically, it is recommended that:

1. *Higher quality/higher resolution cameras* are used to undertake photogrammetric studies. Visual observations as to the quality of images (comparison of the quality between the near infrared images of Figure 15 and Figure 16, for example) indicate that greater imagery detail can be acquired at relatively little cost,
2. *Use of external near-infrared emitters* that produce a wide angle of incidence as opposed to the narrow field of view that was apparent in the images of this Research Project,
3. *Strength of near-infrared emitter* and what relationship exists between strength of emission and distance to target, and the influence of the strength on the blooming effect,
4. *Experimentation* with target types, construction materials, densification of targets, emitter strength, and so on.

5. *Consideration of the use of self-calibrating methods* of camera calibration, thereby negating the need for geodetic control (unless geodetic control has been deemed essential for the running of the project),
6. *Climatic conditions* – does the effect of varying temperature, fog, rain, humidity, aspect, etc. influence the location or differential placement of the targets, and
7. *Static and dynamic monitoring* of the bridge structure with loads of known weight, with image capture using digital still and video camera

6 Conclusions

The literature review to determine previous studies of photogrammetry suggest that much of the work to date has focussed on the use of conventional photogrammetric methods. There is little data on the use of near-infrared photogrammetric work outside of medical applications. In order to rectify this, two Research Projects were conducted concurrently; a comparison of conventional and infrared photogrammetry within the laboratory setting (conducted by Mr. Daniel Pratt), and this project that examined the comparisons between the two methods in the field on a 'live' structure.

The results of the laboratory work suggest that there is no significant difference between the two photogrammetric methods under the examined conditions of daylight, bright (artificial) light and darkness. The differences between the two photogrammetric methods were found to be between 0.1mm – 0.3mm. Similarly, the result fieldwork comparison suggests no significant differences between the two methods, with differences of between 0.16mm-0.24mm. These values were based on the three dimensional distance reduction of the data. Further examination of the three dimensional coordinate distances between randomly selected targets also suggest that there are no significant differences between the methods when considering the distance mean values. Difference values of between 0.28mm-0.51mm were achieved when comparing photogrammetric methods.

If it is considered that there is no significant difference in results between conventional and near-infrared photogrammetry, then there is *no* reason not to consider the use of infrared photogrammetry in place of conventional methods. Unless a required project deliverable is an image that represents human perception of colours (i.e. that of a traditional visible light photograph), then it would make sense to use near-infrared systems to acquire images. Near infrared photogrammetry can capture both diffuse and retro-reflective targets, be used in daylight, low light, or night conditions, additional external lighting is unnecessary, and can be used in restrictive or explosive atmospheres, and achieve the same results as that of conventional photogrammetry. Assuming that as many error

sources can be removed (or minimised as much as possible) from the capture or processing of images, then infrared photogrammetry should be considered a viable alternative to conventional methods.

As discussed in the recommendations there are many aspects of infra-red photogrammetry that would require further examination to determine the benefit (or otherwise) of near-infrared photogrammetry in a wider field of research.

7 References

Barazzetti, L & Scaioni, M 2009, 'Crack measurement: Development, testing and applications of an automatic image-based algorithm', *ISPRS Journal of Photogrammetry and Remote Sensing*, vol. 64, pp. 285-296.

Chong, AK & Matheau, R 2006, 'Near-infrared photography for craniofacial anthropometric landmark measurement' *The Photogrammetric Record*, vol. 21, No. 113, pp. 16-28.

Cooper, MAR & Robson, S 2001, 'Theory of close range photogrammetry', in KB Atkinson (ed), *Close range photogrammetry and machine vision*, Whittles Publishing, Dunbeath, Scotland.

Dias-da-Costa, D, Valença, J & Júlio, ENBS 2011, 'Laboratorial test monitoring applying photogrammetric post-processing procedures to surface displacements' *Measurement*, vol 44, pp. 527-538.

Fraser, CS 2001, 'Network design', in KB Atkinson (ed), *Close range photogrammetry and machine vision*, Whittles Publishing, Dunbeath, Scotland.

Fraser, CS and Al-Ajlouni, S, (2006) 'Zoom-dependent camera calibration in digital close-range photogrammetry', *Photogrammetric Engineering and Remote Sensing*, vol. 72, No. 9, pp. 1017-1026.

Fryer, JG 2001, 'Introduction', in KB Atkinson (ed), *Close range photogrammetry and machine vision*, Whittles Publishing, Dunbeath, Scotland.

Giancoli, DC 2005, *Physics: principles with applications*, 6th edn, Pearson Education Inc., Upper Saddle River, New Jersey.

Jáuregui, DV, White, KR, Woodward, CB & Leitch, KR 2003, 'Noncontact photogrammetric measurement of vertical bridge deflection', *Journal of Bridge Engineering*, vol 8, No. 4, pp. 212-222.

Jiang, R, Jáuregui, DV & White, KR 2008, 'Close-range photogrammetry applications in bridge measurement: Literature review', *Measurement*, vol 41, pp. 823-834.

Jiang, R & Jáuregui, DV 2010, 'Development of a digital close-range photogrammetric bridge deflection measurement system', *Measurement*, vol 43, pp. 1431-1438.

Knight, RD 2004, *Physics for scientists and engineers: a strategic approach*, Addison Wesley, San Francisco.

Lillesand, TM, Kiefer, RW & Chipman, JW 2004, *Remote sensing and image interpretation*, 5th edn, John Wiley & Sons, Inc., New York.

Litwiller, D, 2001, 'CCD vs CMOS: facts and fiction', *Photonics Spectra*, Laurin Publishing Co. Inc., January

Luhmann, T, Robson, S, Kyle, S & Harley, I 2006, *Close range photogrammetry: Principles, techniques and applications*, Whittles Publishing, Dunbeath, Scotland.

Maas, H-G & Hampel, U 2006, 'Photogrammetric techniques in civil engineering material testing and structure monitoring', *Photogrammetric Engineering & Remote Sensing*, vol. 72, No. 1, pp. 39-45.

Maas, H-G & Hampel, U 2009, 'Cascaded image analysis for dynamic crack detection in material testing', *ISPRS Journal of Photogrammetry and Remote Sensing*, vol. 64, pp. 345-350.

Mills, J & Barber, D 2004, 'Geomatics techniques for structural surveying', *Journal of Surveying Engineering*, vol. 130, No. 2, pp. 56-64.

Mikhail, EM, Bethel, JS & McGlone, JC 2001, *Introduction to modern photogrammetry*, John Wiley & Sons, Inc., New York.

Mitchell, H 2007, 'Fundementals of photogrammetry', in J Fryer, H Mitchell & J Chandler (eds), *Applications of 3D measurements from images*, Whittles Publishing, Dunbeath, Scotland.

Roberts, GW, Brown, CJ & Ogundipe, O, 'Monitoring bridges by GNSS', *Proceedings of the FIG Congress 2010*, International Federation of Surveyors, Sydney

Rönnholm, P, Nuikka, M, Suominen, A, Salo, P, Hyyppä, H, Pöntinen, P, Haggrén, H, Vermeer, M, Puttonen, J, Hirsi, H, Kukko, A, Kaartinen, H, Hyypä, J & Jaakkola, A 2009, 'Comparison of measurement techniques and static theory applied to concrete beam deformation', *The Photogrammetric Record*, vol. 24, No. 128, pp. 351-371.

Ruscello , MAC 2010, *Infrared Photography - Part I*, viewed 10 August 2011, http://www.infraredphoto.eu/Site/GentleIntro1.html

Schlessinger, M 1995, *Infrared technology* fundamentals, 2nd edn, Marcel Dekker, Inc., New York.

Teledyne Dalsa, 2011, 'CCD vs. CMOS' viewed 18 May 2011, http://www.dalsa.com/corp/markets/ccd_vs_cmos.aspx

Thomas, H & Cantré, S 2009, 'Applications of low-budget photogrammetry in the geotechnical laboratory', *The Photogrammetric Record*, vol. 24, No. 128, pp. 332-350.

Wikibooks, 2011 'A-level Physics (Advancing Physics)/What is a wave?', Wiki article, 22 February, viewed 19 May 2011, http://en.wikibooks.org/wiki/A-level_Physics_(Advancing_Physics)/What_is_a_wave%3F

Whiteman, T, Lichti, DD & Chandler, I 2002, 'Measurement of deflections in concrete beams by close-range digital photogrammetry', *Symposium on Geospatial Theory, Processing and Applications*, Ottawa, Canada.

Woodhouse, NG, Robson, S & Eyre, JR 1999, 'Vision metrology and three dimensional visualization in structural testing and monitoring', *Photogrammetric Record*, vol. 16, No. 94, pp. 625-641.

Appendix A:

Project Specification

University of Southern Queensland

ENG4111/4112 – RESEARCH PROJECT

PROJECT SPECIFICATION

FOR:	**PAUL LENTON**
TOPIC:	NEAR INFRARED FOR SMALL STRUCTURAL DEFORMATION STUDY
SUPERVISORS:	Dr. Albert Chong
	Faculty of Engineering and Surveying, USQ.
ENROLMENT:	ENG4111 – SEMESTER 1, X, 2011
	ENG4112 – SEMESTER 2, X, 2011
PROJECT AIM:	This project seeks to establish whether the use of near-infrared photogrammetric techniques is suitable for the determination of structural deformation in small scale structures.
SPONSORSHIP:	None obtained.
PROGRAMME:	(Issue 1, 22nd March 2011)

1. Discuss current (non-photogrammetric) methods and their effectiveness for the measurement of structural deformation in structures.
2. Research conventional photogrammetry and its application in determining structural deformation.
3. Determine whether infra-red photogrammetric techniques can be used to better determine structural deformation in small scale structures.
4. Compare and contrast conventional and infra-red photogrammetric techniques in determining deformation in small scale structures within a laboratory context.
5. Prepare and submit an academic dissertation on the research.

If time permits:

6. Negotiate with the Queensland Department of Transport and Main Roads (TMR) to undertake photogrammetric testing of a 'live' structure suspected of having structural deformation.
7. Compare data acquired in Step 6 (above) with any data collated by the TMR, and provide feedback, if required.

AGREED:

(Supervisor)		(Student)	
/ /	(Date)	/ /	(Date)

Appendix B:

Control Traverse Report File

File: C:\Documents and Settings\pdlento\Desktop\Paul\USQ\ENG4111-4112 - Research Project\12d Bridge\Traverse Reduction.rpt 10/07/2011, 7:52:32 AM

Survey Data Reduction

Reduction report for field files

HODGSON CK BRIDGE.fld

Traverse	Start link	End link
1	-	-
2	1	-
3	1	-

Raw traverse details

Traverse	From	To	Description	Instrument Height	Target Height	Horizontal Angle	Vertical Angle	Slope Distance
1	MR16K	STN1	Foresight	1.6620	1.6250	359° 59' 56"	90° 17' 5"	350.1300
1	STN1	MR16K	Backsight	1.6250	1.6620	0° 0' 0"	89° 43' 35"	350.1297
			Reciprocal	point	point	359° 59' 56"	90° 16' 23"	350.1297
1	STN1	TBM1	Foresight	1.6250	1.6160	177° 52' 45"	88° 26' 23"	344.5565
1	TBM1	STN1	Backsight	1.6160	1.6250	0° 0' 0"	91° 34' 6"	344.5568
			Reciprocal	point	point	177° 52' 45"	88° 26' 3"	344.5569
1	TBM1	STN2	Foresight	1.6160	1.6130	175° 30' 1"	88° 48' 52"	149.2703
1	STN2	TBM1	Backsight	1.6130	1.6160	0° 0' 0"	91° 11' 18"	149.2697
			Reciprocal	point	point	175° 30' 1"	88° 48' 43"	149.2701
1	STN2	QT17K	Foresight	1.6130	1.6990	151° 17' 1"	87° 40' 53"	107.9890
1	QT17K	STN2	Backsight	1.6990	1.6130	359° 59' 55"	92° 19' 13"	107.9890
			Reciprocal	point	point	151° 17' 1"	87° 43' 34"	107.9856
2	STN1	STN3	Foresight	1.6250	1.3740	217° 19' 8"	92° 0' 11"	53.7872
2	STN3	STN1	Backsight	1.3740	1.6250	359° 59' 57"	87° 59' 41"	53.7870
			Reciprocal	point	point	217° 19' 8"	91° 44' 13"	53.7789
3	STN1	STN4	Foresight	1.6250	1.4610	222° 3' 25"	91° 53' 48"	56.1997
3	STN4	STN1	Backsight	1.4610	1.6250	359° 59' 56"	88° 6' 5"	56.2000
			Reciprocal	point	point	222° 3' 25"	91° 43' 50"	56.1947

Rotating traverse "1"

Point	Easting	Northing	Height	
MR16K	392241.6930	6936075.7510	482.4060	fixed
QT17K	392656.0680	6935237.7640	497.5450	fixed

	Bearing	Distance (plane)
Actual	153° 41' 17"	934.8416
Surveyed	354° 19' 51"	934.8423
Difference	-159° 21' 26"	-0.0007

Reduced details - Traverse "1"

	Plane Bearing	Plane Distance
MR16K	159° 21' 23"	350.0092
STN1	157° 14' 7"	344.3134
TBM1	152° 44' 8"	149.1880
STN2	124° 1' 9"	107.8643
QT17K		

Bowditch adjustment - Traverse "1"

Point No	Surveyed Easting	Surveyed Northing	Adjusted Easting	Adjusted Northing	Difference Easting	Difference Northing
MR16K	392241.6930	6936075.7510	392241.6930	6936075.7510	0.0000	0.0000
STN1	392365.0909	6935748.2156	392365.0908	6935748.2159	-0.0001	0.0002
TBM1	392498.3222	6935430.7237	392498.3220	6935430.7242	-0.0002	0.0005
STN2	392566.6649	6935298.1102	392566.6646	6935298.1108	-0.0003	0.0006
QT17K	392656.0683	6935237.7634	392656.0680	6935237.7640	-0.0003	0.0006

Final coordinates

Traverse	Point	Easting	Northing		Height	
1	MR16K	392241.6930	6936075.7510	fixed	482.4060	calc'd
1	STN1	392365.0908	6935748.2159	calc'd	480.7368	calc'd
1	TBM1	392498.3220	6935430.7242	calc'd	490.1514	calc'd
1	STN2	392566.6646	6935298.1108	calc'd	493.2464	calc'd
1	QT17K	392656.0680	6935237.7640	fixed	497.5450	calc'd
2	STN1	392365.0908	6935748.2159	calc'd	480.7368	calc'd
2	STN3	392349.6713	6935696.7393	calc'd	479.1068	calc'd
3	STN1	392365.0908	6935748.2159	calc'd	480.7368	calc'd
3	STN4	392344.5907	6935695.9415	calc'd	479.0398	calc'd

End of traversings

Coordinate for station "MR16K" defined from control model "control->"

Occupying Station : MR16K
Coordinates : E 392241.693 N 6936075.751 H 482.406
Code : PBMK
Instrument Ht : 1.662
N Value : 0.000

PointID	Horiz	Vert	SDist	HTar	East	North	Height	Code
1	359° 59' 56"	90° 17' 5"	350.130	1.625	392241.686	6936425.760	480.711	TL 1 STN1

(1 measurement)

Coordinate for station "STN1" defined from network model "SURVEY TRAVERSE->TL"

Occupying Station : STN1
Coordinates : E 392365.091 N 6935748.216 H 480.737
Code : PISP
Instrument Ht : 1.625
N Value : 0.000

Coordinate for Backsight "MR16K" defined from control model "control->"

0° 0' 0"	89° 43' 35"	350.130	1.662	392365.091	6936098.225	482.380	

******** Backsight to "MR16K" Code "TL" ***********

	OBSERVED (SWUNG)	CALCULATED	OBSERVED - CALCULATED	CORRECTED	CORRECTED - CALCULATED
EASTING	392241.693	392241.693	-0.000	392241.693	-0.000
NORTHING	6936075.751	6936075.751	0.000	6936075.751	0.000
HEIGHT	482.380	482.406	-0.026	482.380	-0.026
BEARING (grid)	339° 21' 22"	339° 21' 22"		339° 21' 22"	0° 0' 0"
DISTANCE (ellip)	350.099	350.099	0.000	350.099	0.000

Bearing datum difference 339° 21' 22" applied to subsequent measurements

PointID	Horiz	Vert	SDist	HTar	East	North	Height	Code
1	177° 52' 45"	88° 26' 23"	344.557	1.616	392498.322	6935430.724	490.135	TL 1 TBM1
3	217° 19' 8"	92° 0' 11"	53.787	1.374	392349.671	6935696.739	479.108	TL 2 STN3
4	222° 3' 25"	91° 53' 48"	56.200	1.461	392344.591	6935695.942	479.041	TL 3 STN4

(3 measurements)
Coordinate for station "STN3" defined from network model "SURVEY TRAVERSE->TL"

Occupying Station : STN3
Coordinates : E 392349.671 N 6935696.739 H 479.107
Code : PISP
Instrument Ht : 1.374
N Value : 0.000

Coordinate for Backsight "STN1" defined from network model "SURVEY TRAVERSE->TL"
359° 59' 57" 87° 59' 41" 53.787 1.625 392349.671 6935750.476 480.738

******** Backsight to "STN1" Code "TL" ***********

	OBSERVED (SWUNG)	CALCULATED	OBSERVED - CALCULATED	CORRECTED	CORRECTED - CALCULATED
EASTING	392365.091	392365.091	-0.000	392365.091	-0.000
NORTHING	6935748.216	6935748.216	-0.000	6935748.216	-0.000
HEIGHT	480.738	480.737	0.001	480.738	0.001
BEARING (grid)	16° 40' 31"	16° 40' 31"		16° 40' 31"	0° 0' 0"
DISTANCE (ellip)	53.750	53.750	-0.000	53.750	-0.000

Bearing datum difference 16° 40' 34" applied to subsequent measurements

Coordinate for station "STN4" defined from network model "SURVEY TRAVERSE->TL"

Occupying Station : STN4
Coordinates : E 392344.591 N 6935695.942 H 479.040
Code : PISP
Instrument Ht : 1.461
N Value : 0.000

Coordinate for Backsight "STN1" defined from network model "SURVEY TRAVERSE->TL"
359° 59' 56" 88° 6' 5" 56.200 1.625 392344.590 6935752.092 480.738

******** Backsight to "STN1" Code "TL" ***********

	OBSERVED (SWUNG)	CALCULATED	OBSERVED - CALCULATED	CORRECTED	CORRECTED - CALCULATED
EASTING	392365.091	392365.091	0.000	392365.091	0.000
NORTHING	6935748.216	6935748.216	0.000	6935748.216	0.000
HEIGHT	480.738	480.737	0.001	480.738	0.001
BEARING (grid)	21° 24' 48"	21° 24' 48"		21° 24' 48"	0° 0' 0"
DISTANCE (ellip)	56.165	56.165	0.000	56.165	0.000

Bearing datum difference 21° 24' 52" applied to subsequent measurements

Coordinate for station "TBM1" defined from network model "SURVEY TRAVERSE->TL"

Occupying Station : TBM1
Coordinates : E 392498.322 N 6935430.724 H 490.151
Code : PSMK
Instrument Ht : 1.616
N Value : 0.000

Coordinate for Backsight "STN1" defined from network model "SURVEY TRAVERSE->TL"
0° 0' 0" 91° 34' 6" 344.557 1.625 392498.322 6935775.037 480.720

******** Backsight to "STN1" Code "TL" ***********

	OBSERVED (SWUNG)	CALCULATED	OBSERVED - CALCULATED	CORRECTED	CORRECTED - CALCULATED
EASTING	392365.091	392365.091	-0.000	392365.091	-0.000
NORTHING	6935748.216	6935748.216	0.000	6935748.216	0.000
HEIGHT	480.720	480.737	-0.016	480.720	-0.016
BEARING (grid)	337° 14' 7"	337° 14' 7"		337° 14' 7"	0° 0' 0"
DISTANCE (ellip)	344.402	344.402	0.000	344.402	0.000

Bearing datum difference 337° 14' 7" applied to subsequent measurements

PointID	Horiz	Vert	SDist	HTar	East	North	Height	Code
2	175° 30' 1"	88° 48' 52"	149.270	1.613	392566.665	6935298.110	493.244	TL 1 STN2

(1 measurement)

Coordinate for station "STN2" defined from network model "SURVEY TRAVERSE->TL"

Occupying Station : STN2
Coordinates : E 392566.665 N 6935298.111 H 493.246
Code : PISP
Instrument Ht : 1.613
N Value : 0.000

Coordinate for Backsight "TBM1" defined from network model "SURVEY TRAVERSE->TL"
0° 0' 0" 91° 11' 18" 149.270 1.616 392566.665 6935447.298 490.149

******** Backsight to "TBM1" Code "TL" ***********

	OBSERVED (SWUNG)	CALCULATED	OBSERVED - CALCULATED	CORRECTED	CORRECTED - CALCULATED
EASTING	392498.322	392498.322	0.000	392498.322	0.000
NORTHING	6935430.724	6935430.724	-0.000	6935430.724	-0.000
HEIGHT	490.149	490.151	-0.002	490.149	-0.002
BEARING (grid)	332° 44' 8"	332° 44' 8"		332° 44' 8"	0° 0' 0"
DISTANCE (ellip)	149.226	149.226	-0.000	149.226	-0.000

Bearing datum difference 332° 44' 8" applied to subsequent measurements

PointID Horiz Vert SDist HTar East North Height Code
0 151° 17' 1" 87° 40' 53" 107.989 1.699 392656.068 6935237.764 497.530 TL 1 QT17K
(1 measurement)

Coordinate for station "QT17K" defined from control model "control->"

Occupying Station : QT17K
Coordinates : E 392656.068 N 6935237.764 H 497.545
Code : PBMK
Instrument Ht : 1.699
N Value : 0.000

Coordinate for Backsight "STN2" defined from network model "SURVEY TRAVERSE->TL"
359° 59' 55" 92° 19' 13" 107.989 1.613 392656.065 6935345.628 493.260

******** Backsight to "STN2" Code "TL" **********

	OBSERVED (SWUNG)	CALCULATED	OBSERVED - CALCULATED	CORRECTED	CORRECTED - CALCULATED
EASTING	392566.665	392566.665	-0.000	392566.665	-0.000
NORTHING	6935298.111	6935298.111	0.000	6935298.111	0.000
HEIGHT	493.260	493.246	0.013	93.260	0.013
BEARING (grid)	304° 1' 9"	304° 1' 9"		304° 1' 9"	0° 0' 0"
DISTANCE (ellip)	107.892	107.892	0.000	107.892	0.000

Bearing datum difference 304° 1' 14" applied to subsequent measurements

End of reduction report

Appendix C:

Target Location Report File

Survey Data Reduction
==========

Reduction report for field files
  TARGET COORDINATES.fld

Coordinate for station "STN4" defined from control model "SURVEY TRAVERSE->TL"

Occupying Station : STN4
Coordinates : E 392344.591 N 6935695.942 H 479.040
Code : PISP
Instrument Ht : 1.504
N Value : 0.000

Coordinate for Backsight "STN1" defined from control model "SURVEY TRAVERSE->TL"
0° 0' 0" 88° 9' 8" 56.198 1.619 392344.591 6935752.092 480.737

******** Backsight to "STN1" Code "" ***********

	OBSERVED (SWUNG)	CALCULATED	OBSERVED - CALCULATED	CORRECTED	CORRECTED - CALCULATED
EASTING	392365.091	392365.091	-0.000	392365.091	-0.000
NORTHING	6935748.216	6935748.216	-0.000	6935748.216	-0.000
HEIGHT	480.737	480.737	0.000	480.737	0.000
BEARING (grid)	21° 24' 48"	21° 24' 48"		21° 24' 48"	0° 0' 0"
DISTANCE (ellip)	56.165	56.165	-0.000	56.165	-0.000

Bearing datum difference 21° 24' 48" applied to subsequent measurements

Coordinate for Check measurement "STN3" defined from control model "SURVEY TRAVERSE->TL"

******** Check Measurement to "STN3" Code "" ***********

	OBSERVED	CALCULATED	OBSERVED - CALCULATED
EASTING	392349.671	392349.671	-0.000
NORTHING	6935696.739	6935696.739	-0.001
HEIGHT	479.106	479.107	-0.001
BEARING (grid)	81° 4' 52"	81° 4' 32"	- 0° 0' 20"
DISTANCE (ellip)	5.144	5.144	-0.001

PointID	Horiz	Vert	SDist	HTar	East	North	Height	Code
A100	295° 15' 39"	76° 52' 27"	4.588	0.000	392341.526	6935699.191	481.586	PSMK 0
B100	295° 12' 30"	79° 54' 4"	4.536	0.000	392341.525	6935699.186	481.339	PSMK 0
C100	295° 9' 49"	83° 4' 39"	4.497	0.000	392341.523	6935699.183	481.086	PSMK 0
D100	295° 56' 2"	86° 9' 40"	4.568	0.000	392341.504	6935699.292	480.850	PSMK 0
E100	295° 56' 8"	89° 19' 33"	4.556	0.000	392341.505	6935699.291	480.597	PSMK 0
F100	295° 58' 24"	92° 31' 56"	4.555	0.000	392341.511	6935699.289	480.343	PSMK 0
G100	295° 56' 44"	95° 38' 45"	4.573	0.000	392341.509	6935699.288	480.094	PSMK 0
A101	296° 18' 15"	76° 41' 22"	4.533	0.000	392341.624	6935699.204	481.587	PSMK 0
B101	296° 16' 27"	79° 47' 54"	4.477	0.000	392341.626	6935699.199	481.337	PSMK 0
C101	296° 11' 39"	83° 1' 56"	4.440	0.000	392341.620	6935699.195	481.082	PSMK 0
D101	296° 58' 2"	86° 9' 27"	4.506	0.000	392341.606	6935699.301	480.846	PSMK 0
E101	296° 57' 54"	89° 18' 47"	4.495	0.000	392341.606	6935699.300	480.598	PSMK 0
F101	296° 59' 10"	92° 30' 54"	4.496	0.000	392341.610	6935699.299	480.346	PSMK 0
G101	296° 58' 20"	95° 43' 9"	4.515	0.000	392341.608	6935699.299	480.094	PSMK 0
A102	304° 18' 57"	75° 54' 39"	4.191	0.000	392342.302	6935699.300	481.564	PSMK 0
B102	304° 19' 42"	79° 18' 5"	4.133	0.000	392342.305	6935699.297	481.311	PSMK 0
C102	304° 12' 30"	82° 40' 28"	4.093	0.000	392342.299	6935699.291	481.066	PSMK 0
A103	305° 37' 44"	75° 49' 35"	4.146	0.000	392342.405	6935699.313	481.559	PSMK 0
B103	305° 32' 56"	79° 14' 23"	4.091	0.000	392342.400	6935699.310	481.308	PSMK 0
C103	305° 27' 31"	82° 37' 6"	4.051	0.000	392342.396	6935699.305	481.064	PSMK 0
A104	315° 20' 27"	75° 8' 59"	3.905	0.000	392343.101	6935699.409	481.545	PSMK 0
B104	315° 17' 41"	78° 49' 20"	3.846	0.000	392343.099	6935699.406	481.289	PSMK 0
C104	315° 16' 2"	82° 31' 8"	3.801	0.000	392343.099	6935699.401	481.039	PSMK 0
A105	325° 59' 47"	75° 1' 37"	3.781	0.000	392343.795	6935699.505	481.521	PSMK 0
B105	325° 56' 3"	78° 45' 39"	3.719	0.000	392343.792	6935699.499	481.269	PSMK 0
C105	325° 57' 43"	82° 48' 40"	3.671	0.000	392343.795	6935699.494	481.003	PSMK 0
D105	325° 58' 30"	86° 22' 46"	3.731	0.000	392343.778	6935699.574	480.779	PSMK 0
E105	325° 57' 31"	90° 19' 45"	3.722	0.000	392343.777	6935699.572	480.522	PSMK 0
F105	325° 56' 33"	94° 10' 14"	3.731	0.000	392343.776	6935699.571	480.272	PSMK 0
G105	325° 51' 1"	97° 58' 34"	3.759	0.000	392343.770	6935699.571	480.022	PSMK 0
A106	327° 31' 58"	74° 59' 1"	3.773	0.000	392343.892	6935699.517	481.521	PSMK 0
B106	327° 33' 43"	78° 41' 33"	3.711	0.000	392343.895	6935699.512	481.271	PSMK 0
C106	327° 32' 22"	82° 50' 43"	3.664	0.000	392343.894	6935699.508	481.000	PSMK 0
D106	327° 28' 1"	86° 26' 9"	3.721	0.000	392343.875	6935699.584	480.775	PSMK 0
E106	327° 31' 21"	90° 23' 30"	3.718	0.000	392343.877	6935699.589	480.518	PSMK 0
F106	327° 26' 0"	94° 12' 18"	3.730	0.000	392343.871	6935699.590	480.270	PSMK 0
G106	327° 24' 6"	97° 58' 6"	3.755	0.000	392343.870	6935699.588	480.023	PSMK 0
A107	338° 20' 5"	75° 24' 39"	3.796	0.000	392344.575	6935699.614	481.500	PSMK 0
B107	338° 14' 17"	79° 11' 9"	3.735	0.000	392344.568	6935699.609	481.245	PSMK 0
C107	338° 17' 28"	82° 59' 23"	3.692	0.000	392344.572	6935699.605	480.994	PSMK 0
A108	339° 49' 51"	75° 31' 21"	3.809	0.000	392344.671	6935699.627	481.496	PSMK 0
B108	339° 50' 58"	79° 16' 13"	3.749	0.000	392344.672	6935699.623	481.242	PSMK 0
C108	339° 50' 9"	83° 6' 14"	3.706	0.000	392344.671	6935699.619	480.989	PSMK 0
A109	347° 27' 42"	76° 9' 31"	3.915	0.000	392345.177	6935699.696	481.480	PSMK 0
B109	347° 35' 7"	79° 51' 53"	3.859	0.000	392345.185	6935699.692	481.223	PSMK 0
C109	347° 36' 5"	83° 34' 56"	3.819	0.000	392345.185	6935699.688	480.971	PSMK 0
A110	356° 59' 30"	77° 17' 7"	4.162	0.000	392345.872	6935699.792	481.460	PSMK 0
B110	357° 0' 54"	80° 43' 51"	4.110	0.000	392345.873	6935699.789	481.206	PSMK 0
C110	357° 0' 45"	84° 25' 58"	4.071	0.000	392345.871	6935699.784	480.939	PSMK 0
D110	356° 25' 16"	87° 33' 46"	4.148	0.000	392345.860	6935699.885	480.720	PSMK 0
E110	356° 25' 1"	91° 2' 40"	4.143	0.000	392345.859	6935699.884	480.468	PSMK 0
F110	356° 21' 54"	94° 37' 28"	4.157	0.000	392345.855	6935699.886	480.209	PSMK 0
G110	356° 32' 36"	98° 1' 24"	4.184	0.000	392345.868	6935699.881	479.960	PSMK 0

Coordinate for Check measurement "STN3" defined from control model "SURVEY TRAVERSE->TL"

******** Check Measurement to "STN3" Code "" ***********

```
                        OBSERVED      CALCULATED      OBSERVED -
                                                      CALCULATED
EASTING               392349.671      392349.671          -0.000
NORTHING             6935696.739     6935696.739          -0.001
HEIGHT                   479.106         479.107          -0.001
BEARING  (grid)     81°  4' 58"     81°  4' 32"   -  0°  0' 26"
DISTANCE (ellip)          5.144           5.144          -0.001

Coordinate for Check measurement "STN1" defined from control model "SURVEY TRAVERSE->TL"

******** Check Measurement to "STN1" Code "" ***********

                        OBSERVED      CALCULATED      OBSERVED -
                                                      CALCULATED
EASTING               392365.092      392365.091           0.001
NORTHING             6935748.216     6935748.216           0.000
HEIGHT                   480.737         480.737           0.001
BEARING  (grid)     21° 24' 51"     21° 24' 48"   -  0°  0'  3"
DISTANCE (ellip)          56.166          56.165           0.001

 (53 measurements)
Coordinate for station "STN3" defined from control model "SURVEY TRAVERSE->TL"

Occupying Station           : STN3
Coordinates                 : E 392349.671   N 6935696.739   H 479.107
Code                        :
Instrument Ht               : 1.236
N Value                     : 0.000

PointID    Horiz        Vert      SDist   HTar        East       North    Height   Code
   STN1   0°  0'  0"  87° 51' 11"  53.794  1.619  392349.671 6935750.478   480.739
Coordinate for Backsight "STN1" defined from control model "SURVEY TRAVERSE->TL"
          0°  0'  1"  87° 51' 12"  53.793  1.619  392349.672 6935750.477   480.739

******** Backsight to "STN1" Code "" ***********

                        OBSERVED      CALCULATED      OBSERVED -       CORRECTED     CORRECTED -
                        (SWUNG)                       CALCULATED                     CALCULATED
EASTING               392365.091      392365.091           0.000     392365.091           0.000
NORTHING             6935748.217     6935748.216           0.001    6935748.217           0.001
HEIGHT                   480.739         480.737           0.002        480.739           0.002
BEARING  (grid)     16° 40' 31"     16° 40' 31"                    16° 40' 31"      0°  0'  0"
DISTANCE (ellip)          53.751          53.750           0.001         53.751           0.001

Bearing datum difference   16° 40' 30" applied to subsequent measurements

Coordinate for Check measurement "STN4" defined from control model "SURVEY TRAVERSE->TL"

******** Check Measurement to "STN4" Code "" ***********

                        OBSERVED      CALCULATED      OBSERVED -
                                                      CALCULATED
EASTING               392344.591      392344.591           0.000
NORTHING             6935695.942     6935695.942           0.001
HEIGHT                   479.040         479.040           0.000
BEARING  (grid)    261°  5'  4"    261°  4' 32"   -  0°  0' 32"
DISTANCE (ellip)          5.144           5.144          -0.001

   A111 292° 58' 53"  76° 53' 45"   4.937  0.000  392345.971 6935699.807   481.462 PSMK 0
   B111 292° 55' 55"  79° 48'  4"   4.882  0.000  392345.971 6935699.801   481.207 PSMK 0
   C111 292° 53' 32"  82° 53' 49"   4.837  0.000  392345.972 6935699.796   480.941 PSMK 0
   D111 293° 46' 56"  85° 34' 15"   4.899  0.000  392345.956 6935699.908   480.721 PSMK 0
   E111 293° 45' 15"  88° 29' 40"   4.883  0.000  392345.957 6935699.904   480.471 PSMK 0
   F111 293° 39'  3"  91° 31' 18"   4.886  0.000  392345.949 6935699.899   480.213 PSMK 0
   G111 293° 44' 47"  94° 28' 52"   4.893  0.000  392345.959 6935699.901   479.961 PSMK 0
   A112 299° 36' 27"  75° 55' 51"   4.511  0.000  392346.648 6935699.901   481.439 PSMK 0
   B112 299° 30' 49"  79°  3' 30"   4.457  0.000  392346.643 6935699.896   481.189 PSMK 0
   C112 299° 32' 37"  82° 15' 53"   4.409  0.000  392346.649 6935699.893   480.936 PSMK 0
   A113 300° 42' 12"  75° 46' 44"   4.451  0.000  392346.751 6935699.913   481.436 PSMK 0
   B113 300° 37' 23"  78° 56' 40"   4.397  0.000  392346.746 6935699.910   481.186 PSMK 0
   C113 300° 34' 20"  82° 13'  3"   4.353  0.000  392346.745 6935699.905   480.932 PSMK 0
   A114 308° 34' 21"  74° 51' 26"   4.117  0.000  392347.407 6935700.003   481.418 PSMK 0
   B114 308° 32'  1"  78° 21' 21"   4.053  0.000  392347.407 6935699.998   481.161 PSMK 0
   C114 308° 27' 35"  81° 51' 36"   4.010  0.000  392347.403 6935699.995   480.911 PSMK 0
   A115 318°  9' 48"  74°  9' 40"   3.857  0.000  392348.094 6935700.097   481.396 PSMK 0
   B115 318°  9'  9"  77° 47' 18"   3.795  0.000  392348.094 6935700.095   481.146 PSMK 0
   C115 318°  3'  5"  81° 41' 18"   3.749  0.000  392348.088 6935700.093   480.885 PSMK 0
   D115 318° 30'  9"  85° 14'  9"   3.799  0.000  392348.083 6935700.174   480.658 PSMK 0
   E115 318° 32' 18"  89°  8'  7"   3.782  0.000  392348.086 6935700.171   480.400 PSMK 0
   F115 318° 28' 50"  92° 58' 13"   3.785  0.000  392348.084 6935700.168   480.147 PSMK 0
   G115 318° 29' 13"  96° 46' 34"   3.802  0.000  392348.086 6935700.164   479.894 PSMK 0
   A116 319° 40' 48"  74°  4'  5"   3.827  0.000  392348.196 6935700.109   481.393 PSMK 0
   B116 319° 40' 19"  77° 42'  7"   3.764  0.000  392348.196 6935700.107   481.145 PSMK 0
   C116 319° 37' 55"  81° 38' 51"   3.718  0.000  392348.194 6935700.107   480.883 PSMK 0
   D116 319° 51' 44"  85° 14' 32"   3.776  0.000  392348.174 6935700.190   480.656 PSMK 0
   E116 320°  0' 17"  89°  6' 44"   3.760  0.000  392348.184 6935700.191   480.401 PSMK 0
   F116 319° 55' 45"  93°  1' 37"   3.763  0.000  392348.180 6935700.187   480.144 PSMK 0
   G116 319° 52' 44"  96° 48' 57"   3.781  0.000  392348.178 6935700.182   479.894 PSMK 0
   A117 330° 17' 37"  73° 51' 35"   3.703  0.000  392348.870 6935700.204   481.372 PSMK 0
   B117 330° 16' 51"  77° 35'  7"   3.639  0.000  392348.869 6935700.200   481.125 PSMK 0
   C117 330° 17' 53"  81° 33' 24"   3.589  0.000  392348.871 6935700.197   480.870 PSMK 0
   A118 332°  1' 10"  73° 54' 36"   3.693  0.000  392348.976 6935700.218   481.366 PSMK 0
   B118 331° 53' 45"  77° 34' 51"   3.631  0.000  392348.969 6935700.214   481.124 PSMK 0
   C118 331° 57' 55"  81° 32' 58"   3.580  0.000  392348.974 6935700.210   480.869 PSMK 0
   A119 342° 59'  9"  74° 25'  6"   3.709  0.000  392349.650 6935700.311   481.339 PSMK 0
   B119 342° 56'  3"  78° 14' 48"   3.646  0.000  392349.647 6935700.308   481.086 PSMK 0
   C119 342° 57' 10"  81° 50' 16"   3.600  0.000  392349.648 6935700.302   480.854 PSMK 0
```

```
   A120 353° 43' 44"  74° 57' 59"   3.862  0.000  392350.345 6935700.407   481.345 PSMK 0
   B120 353° 45' 33"  78° 42' 55"   3.799  0.000  392350.346 6935700.402   481.086 PSMK 0
   C120 353° 40' 50"  82° 29' 11"   3.752  0.000  392350.340 6935700.397   480.833 PSMK 0
   D120 353° 18' 55"  85° 57' 16"   3.819  0.000  392350.332 6935700.490   480.612 PSMK 0
   E120 353° 14' 27"  89° 51' 33"   3.807  0.000  392350.327 6935700.488   480.352 PSMK 0
   F120 353° 19' 53"  93° 36' 28"   3.814  0.000  392350.333 6935700.487   480.103 PSMK 0
   G120 353° 16' 49"  97° 25' 14"   3.835  0.000  392350.329 6935700.484   479.848 PSMK 0
   A121 355°  9' 50"  75°  8'  5"   3.889  0.000  392350.442 6935700.417   481.341 PSMK 0
   B121 355° 12' 23"  78° 49' 49"   3.830  0.000  392350.445 6935700.415   481.085 PSMK 0
   C121 355°  9'  8"  82° 35' 35"   3.783  0.000  392350.440 6935700.410   480.831 PSMK 0
   D121 354° 38' 52"  86°  0' 45"   3.850  0.000  392350.425 6935700.504   480.611 PSMK 0
   E121 354° 39' 27"  89° 56' 40"   3.840  0.000  392350.426 6935700.503   480.347 PSMK 0
   F121 354° 38' 55"  93° 37'  2"   3.846  0.000  392350.425 6935700.502   480.100 PSMK 0
   G121 354° 38' 39"  97° 25' 44"   3.871  0.000  392350.424 6935700.502   479.842 PSMK 0
Coordinate for Check measurement "STN4" defined from control model "SURVEY TRAVERSE->TL"

******** Check Measurement to "STN4" Code "" ***********

                       OBSERVED      CALCULATED      OBSERVED -
                                                     CALCULATED
EASTING              392344.591      392344.591           0.000
NORTHING            6935695.942     6935695.942           0.001
HEIGHT                  479.040         479.040           0.000
BEARING  (grid)    261°  5'  5"    261°  4' 32"   -  0°  0' 33"
DISTANCE (ellip)          5.144           5.144          -0.001

Coordinate for Check measurement "STN1" defined from control model "SURVEY TRAVERSE->TL"

******** Check Measurement to "STN1" Code "" ***********

                       OBSERVED      CALCULATED      OBSERVED -
                                                     CALCULATED
EASTING              392365.091      392365.091           0.001
NORTHING            6935748.217     6935748.216           0.001
HEIGHT                  480.740         480.737           0.003
BEARING  (grid)     16° 40' 32"     16° 40' 31"   -  0°  0'  1"
DISTANCE (ellip)         53.751          53.750           0.001


End of reduction report
```

```
Survey Data Reduction
=====================

Reduction report for field files
  TARGET COORDINATES 2.fld

Coordinate for station "STN4" defined from control model "SURVEY TRAVERSE->TL"

Occupying Station           : STN4
Coordinates                 : E 392344.591   N 6935695.942   H 479.040
Code                        :
Instrument Ht               : 1.541
N Value                     : 0.000

Coordinate for Backsight "STN1" defined from control model "SURVEY TRAVERSE->TL"
          0°  0'  8"  88° 31' 19"  56.186  1.293  392344.593 6935752.090   480.737

******** Backsight to "STN1" Code "" ***********

                       OBSERVED      CALCULATED      OBSERVED -       CORRECTED     CORRECTED -
                       (SWUNG)                       CALCULATED                     CALCULATED
EASTING              392365.090      392365.091          -0.001      392365.090          -0.001
NORTHING            6935748.214     6935748.216          -0.002     6935748.214          -0.002
HEIGHT                  480.737         480.737           0.000         480.737           0.000
BEARING  (grid)     21° 24' 48"     21° 24' 48"                     21° 24' 48"      0°  0'  0"
DISTANCE (ellip)         56.163          56.165          -0.002          56.163          -0.002

Bearing datum difference   21° 24' 39" applied to subsequent measurements

Coordinate for Check measurement "STN3" defined from control model "SURVEY TRAVERSE->TL"

******** Check Measurement to "STN3" Code "" ***********

                       OBSERVED      CALCULATED      OBSERVED -
                                                     CALCULATED
EASTING              392349.671      392349.671          -0.001
NORTHING            6935696.742     6935696.739           0.003
HEIGHT                  479.106         479.107          -0.001
BEARING  (grid)     81°  2' 30"     81°  4' 32"      0°  2'  2"
DISTANCE (ellip)          5.144           5.144          -0.000
```

PointID	Horiz	Vert	SDist	HTar	East	North	Height	Code
A100	295° 15' 44"	77° 20' 17"	4.579	0.000	392341.526	6935699.190	481.584	PSMK A100
A101	296° 18' 5"	77° 9' 23"	4.523	0.000	392341.625	6935699.203	481.586	PSMK A101
A102	304° 19' 52"	76° 25' 19"	4.182	0.000	392342.303	6935699.300	481.563	PSMK A102
A103	305° 37' 47"	76° 18' 7"	4.137	0.000	392342.405	6935699.313	481.560	PSMK A103
A104	315° 20' 21"	75° 41' 31"	3.896	0.000	392343.101	6935699.409	481.544	PSMK A104
A105	325° 59' 47"	75° 33' 53"	3.772	0.000	392343.795	6935699.505	481.521	PSMK A105
A106	327° 30' 48"	75° 32' 24"	3.763	0.000	392343.891	6935699.516	481.520	PSMK A106
A107	338° 18' 11"	75° 58' 58"	3.787	0.000	392344.572	6935699.614	481.498	PSMK A107
A108	339° 49' 41"	76° 3' 55"	3.800	0.000	392344.670	6935699.628	481.496	PSMK A108
A109	347° 29' 12"	76° 40' 35"	3.908	0.000	392345.179	6935699.697	481.481	PSMK A109
A110	356° 59' 32"	77° 46' 28"	4.156	0.000	392345.873	6935699.794	481.461	PSMK A110
A111	358° 14' 53"	77° 54' 49"	4.199	0.000	392345.972	6935699.807	481.460	PSMK A111
B100	295° 12' 51"	80° 21' 31"	4.530	0.000	392341.525	6935699.187	481.339	PSMK B100
B101	296° 16' 47"	80° 15' 54"	4.471	0.000	392341.625	6935699.199	481.337	PSMK B101
B102	304° 20' 47"	79° 48' 58"	4.126	0.000	392342.306	6935699.297	481.310	PSMK B102
B103	305° 32' 39"	79° 45' 56"	4.084	0.000	392342.400	6935699.309	481.306	PSMK B103
B104	315° 15' 45"	79° 22' 41"	3.839	0.000	392343.097	6935699.405	481.288	PSMK B104
B105	325° 56' 29"	79° 19' 24"	3.713	0.000	392343.792	6935699.501	481.269	PSMK B105
B106	327° 35' 56"	79° 15' 6"	3.705	0.000	392343.897	6935699.514	481.272	PSMK B106
B107	338° 14' 8"	79° 45' 22"	3.728	0.000	392344.568	6935699.609	481.244	PSMK B107
B108	339° 50' 56"	79° 49' 32"	3.742	0.000	392344.672	6935699.623	481.242	PSMK B108
B109	347° 35' 2"	80° 25' 6"	3.854	0.000	392345.185	6935699.694	481.222	PSMK B109
B110	356° 58' 57"	81° 14' 26"	4.104	0.000	392345.870	6935699.789	481.206	PSMK B110
B111	358° 16' 46"	81° 19' 41"	4.147	0.000	392345.972	6935699.800	481.206	PSMK B111
C100	295° 10' 42"	83° 34' 14"	4.491	0.000	392341.525	6935699.182	481.084	PSMK C100
C101	296° 11' 28"	83° 30' 29"	4.434	0.000	392341.621	6935699.194	481.082	PSMK C101
C102	304° 12' 26"	83° 11' 27"	4.090	0.000	392342.298	6935699.292	481.066	PSMK C102
C103	305° 27' 22"	83° 8' 57"	4.047	0.000	392342.395	6935699.305	481.064	PSMK C103
C104	315° 17' 16"	83° 6' 9"	3.796	0.000	392343.101	6935699.402	481.037	PSMK C104
C105	325° 58' 10"	83° 24' 50"	3.667	0.000	392343.795	6935699.495	481.001	PSMK C105
C106	327° 31' 27"	83° 24' 34"	3.659	0.000	392343.893	6935699.508	481.001	PSMK C106
C107	338° 16' 39"	83° 34' 59"	3.688	0.000	392344.571	6935699.605	480.993	PSMK C107
C108	339° 50' 29"	83° 41' 41"	3.701	0.000	392344.671	6935699.618	480.987	PSMK C108
C109	347° 35' 34"	84° 7' 59"	3.815	0.000	392345.184	6935699.689	480.971	PSMK C109
C110	357° 0' 37"	84° 57' 5"	4.068	0.000	392345.871	6935699.785	480.939	PSMK C110
C111	358° 18' 6"	85° 1' 13"	4.110	0.000	392345.971	6935699.795	480.938	PSMK C111
D100	295° 56' 28"	86° 38' 1"	4.564	0.000	392341.505	6935699.292	480.849	PSMK D100
D101	296° 59' 40"	86° 37' 28"	4.503	0.000	392341.608	6935699.302	480.846	PSMK D101
D105	325° 58' 49"	86° 57' 1"	3.729	0.000	392343.778	6935699.574	480.779	PSMK D105
D106	327° 28' 26"	87° 0' 7"	3.721	0.000	392343.875	6935699.587	480.775	PSMK D106
D110	356° 25' 25"	88° 5' 29"	4.148	0.000	392345.860	6935699.887	480.719	PSMK D110
D111	357° 38' 9"	88° 7' 20"	4.198	0.000	392345.959	6935699.906	480.718	PSMK D111
E100	295° 56' 21"	89° 47' 52"	4.556	0.000	392341.505	6935699.291	480.597	PSMK E100
E101	296° 57' 44"	89° 47' 59"	4.494	0.000	392341.606	6935699.300	480.596	PSMK E101
E105	325° 57' 19"	90° 53' 27"	3.724	0.000	392343.777	6935699.574	480.523	PSMK E105
E106	327° 33' 7"	90° 58' 29"	3.719	0.000	392343.879	6935699.590	480.517	PSMK E106
E110	356° 25' 19"	91° 33' 34"	4.145	0.000	392345.859	6935699.885	480.468	PSMK E110
E111	357° 36' 34"	91° 32' 2"	4.193	0.000	392345.956	6935699.903	480.469	PSMK E110
F100	295° 59' 1"	93° 1' 23"	4.555	0.000	392341.513	6935699.288	480.341	PSMK F100
F101	296° 59' 37"	93° 0' 16"	4.499	0.000	392341.609	6935699.300	480.345	PSMK F101
F105	325° 57' 27"	94° 44' 0"	3.734	0.000	392343.777	6935699.572	480.273	PSMK F105
F106	327° 28' 30"	94° 47' 7"	3.733	0.000	392343.874	6935699.591	480.269	PSMK F106
F110	356° 22' 2"	95° 7' 45"	4.160	0.000	392345.855	6935699.886	480.209	PSMK F110
F111	357° 32' 59"	95° 3' 21"	4.201	0.000	392345.950	6935699.898	480.211	PSMK F111
G100	295° 57' 3"	96° 7' 43"	4.576	0.000	392341.510	6935699.287	480.092	PSMK G100
G101	296° 58' 43"	96° 13' 7"	4.519	0.000	392341.608	6935699.299	480.091	PSMK G101
G105	325° 51' 9"	98° 33' 14"	3.764	0.000	392343.770	6935699.571	480.021	PSMK G105
G106	327° 26' 28"	98° 32' 34"	3.762	0.000	392343.872	6935699.590	480.022	PSMK G106
G110	356° 31' 5"	98° 33' 22"	4.190	0.000	392345.866	6935699.882	479.957	PSMK G110
G111	357° 40' 27"	98° 27' 26"	4.237	0.000	392345.961	6935699.901	479.958	PSMK G111
1001	299° 52' 46"	79° 32' 36"	4.308	0.000	392341.942	6935699.246	481.363	PSMK 1001
1002	320° 9' 16"	79° 11' 54"	3.764	0.000	392343.422	6935699.448	481.286	PSMK 1002
1003	333° 40' 15"	79° 30' 35"	3.702	0.000	392344.279	6935699.567	481.255	PSMK 1003
1004	352° 6' 16"	79° 45' 0"	3.970	0.000	392345.503	6935699.739	481.287	PSMK 1004
2001	299° 54' 27"	80° 51' 2"	4.287	0.000	392341.946	6935699.244	481.262	PSMK 2001
2002	320° 9' 23"	80° 40' 27"	3.747	0.000	392343.422	6935699.448	481.188	PSMK 2002
2003	333° 39' 25"	81° 2' 1"	3.684	0.000	392344.278	6935699.566	481.155	PSMK 2003
2004	352° 9' 59"	81° 8' 28"	3.954	0.000	392345.508	6935699.738	481.190	PSMK 2004
3001	296° 0' 33"	91° 36' 48"	4.549	0.000	392341.515	6935699.289	480.453	PSMK 3001
3002	296° 58' 25"	91° 38' 32"	4.496	0.000	392341.607	6935699.300	480.452	PSMK 3002
3003	325° 54' 10"	93° 9' 6"	3.727	0.000	392343.774	6935699.571	480.376	PSMK 3003
3004	327° 29' 21"	93° 9' 0"	3.726	0.000	392343.875	6935699.591	480.376	PSMK 3004
3005	356° 21' 38"	93° 30' 49"	4.150	0.000	392345.855	6935699.885	480.326	PSMK 3005
3006	357° 34' 41"	93° 28' 56"	4.198	0.000	392345.954	6935699.902	480.326	PSMK 3006

Coordinate for Check measurement "STN3" defined from control model "SURVEY TRAVERSE->TL"

******** Check Measurement to "STN3" Code "" ***********

	OBSERVED	CALCULATED	OBSERVED - CALCULATED
EASTING	392349.672	392349.671	0.000
NORTHING	6935696.742	6935696.739	0.003
HEIGHT	479.106	479.107	-0.001
BEARING (grid)	81° 2' 49"	81° 4' 32"	0° 1' 43"
DISTANCE (ellip)	5.145	5.144	0.001

Coordinate for Check measurement "STN1" defined from control model "SURVEY TRAVERSE->TL"

******** Check Measurement to "STN1" Code "" ***********

	OBSERVED	CALCULATED	OBSERVED - CALCULATED
EASTING	392365.090	392365.091	-0.001
NORTHING	6935748.215	6935748.216	-0.001
HEIGHT	480.737	480.737	0.000
BEARING (grid)	21° 24' 47"	21° 24' 48"	0° 0' 1"

```
DISTANCE (ellip)         56.164          56.165          -0.001

 (74 measurements)
Coordinate for station "STN3" defined from control model "SURVEY TRAVERSE->TL"

Occupying Station           : STN3
Coordinates                 : E 392349.671   N 6935696.739   H 479.107
Code                        :
Instrument Ht               : 1.281
N Value                     : 0.000

Coordinate for Backsight "STN1" defined from control model "SURVEY TRAVERSE->TL"
        359° 59' 59"  88° 14' 53"  53.777  1.293  392349.671 6935750.473   480.739

******** Backsight to "STN1" Code "" ***********

                       OBSERVED      CALCULATED      OBSERVED -       CORRECTED     CORRECTED -
                       (SWUNG)                       CALCULATED                     CALCULATED
EASTING              392365.090      392365.091          -0.001      392365.090          -0.001
NORTHING            6935748.214     6935748.216          -0.002     6935748.214          -0.002
HEIGHT                  480.739         480.737           0.002         480.739           0.002
BEARING  (grid)     16° 40' 31"     16° 40' 31"                     16° 40' 31"      0°  0'  0"
DISTANCE (ellip)         53.748          53.750          -0.002          53.748          -0.002

Bearing datum difference   16° 40' 32" applied to subsequent measurements

Coordinate for Check measurement "STN4" defined from control model "SURVEY TRAVERSE->TL"

******** Check Measurement to "STN4" Code "" ***********

                       OBSERVED      CALCULATED      OBSERVED -
                                                     CALCULATED
EASTING              392344.590      392344.591          -0.000
NORTHING            6935695.939     6935695.942          -0.003
HEIGHT                  479.043         479.040           0.003
BEARING  (grid)     261°  2' 52"    261°  4' 32"      0°  1' 40"
DISTANCE (ellip)         5.145           5.144           0.001

PointID    Horiz        Vert       SDist   HTar        East       North    Height   Code
   2005 295° 53' 47"  80° 16' 28"   4.657  0.000  392346.292 6935699.844   481.175 PSMK 2005
   1005 295° 56' 10"  79°  2' 24"   4.673  0.000  392346.296 6935699.844   481.276 PSMK 1005
   1006 313° 18' 10"  78°  3' 54"   3.904  0.000  392347.761 6935700.045   481.195 PSMK 1006
   1007 324° 37' 44"  77° 49' 46"   3.685  0.000  392348.517 6935700.150   481.165 PSMK 1007
   STN1 349° 26' 30"  77° 51' 32"   3.729  0.000  392350.060 6935700.363   481.172 PSMK 1008
   1008 349° 26' 38"  77° 51' 37"   3.729  0.000  392350.060 6935700.363   481.172 PSMK 1008
   2006 313° 18' 32"  79° 30' 21"   3.885  0.000  392347.761 6935700.046   481.095 PSMK 2006
   2007 324° 32' 53"  79° 17' 55"   3.666  0.000  392348.512 6935700.149   481.069 PSMK 2007
   2008 349° 22' 30"  79° 14' 33"   3.709  0.000  392350.055 6935700.362   481.080 PSMK 2008
   3007 318° 26' 42"  92°  4' 12"   3.782  0.000  392348.082 6935700.167   480.251 PSMK 3007
   3008 319° 57' 35"  92°  5' 38"   3.761  0.000  392348.181 6935700.188   480.250 PSMK 3008
   3009 353° 12' 16"  92° 48'  2"   3.809  0.000  392350.324 6935700.486   480.202 PSMK 3009
   3010 354° 38' 58"  92° 52' 49"   3.843  0.000  392350.425 6935700.502   480.195 PSMK 3010
   A112 299° 34' 15"  76° 28' 39"   4.499  0.000  392346.647 6935699.898   481.440 PSMK A112
   A113 300° 39' 31"  76° 20'  4"   4.440  0.000  392346.748 6935699.911   481.437 PSMK A113
   A114 308° 32' 43"  75° 26' 51"   4.104  0.000  392347.406 6935700.001   481.419 PSMK A114
   A115 318°  9'  2"  74° 46' 25"   3.842  0.000  392348.095 6935700.093   481.397 PSMK A115
   A116 319° 39' 42"  74° 41' 10"   3.813  0.000  392348.196 6935700.107   481.395 PSMK A116
   A117 330° 15' 49"  74° 32' 40"   3.689  0.000  392348.868 6935700.202   481.371 PSMK A117
   A118 331° 59' 23"  74° 34' 39"   3.678  0.000  392348.975 6935700.215   481.366 PSMK A118
   A119 342° 58' 49"  75°  1' 22"   3.697  0.000  392349.650 6935700.309   481.343 PSMK A119
   A120 353° 43' 38"  75° 36' 30"   3.847  0.000  392350.344 6935700.403   481.344 PSMK A120
   A121 355° 10' 27"  75° 44' 42"   3.877  0.000  392350.443 6935700.416   481.342 PSMK A121
   B112 299° 30' 13"  79° 37' 26"   4.445  0.000  392346.645 6935699.893   481.188 PSMK B112
   B113 300° 36' 16"  79° 31' 18"   4.386  0.000  392346.746 6935699.907   481.185 PSMK B113
   B114 308° 29' 26"  78° 57' 55"   4.044  0.000  392347.405 6935699.996   481.162 PSMK B114
   B115 318°  6' 17"  78° 27'  2"   3.784  0.000  392348.092 6935700.092   481.145 PSMK B115
   B116 319° 39' 48"  78° 21' 25"   3.753  0.000  392348.197 6935700.105   481.145 PSMK B116
   B117 330° 17' 20"  78° 17' 41"   3.626  0.000  392348.871 6935700.197   481.123 PSMK B117
   B118 331° 52' 42"  78° 16' 30"   3.619  0.000  392348.968 6935700.211   481.123 PSMK B118
   B119 342° 57' 12"  78° 55' 18"   3.635  0.000  392349.648 6935700.305   481.086 PSMK B119
   B120 353° 46' 37"  79° 22' 23"   3.789  0.000  392350.347 6935700.400   481.087 PSMK B120
   B121 355° 11' 16"  79° 29' 38"   3.816  0.000  392350.442 6935700.410   481.084 PSMK B121
   C112 299° 32' 26"  82° 52' 31"   4.400  0.000  392346.651 6935699.890   480.934 PSMK C112
   C113 300° 31'  7"  82° 49' 50"   4.345  0.000  392346.743 6935699.901   480.930 PSMK C113
   C114 308° 25' 11"  82° 31'  7"   4.001  0.000  392347.402 6935699.992   480.909 PSMK C114
   C115 318°  2' 43"  82° 22'  4"   3.740  0.000  392348.089 6935700.090   480.885 PSMK C115
   C116 319° 35' 44"  82° 19' 13"   3.710  0.000  392348.192 6935700.104   480.884 PSMK C116
   C117 330° 17' 43"  82° 16' 15"   3.581  0.000  392348.872 6935700.195   480.869 PSMK C117
   C118 331° 57' 10"  82° 13' 19"   3.571  0.000  392348.974 6935700.207   480.871 PSMK C118
   C119 342° 55' 50"  82° 33'  5"   3.592  0.000  392349.647 6935700.300   480.853 PSMK C119
   C120 353° 41'  7"  83° 11' 12"   3.744  0.000  392350.340 6935700.395   480.832 PSMK C120
   C121 355°  9' 21"  83° 16' 38"   3.774  0.000  392350.440 6935700.407   480.830 PSMK C121
   D115 318° 30'  7"  85° 55' 11"   3.792  0.000  392348.084 6935700.171   480.658 PSMK D115
   D116 319° 50' 56"  85° 53' 22"   3.771  0.000  392348.173 6935700.188   480.658 PSMK D116
   D120 353° 18' 54"  86° 37' 16"   3.814  0.000  392350.332 6935700.488   480.613 PSMK D120
   D121 354° 39'  6"  86° 41' 21"   3.843  0.000  392350.425 6935700.500   480.610 PSMK D121
   E115 318° 31' 45"  89° 48' 26"   3.779  0.000  392348.087 6935700.169   480.401 PSMK E115
   E116 319° 59' 47"  89° 48' 46"   3.757  0.000  392348.184 6935700.188   480.400 PSMK E116
   E120 353° 13' 30"  90° 32' 28"   3.806  0.000  392350.325 6935700.487   480.352 PSMK E120
   E121 354° 40'  4"  90° 39' 11"   3.836  0.000  392350.426 6935700.499   480.344 PSMK E121
   F115 318° 28' 12"  93° 40'  4"   3.785  0.000  392348.084 6935700.166   480.146 PSMK F115
   F116 319° 54' 21"  93° 40' 19"   3.761  0.000  392348.180 6935700.182   480.147 PSMK F116
   F120 353° 19' 51"  94° 18' 14"   3.814  0.000  392350.332 6935700.483   480.102 PSMK F120
   F121 354° 37' 12"  94° 19'  4"   3.846  0.000  392350.422 6935700.499   480.098 PSMK F121
   G115 318° 27' 51"  97° 27' 20"   3.806  0.000  392348.085 6935700.162   479.894 PSMK G115
   G116 319° 51'  8"  97° 31' 45"   3.784  0.000  392348.178 6935700.179   479.892 PSMK G116
   G120 353° 16' 40"  98°  5' 49"   3.840  0.000  392350.328 6935700.483   479.847 PSMK G120
   G121 354° 38' 44"  98°  3' 58"   3.873  0.000  392350.424 6935700.498   479.844 PSMK G121
```

Coordinate for Check measurement "STN4" defined from control model "SURVEY TRAVERSE->TL"

******** Check Measurement to "STN4" Code "" ***********

	OBSERVED	CALCULATED	OBSERVED - CALCULATED
EASTING	392344.591	392344.591	-0.000
NORTHING	6935695.938	6935695.942	-0.003
HEIGHT	479.043	479.040	0.003
BEARING (grid)	261° 2' 31"	261° 4' 32"	0° 2' 1"
DISTANCE (ellip)	5.145	5.144	0.001

Coordinate for Check measurement "STN1" defined from control model "SURVEY TRAVERSE->TL"

******** Check Measurement to "STN1" Code "" ***********

	OBSERVED	CALCULATED	OBSERVED - CALCULATED
EASTING	392365.084	392365.091	-0.006
NORTHING	6935748.214	6935748.216	-0.002
HEIGHT	480.740	480.737	0.003
BEARING (grid)	16° 40' 9"	16° 40' 31"	0° 0' 22"
DISTANCE (ellip)	53.747	53.750	-0.003

(59 measurements)

End of reduction report

Appendix D:

Bundle Adjustment Results

Australis Bundle Adjustment Results File: Bundle.txt

12 September, 2011 19:17:56

Quick Summary
Project: C:\Documents and Settings\pdlento\Desktop\Australis 2\Paper colour\Paper colour.aus
Adjustment: Preferred control points specified
Simulated Network: No
Folding Method: Standard
Scaling: N/A
Units: m
Number of Points: 59
Number of Images: 13
Number of Scale Bars: 1
Number of Iterations: 5
Elapsed CPU Time: 0.172 seconds

Adjusted Exterior Orientation Parameters (angles are decimal degrees, XYZ are m)

Results for Station Image002 FileName Camera 1 Mideast 1 Colour.tif Camera Colour 1 Lens

Station Variable	Initial Value	Total Adjustment	Final Value	Initial Standard Error	Final Standard Error
X	348.6319	0.0549	348.6869	1.0000E+003	6.2878E-003
Y	480.6525	-0.0110	480.6415	1.0000E+003	3.1808E-002
Z	706.0972	0.0063	706.1035	1.0000E+003	1.3315E-002
AZ	-158.3127	-16.2619	-174.5747	1.0000E+003	1.2101E+000
EL	-87.1865	0.2860	-86.9006	1.0000E+003	3.0314E-001
ROLL	155.9065	16.8922	172.7987	1.0000E+003	1.1861E+000

Results for Station Image003 FileName Camera 1 Mideast 2 Colour.tif Camera Colour 1 Lens

Station Variable	Initial Value	Total Adjustment	Final Value	Initial Standard Error	Final Standard Error
X	348.6479	0.0093	348.6572	1.0000E+003	6.6281E-003
Y	480.6057	0.0339	480.6396	1.0000E+003	3.1281E-002
Z	706.0873	0.0308	706.1181	1.0000E+003	1.2792E-002
AZ	97.7168	2.5248	100.2416	1.0000E+003	7.1625E-001
EL	-68.8567	0.3850	-68.4717	1.0000E+003	8.3637E-002
ROLL	-98.5328	-2.4058	-100.9386	1.0000E+003	8.1099E-001

Results for Station Image004 FileName Camera 1 Midwest 1 Colour.tif Camera Colour 1 Lens

Station Variable	Initial Value	Total Adjustment	Final Value	Initial Standard Error	Final Standard Error
X	345.6173	-0.0134	345.6039	1.0000E+003	8.0899E-003
Y	480.7000	-0.0681	480.6319	1.0000E+003	3.2460E-002
Z	705.8121	0.0112	705.8233	1.0000E+003	1.2121E-002
AZ	-96.9188	-0.2431	-97.1619	1.0000E+003	1.3281E+000
EL	-76.5194	-0.1513	-76.6707	1.0000E+003	5.0424E-002
ROLL	95.8105	0.3287	96.1391	1.0000E+003	1.3214E+000

Results for Station Image005 FileName Camera 1 Midwest 2 Colour.tif Camera Colour 1 Lens

Station Variable	Initial Value	Total Adjustment	Final Value	Initial Standard Error	Final Standard Error
X	345.5617	-0.0007	345.5610	1.0000E+003	6.1944E-003
Y	480.5484	0.0825	480.6308	1.0000E+003	3.2555E-002
Z	705.7849	0.0621	705.8470	1.0000E+003	1.3102E-002

AZ	93.4624	7.1003	100.5627	1.0000E+003	1.4347E+000
EL	-78.8552	0.3898	-78.4654	1.0000E+003	9.1213E-002
ROLL	-93.0990	-7.4205	-100.5195	1.0000E+003	1.5056E+000

Results for Station Image006 FileName Camera 1 West 1 Colour.tif Camera Colour 1 Lens

Station Variable	Initial Value	Total Adjustment	Final Value	Initial Standard Error	Final Standard Error
X	341.7353	-0.0031	341.7322	1.0000E+003	1.0807E-002
Y	480.6978	0.0674	480.7653	1.0000E+003	3.1412E-002
Z	705.1120	0.0471	705.1592	1.0000E+003	9.9281E-003
AZ	-92.7548	-4.2193	-96.9740	1.0000E+003	9.9320E-001
EL	-71.9957	-0.3195	-72.3151	1.0000E+003	6.9402E-002
ROLL	91.2346	3.8335	95.0681	1.0000E+003	9.9727E-001

Results for Station Image007 FileName Camera 1 West 2 Colour.tif Camera Colour 1 Lens

Station Variable	Initial Value	Total Adjustment	Final Value	Initial Standard Error	Final Standard Error
X	341.6601	0.0529	341.7130	1.0000E+003	9.7983E-003
Y	480.6643	0.1020	480.7662	1.0000E+003	3.1833E-002
Z	705.0828	0.0820	705.1647	1.0000E+003	1.1477E-002
AZ	-92.7852	-15.9296	-108.7147	1.0000E+003	2.8928E+000
EL	-83.4417	-0.6563	-84.0980	1.0000E+003	1.1514E-001
ROLL	93.3619	15.4108	108.7726	1.0000E+003	2.8657E+000

Results for Station Image022 FileName Camera 2 East 1 Colour.tif Camera Colour 2 Lens

Station Variable	Initial Value	Total Adjustment	Final Value	Initial Standard Error	Final Standard Error
X	351.6551	-0.0127	351.6424	1.0000E+003	9.4499E-003
Y	481.0627	0.0101	481.0728	1.0000E+003	3.3012E-002
Z	706.8722	-0.0389	706.8333	1.0000E+003	1.3064E-002
AZ	96.7630	1.5273	98.2903	1.0000E+003	5.4781E-001
EL	-63.2791	0.3366	-62.9425	1.0000E+003	7.7727E-002
ROLL	-95.7601	-0.8187	-96.5789	1.0000E+003	6.5742E-001

Results for Station Image023 FileName Camera 2 Mideast 1 Colour.tif Camera Colour 2 Lens

Station Variable	Initial Value	Total Adjustment	Final Value	Initial Standard Error	Final Standard Error
X	348.2073	0.0645	348.2718	1.0000E+003	6.5378E-003
Y	480.6040	0.0382	480.6422	1.0000E+003	3.1512E-002
Z	706.0098	-0.0034	706.0064	1.0000E+003	1.2685E-002
AZ	-131.5763	-13.8715	-145.4478	1.0000E+003	2.0414E+000
EL	-84.9407	0.2176	-84.7231	1.0000E+003	2.4862E-001
ROLL	130.4627	14.4278	144.8905	1.0000E+003	2.0095E+000

Results for Station Image024 FileName Camera 2 Mideast2 Colour.tif Camera Colour 2 Lens

Station Variable	Initial Value	Total Adjustment	Final Value	Initial Standard Error	Final Standard Error
X	348.2022	0.0094	348.2116	1.0000E+003	6.1041E-003
Y	480.6043	0.0372	480.6415	1.0000E+003	3.1157E-002
Z	706.0257	-0.0004	706.0253	1.0000E+003	1.2222E-002
AZ	96.7886	3.1366	99.9252	1.0000E+003	8.6084E-001
EL	-72.0373	0.4368	-71.6005	1.0000E+003	8.5313E-002
ROLL	-96.1703	-3.0225	-99.1928	1.0000E+003	9.4759E-001

Results for Station Image025 FileName Camera 2 Midwest 1 Colour.tif Camera Colour 2 Lens

Station Variable	Initial Value	Total Adjustment	Final Value	Initial Standard Error	Final Standard Error
X	345.1826	-0.0040	345.1786	1.0000E+003	8.3123E-003
Y	480.7401	-0.1063	480.6339	1.0000E+003	3.2516E-002
Z	705.8026	-0.0169	705.7857	1.0000E+003	1.1388E-002
AZ	-92.2865	1.2121	-91.0744	1.0000E+003	1.2770E+000
EL	-75.9115	-0.1584	-76.0699	1.0000E+003	4.4135E-002
ROLL	92.4041	-1.1337	91.2704	1.0000E+003	1.2718E+000

Results for Station Image026 FileName Camera 2 Midwest 2 Colour.tif Camera Colour 2 Lens

Station Variable	Initial Value	Total Adjustment	Final Value	Initial Standard Error	Final Standard Error
X	345.1391	-0.0235	345.1156	1.0000E+003	6.5499E-003
Y	480.5392	0.1002	480.6395	1.0000E+003	3.2799E-002
Z	705.7703	0.0355	705.8059	1.0000E+003	1.2653E-002
AZ	86.4949	10.1023	96.5971	1.0000E+003	1.8621E+000
EL	-80.9378	0.0863	-80.8515	1.0000E+003	8.3871E-002
ROLL	-86.4614	-10.4526	-96.9140	1.0000E+003	1.9273E+000

Results for Station Image027 FileName Camera 2 West 1 Colour.tif Camera Colour 2 Lens

Station Variable	Initial Value	Total Adjustment	Final Value	Initial Standard Error	Final Standard Error
X	341.2981	0.0299	341.3280	1.0000E+003	1.0033E-002
Y	480.7087	0.0757	480.7844	1.0000E+003	3.0839E-002
Z	704.9587	0.0415	705.0002	1.0000E+003	9.8708E-003
AZ	-88.8393	-4.2639	-93.1032	1.0000E+003	9.6511E-001
EL	-71.0662	-0.6676	-71.7338	1.0000E+003	6.9133E-002
ROLL	87.6421	3.8770	91.5191	1.0000E+003	9.7064E-001

Results for Station Image028 FileName Camera 2 West 2 Colour.tif Camera Colour 2 Lens

Station Variable	Initial Value	Total Adjustment	Final Value	Initial Standard Error	Final Standard Error
X	341.2560	0.0618	341.3178	1.0000E+003	9.6835E-003
Y	480.6637	0.1117	480.7754	1.0000E+003	3.1301E-002
Z	704.9413	0.0669	705.0082	1.0000E+003	1.1336E-002
AZ	-84.2314	-10.3816	-94.6129	1.0000E+003	2.0233E+000
EL	-80.1542	-1.0563	-81.2105	1.0000E+003	8.6788E-002
ROLL	84.7590	9.8618	94.6208	1.0000E+003	2.0040E+000

Summary of Image Coordinate Residuals (units are micrometres)

Sta #	RMS of Image Residuals x	y	xy	Number of non-rejected points
Image002	0.15	0.16	0.15	26
Image003	0.13	0.18	0.16	29
Image004	0.13	0.20	0.17	32
Image005	0.11	0.17	0.14	29
Image006	0.11	0.18	0.15	33
Image007	0.12	0.11	0.11	23
Image022	0.13	0.26	0.20	25
Image023	0.12	0.16	0.14	26
Image024	0.10	0.15	0.13	26
Image025	0.09	0.11	0.10	29
Image026	0.13	0.10	0.12	29
Image027	0.10	0.17	0.14	33
Image028	0.13	0.11	0.12	23

Total Residuals (RMS)				Degrees of			
x	y	xy	Sigma0	Freedom	Observations	Parameters	Constraints
0.12	0.16	0.14	0.396	549	726	275	98

Standard Errors From Limiting Error and Total Error Propogation (XYZ are in m)

	Limiting Sigma Estimates			Total Sigma Estimates				Sightings #	List 1111111111222222222223
Label	sX	sY	sZ	sX	sY	sZ	RMS	Rays	12345678901234567890123456789 0
A100	0.0002	0.0005	0.0031	0.0019	0.0019	0.0034	0.2	4	NNNNYYNNNNNYY
A102	0.0002	0.0002	0.0006	0.0016	0.0016	0.0031	0.2	6	NNNYYYNNNNYYY
A104	0.0002	0.0002	0.0006	0.0014	0.0014	0.0026	0.1	6	NNNYYYNNNNYYY
A105	0.0002	0.0002	0.0006	0.0013	0.0013	0.0023	0.1	6	NNNYYYNNNNYYY
A107	0.0001	0.0001	0.0003	0.0012	0.0012	0.0021	0.2	10	NYYYYYNNYYYYY
A109	0.0001	0.0002	0.0004	0.0012	0.0011	0.0020	0.2	8	NYYYYNNNYYYYN
A110	0.0002	0.0001	0.0004	0.0012	0.0011	0.0020	0.1	8	NYYYYNNNYYYYN
A112	0.0001	0.0001	0.0005	0.0012	0.0011	0.0020	0.2	9	YYYYNNYYYYYNN
A114	0.0002	0.0002	0.0006	0.0013	0.0012	0.0020	0.1	7	YYYNNNYYYYNNN
A115	0.0002	0.0002	0.0005	0.0013	0.0013	0.0020	0.2	7	YYYNNNYYYYNNN
A117	0.0002	0.0002	0.0005	0.0015	0.0014	0.0021	0.1	6	YYYNNNYYNYNNN
A119	0.0002	0.0002	0.0006	0.0016	0.0016	0.0023	0.2	4	YNYNNNYYNNNNN
A120	0.0003	0.0002	0.0009	0.0019	0.0018	0.0025	0.1	3	YNNNNNYYNNNNN
B100	0.0002	0.0004	0.0032	0.0019	0.0018	0.0034	0.1	4	NNNNYYNNNNNYY
B102	0.0002	0.0002	0.0006	0.0016	0.0016	0.0028	0.1	6	NNNYYYNNNNYYY
B104	0.0002	0.0002	0.0006	0.0014	0.0014	0.0022	0.1	6	NNNYYYNNNNYYY
B105	0.0002	0.0002	0.0006	0.0013	0.0013	0.0018	0.1	6	NNNYYYNNNNYYY
B107	0.0001	0.0001	0.0003	0.0012	0.0011	0.0016	0.2	10	NYYYYYNNYYYYY
B109	0.0002	0.0001	0.0004	0.0012	0.0011	0.0015	0.2	8	NYYYYNNNYYYYN
B110	0.0002	0.0001	0.0004	0.0012	0.0011	0.0015	0.1	8	NYYYYNNNYYYYN
B112	0.0001	0.0001	0.0005	0.0012	0.0011	0.0016	0.2	9	YYYYNNYYYYYNN
B114	0.0002	0.0002	0.0006	0.0012	0.0012	0.0015	0.1	7	YYYNNNYYYYNNN
B115	0.0002	0.0002	0.0005	0.0013	0.0013	0.0015	0.1	7	YYYNNNYYYYNNN
B117	0.0002	0.0002	0.0005	0.0014	0.0014	0.0016	0.1	6	YYYNNNYYNYNNN
B119	0.0002	0.0002	0.0006	0.0016	0.0016	0.0019	0.1	4	YNYNNNYYNNNNN
B120	0.0003	0.0002	0.0009	0.0019	0.0018	0.0021	0.1	3	YNNNNNYYNNNNN
C100	0.0002	0.0003	0.0032	0.0019	0.0018	0.0034	0.1	4	NNNNYYNNNNNYY
C102	0.0002	0.0002	0.0006	0.0016	0.0016	0.0031	0.1	6	NNNYYYNNNNYYY
C104	0.0002	0.0002	0.0006	0.0014	0.0014	0.0026	0.1	6	NNNYYYNNNNYYY
C105	0.0002	0.0002	0.0006	0.0013	0.0013	0.0023	0.1	6	NNNYYYNNNNYYY
C107	0.0001	0.0001	0.0003	0.0012	0.0011	0.0021	0.1	10	NYYYYYNNYYYYY
C109	0.0002	0.0001	0.0004	0.0012	0.0011	0.0020	0.1	8	NYYYYNNNYYYYN
C110	0.0002	0.0001	0.0004	0.0012	0.0011	0.0020	0.1	8	NYYYYNNNYYYYN
C112	0.0001	0.0001	0.0005	0.0012	0.0011	0.0021	0.1	8	YYYYNN*YYYYNN
C114	0.0002	0.0002	0.0006	0.0013	0.0012	0.0020	0.2	7	YYYNNNYYYYNNN
C115	0.0002	0.0002	0.0005	0.0013	0.0013	0.0020	0.1	7	YYYNNNYYYYNNN
C117	0.0002	0.0002	0.0005	0.0015	0.0014	0.0021	0.1	6	YYYNNNYYNYNNN
C119	0.0002	0.0002	0.0006	0.0017	0.0016	0.0023	0.1	4	YNYNNNYYNNNNN
C120	0.0003	0.0002	0.0009	0.0019	0.0018	0.0025	0.1	3	YNNNNNYYNNNNN
D100	0.0002	0.0002	0.0055	0.0019	0.0019	0.0072	0.1	4	NNNNYYNNNNNYY
D105	0.0002	0.0002	0.0006	0.0014	0.0014	0.0031	0.1	6	NNNYYYNNNNYYY
D110	0.0002	0.0001	0.0004	0.0013	0.0012	0.0030	0.1	8	NYYYYNNNYYYYN
D115	0.0002	0.0002	0.0006	0.0014	0.0014	0.0030	0.1	7	YYYNNNYYYYNNN
D120	0.0003	0.0002	0.0009	0.0019	0.0019	0.0033	0.1	3	YNNNNNYYNNNNN
E100	0.0002	0.0002	0.0056	0.0020	0.0020	0.0079	0.2	4	NNNNYYNNNNNYY
E105	0.0002	0.0002	0.0006	0.0014	0.0014	0.0043	0.2	6	NNNYYYNNNNYYY
E110	0.0002	0.0001	0.0004	0.0013	0.0013	0.0041	0.1	8	NYYYYNNNYYYYN
E115	0.0002	0.0002	0.0006	0.0014	0.0014	0.0042	0.1	7	YYYNNNYYYYNNN
E120	0.0003	0.0002	0.0009	0.0020	0.0019	0.0044	0.1	3	YNNNNNYYNNNNN
F100	0.0002	0.0004	0.0056	0.0020	0.0021	0.0087	0.1	4	NNNNYYNNNNNYY
F105	0.0002	0.0002	0.0006	0.0016	0.0014	0.0055	0.1	6	NNNYYYNNNNYYY
F110	0.0002	0.0001	0.0004	0.0014	0.0013	0.0054	0.1	8	NYYYYNNNYYYYN
F115	0.0002	0.0002	0.0006	0.0015	0.0014	0.0054	0.2	7	YYYNNNYYYYNNN
F120	0.0003	0.0002	0.0009	0.0021	0.0020	0.0056	0.1	3	YNNNNNYYNNNNN
G100	0.0002	0.0006	0.0056	0.0021	0.0022	0.0097	0.1	4	NNNNYYNNNNNYY
G105	0.0002	0.0002	0.0006	0.0017	0.0015	0.0068	0.2	6	NNNYYYNNNNYYY
G110	0.0002	0.0002	0.0004	0.0016	0.0013	0.0067	0.1	8	NYYYYNNNYYYYN
G115	0.0002	0.0002	0.0006	0.0017	0.0015	0.0067	0.2	7	YYYNNNYYYYNNN
G120	0.0003	0.0003	0.0009	0.0022	0.0020	0.0068	0.2	3	YNNNNNYYNNNNN

	Summary of Limiting STD Error Estimates			Summary of Total STD Error Estimates		
	X	Y	Z	X	Y	Z
RMS is	0.0002	0.0002	0.0017	0.0015	0.0015	0.0039
Minimum is	0.0001	0.0001	0.0003	0.0012	0.0011	0.0015
at point	A112	C107	A107	B110	B110	B110
Maximum is	0.0003	0.0006	0.0056	0.0022	0.0022	0.0097
at point	G120	G100	G100	G120	G100	G100

Triangulated Object Space Coordinates (XYZ are in m)

				Sightings #	List	1111111111222222222223
Label	X	Y	Z	RMS	Rays	12345678901234567890123456789O
A100	341.5227	481.6002	699.1960	0.2	4	NNNNYYNNNNNYY
A102	342.3042	481.5695	699.2939	0.2	6	NNNYYYNNNNYYY
A104	343.1048	481.5429	699.4081	0.1	6	NNNYYYNNNNYYY
A105	343.7998	481.5144	699.5026	0.1	6	NNNYYYNNNNYYY
A107	344.5807	481.4894	699.6086	0.2	10	NYYYYYNNYYYYY
A109	345.1839	481.4691	699.6926	0.2	8	NYYYYNNNYYYYN
A110	345.8796	481.4482	699.7864	0.1	8	NYYYYNNNYYYYN
A112	346.6563	481.4254	699.8965	0.2	9	YYYYNNYYYYYNN
A114	347.4116	481.4064	700.0025	0.1	7	YYYNNNYYYYNNN
A115	348.0964	481.3874	700.0989	0.2	7	YYYNNNYYYYNNN
A117	348.8690	481.3697	700.2036	0.1	6	YYYNNNYYNYNNN
A119	349.6452	481.3441	700.3108	0.2	4	YNYNNNYYNNNNN
A120	350.3349	481.3561	700.4082	0.1	3	YNNNNNYYNNNNN
B100	341.5177	481.3530	699.1862	0.1	4	NNNNYYNNNNNYY
B102	342.3046	481.3155	699.2896	0.1	6	NNNYYYNNNNYYY
B104	343.1011	481.2873	699.4024	0.1	6	NNNYYYNNNNYYY
B105	343.7953	481.2620	699.5005	0.1	6	NNNYYYNNNNYYY
B107	344.5736	481.2341	699.6045	0.2	10	NYYYYYNNYYYYY
B109	345.1908	481.2110	699.6908	0.2	8	NYYYYNNNYYYYN
B110	345.8792	481.1936	699.7839	0.1	8	NYYYYNNNYYYYN
B112	346.6502	481.1754	699.8930	0.2	9	YYYYNNYYYYYNN
B114	347.4125	481.1504	700.0000	0.1	7	YYYNNNYYYYNNN
B115	348.0980	481.1384	700.0935	0.1	7	YYYNNNYYYYNNN
B117	348.8714	481.1240	700.2008	0.1	6	YYYNNNYYNYNNN
B119	349.6454	481.0917	700.3077	0.1	4	YNYNNNYYNNNNN
B120	350.3389	481.0996	700.4057	0.1	3	YNNNNNYYNNNNN
C100	341.5135	481.0974	699.1833	0.1	4	NNNNYYNNNNNYY
C102	342.2949	481.0692	699.2868	0.1	6	NNNYYYNNNNYYY
C104	343.0992	481.0358	699.3994	0.1	6	NNNYYYNNNNYYY
C105	343.7964	480.9959	699.4983	0.1	6	NNNYYYNNNNYYY
C107	344.5757	480.9843	699.6021	0.1	10	NYYYYYNNYYYYY
C109	345.1901	480.9590	699.6893	0.1	8	NYYYYNNNYYYYN
C110	345.8772	480.9266	699.7817	0.1	8	NYYYYNNNYYYYN
C112	346.6576	480.9229	699.8902	0.1	8	YYYYNN*YYYYNN
C114	347.4094	480.8999	699.9969	0.2	7	YYYNNNYYYYNNN
C115	348.0941	480.8787	700.0871	0.1	7	YYYNNNYYYYNNN
C117	348.8750	480.8698	700.1971	0.1	6	YYYNNNYYNYNNN
C119	349.6474	480.8616	700.3064	0.1	4	YNYNNNYYNNNNN
C120	350.3353	480.8484	700.4018	0.1	3	YNNNNNYYNNNNN
D100	341.5225	480.8627	699.0590	0.1	4	NNNNYYNNNNNYY
D105	343.8013	480.7731	699.4109	0.1	6	NNNYYYNNNNYYY
D110	345.8953	480.7106	699.6740	0.1	8	NYYYYNNNYYYYN
D115	348.1134	480.6552	700.0015	0.1	7	YYYNNNYYYYNNN
D120	350.3567	480.6316	700.3066	0.1	3	YNNNNNYYNNNNN
E100	341.5212	480.6084	699.0524	0.2	4	NNNNYYNNNNNYY
E105	343.7995	480.5159	699.4054	0.2	6	NNNYYYNNNNYYY
E110	345.8951	480.4585	699.6692	0.1	8	NYYYYNNNYYYYN
E115	348.1189	480.3978	699.9984	0.1	7	YYYNNNYYYYNNN
E120	350.3552	480.3735	700.2996	0.1	3	YNNNNNYYNNNNN
F100	341.5250	480.3502	699.0462	0.1	4	NNNNYYNNNNNYY
F105	343.7988	480.2647	699.3997	0.1	6	NNNYYYNNNNYYY

F110	345.8931	480.1987	699.6611	0.1	8	NYYYYNNNYYYYN
F115	348.1186	480.1448	699.9927	0.2	7	YYYNNNYYYYNNN
F120	350.3640	480.1255	700.2989	0.1	3	YNNNNNYYNNNNN
G100	341.5220	480.1001	699.0466	0.1	4	NNNNYYNNNNNYY
G105	343.7928	480.0135	699.3907	0.2	6	NNNYYYNNNNYYY
G110	345.9059	479.9487	699.6606	0.1	8	NYYYYNNNYYYYN
G115	348.1224	479.8927	699.9907	0.2	7	YYYNNNYYYYNNN
G120	350.3642	479.8716	700.2919	0.2	3	YNNNNNYYNNNNN

Image Coordinate Rejections

Image Number Image002

Image Number Image003

Image Number Image004

Image Number Image005

Image Number Image006

Image Number Image007

Image Number Image022
C112
Image Number Image023

Image Number Image024

Image Number Image025

Image Number Image026

Image Number Image027

Image Number Image028

Total Rejections 1

Australis Bundle Adjustment Results File: Bundle.txt

12 September, 2011 20:21:31

Quick Summary
Project: C:\Documents and Settings\pdlento\Desktop\Australis 2\Retro colour\Retro colour.aus
Adjustment: Preferred control points specified
Simulated Network: No
Folding Method: Standard
Scaling: N/A
Units: m
Number of Points: 47
Number of Images: 12
Number of Scale Bars: 1
Number of Iterations: 6
Elapsed CPU Time: 0.157 seconds

Adjusted Exterior Orientation Parameters (angles are decimal degrees, XYZ are m)

Results for Station Image002 FileName Camera 1 Mideast 1 Colour.tif Camera Colour 1 Lens

Station Variable	Initial Value	Total Adjustment	Final Value	Initial Standard Error	Final Standard Error
X	348.6977	0.0030	348.7007	1.0000E+003	8.6955E-003
Y	480.6348	-0.0019	480.6329	1.0000E+003	4.0794E-002
Z	706.0957	-0.0084	706.0873	1.0000E+003	1.9706E-002
AZ	-176.7045	-0.9090	-177.6136	1.0000E+003	1.3614E+000
EL	-87.0291	-0.0321	-87.0612	1.0000E+003	3.9139E-001
ROLL	174.8637	0.9277	175.7914	1.0000E+003	1.3402E+000

Results for Station Image003 FileName Camera 1 Mideast 2 Colour.tif Camera Colour 1 Lens

Station Variable	Initial Value	Total Adjustment	Final Value	Initial Standard Error	Final Standard Error
X	348.6612	-0.0029	348.6583	1.0000E+003	9.4581E-003
Y	480.6164	0.0030	480.6194	1.0000E+003	4.0336E-002
Z	706.1081	-0.0008	706.1074	1.0000E+003	1.9505E-002
AZ	99.6812	-0.1460	99.5352	1.0000E+003	9.2691E-001
EL	-68.4806	0.0280	-68.4526	1.0000E+003	1.1668E-001
ROLL	-100.3431	0.1303	-100.2128	1.0000E+003	1.0486E+000

Results for Station Image004 FileName Camera 1 Midwest 1 Colour.tif Camera Colour 1 Lens

Station Variable	Initial Value	Total Adjustment	Final Value	Initial Standard Error	Final Standard Error
X	345.6201	-0.0097	345.6104	1.0000E+003	1.4406E-002
Y	480.5997	0.0046	480.6043	1.0000E+003	4.2064E-002
Z	705.8212	-0.0083	705.8129	1.0000E+003	1.7332E-002
AZ	-95.8941	0.1679	-95.7262	1.0000E+003	1.7508E+000
EL	-76.8809	0.0969	-76.7839	1.0000E+003	6.4379E-002
ROLL	94.8490	-0.1674	94.6816	1.0000E+003	1.7415E+000

Results for Station Image005 FileName Camera 1 Midwest 2 Colour.tif Camera Colour 1 Lens

Station Variable	Initial Value	Total Adjustment	Final Value	Initial Standard Error	Final Standard Error
X	345.5744	-0.0018	345.5725	1.0000E+003	6.5702E-003
Y	480.6305	0.0049	480.6354	1.0000E+003	4.1535E-002

Z	705.8390	-0.0011	705.8379	1.0000E+003	2.0117E-002
AZ	100.4936	-0.2706	100.2230	1.0000E+003	1.8183E+000
EL	-78.4014	0.0715	-78.3299	1.0000E+003	1.1822E-001
ROLL	-100.4258	0.2613	-100.1646	1.0000E+003	1.9086E+000

Results for Station Image007 FileName Camera 1 West 2 Colour.tif Camera Colour 1 Lens

Station Variable	Initial Value	Total Adjustment	Final Value	Initial Standard Error	Final Standard Error
X	341.7061	0.0020	341.7081	1.0000E+003	1.2460E-002
Y	480.7281	0.0027	480.7307	1.0000E+003	4.1628E-002
Z	705.1584	0.0010	705.1594	1.0000E+003	1.8087E-002
AZ	-104.6622	-0.1757	-104.8379	1.0000E+003	3.9027E+000
EL	-84.2189	0.0088	-84.2101	1.0000E+003	1.3495E-001
ROLL	104.7902	0.1851	104.9753	1.0000E+003	3.8672E+000

Results for Station Image015 FileName Camera 2 East 1 Colour.tif Camera Colour 2 Lens

Station Variable	Initial Value	Total Adjustment	Final Value	Initial Standard Error	Final Standard Error
X	351.6614	-0.0127	351.6487	1.0000E+003	1.1824E-002
Y	481.0321	0.0057	481.0379	1.0000E+003	4.2642E-002
Z	706.8622	-0.0183	706.8439	1.0000E+003	1.5980E-002
AZ	97.5659	-0.0383	97.5276	1.0000E+003	7.0831E-001
EL	-62.9191	-0.0157	-62.9348	1.0000E+003	9.5606E-002
ROLL	-95.8417	0.0136	-95.8281	1.0000E+003	8.4917E-001

Results for Station Image016 FileName Camera 2 Mideast 1 Colour.tif Camera Colour 2 Lens

Station Variable	Initial Value	Total Adjustment	Final Value	Initial Standard Error	Final Standard Error
X	348.2626	0.0089	348.2715	1.0000E+003	8.4128E-003
Y	480.6300	0.0035	480.6335	1.0000E+003	4.0565E-002
Z	706.0419	-0.0242	706.0176	1.0000E+003	1.5640E-002
AZ	-158.2841	13.2535	-145.0306	1.0000E+003	2.6867E+000
EL	-85.2341	0.3455	-84.8886	1.0000E+003	3.1880E-001
ROLL	157.6767	-13.2452	144.4315	1.0000E+003	2.6446E+000

Results for Station Image017 FileName Camera 2 Mideast2 Colour.tif Camera Colour 2 Lens

Station Variable	Initial Value	Total Adjustment	Final Value	Initial Standard Error	Final Standard Error
X	348.2348	-0.0079	348.2269	1.0000E+003	7.0185E-003
Y	480.6157	0.0024	480.6181	1.0000E+003	4.0279E-002
Z	706.0517	-0.0133	706.0384	1.0000E+003	1.5234E-002
AZ	99.1625	-0.1992	98.9632	1.0000E+003	1.1054E+000
EL	-71.5064	-0.0113	-71.5177	1.0000E+003	1.0041E-001
ROLL	-98.3860	0.1861	-98.1999	1.0000E+003	1.2176E+000

Results for Station Image018 FileName Camera 2 Midwest 1 Colour.tif Camera Colour 2 Lens

Station Variable	Initial Value	Total Adjustment	Final Value	Initial Standard Error	Final Standard Error
X	345.1750	-0.0007	345.1743	1.0000E+003	1.1413E-002
Y	480.5980	0.0059	480.6039	1.0000E+003	4.2311E-002
Z	705.8178	-0.0196	705.7983	1.0000E+003	1.3905E-002
AZ	-89.7056	0.1152	-89.5903	1.0000E+003	1.6655E+000
EL	-76.2052	0.0830	-76.1222	1.0000E+003	5.7080E-002
ROLL	89.8786	-0.1093	89.7693	1.0000E+003	1.6585E+000

Results for Station Image019 FileName Camera 2 Midwest 2 Colour.tif Camera Colour 2 Lens

Station Variable	Initial Value	Total Adjustment	Final Value	Initial Standard Error	Final Standard Error
X	345.1431	-0.0036	345.1395	1.0000E+003	6.3104E-003
Y	480.6320	0.0040	480.6360	1.0000E+003	4.1869E-002
Z	705.8330	-0.0147	705.8183	1.0000E+003	1.5645E-002
AZ	96.2065	-0.4576	95.7489	1.0000E+003	2.3176E+000
EL	-80.6757	0.0580	-80.6177	1.0000E+003	9.3146E-002
ROLL	-96.4849	0.4505	-96.0344	1.0000E+003	2.4012E+000

Results for Station Image020 FileName Camera 2 West 1 Colour.tif Camera Colour 2 Lens

Station Variable	Initial Value	Total Adjustment	Final Value	Initial Standard Error	Final Standard Error
X	341.3098	0.0120	341.3218	1.0000E+003	1.1954E-002
Y	480.7464	0.0039	480.7504	1.0000E+003	4.0126E-002
Z	705.0273	-0.0102	705.0172	1.0000E+003	1.1786E-002
AZ	-91.7377	-0.0915	-91.8292	1.0000E+003	1.2521E+000
EL	-71.7889	-0.0214	-71.8104	1.0000E+003	7.7773E-002
ROLL	90.1802	0.1075	90.2877	1.0000E+003	1.2593E+000

Results for Station Image021 FileName Camera 2 West 2 Colour.tif Camera Colour 2 Lens

Station Variable	Initial Value	Total Adjustment	Final Value	Initial Standard Error	Final Standard Error
X	341.2891	0.0080	341.2971	1.0000E+003	1.1699E-002
Y	480.7569	0.0023	480.7593	1.0000E+003	4.0977E-002
Z	705.0302	-0.0099	705.0202	1.0000E+003	1.3922E-002
AZ	-93.1041	-0.0016	-93.1057	1.0000E+003	2.6035E+000
EL	-81.1023	-0.0113	-81.1137	1.0000E+003	1.0420E-001
ROLL	93.1513	0.0134	93.1646	1.0000E+003	2.5788E+000

Summary of Image Coordinate Residuals (units are micrometres)

Sta #	RMS of Image Residuals x	y	xy	Number of non-rejected points
Image002	0.29	0.35	0.32	23
Image003	0.17	0.15	0.16	27
Image004	0.23	0.36	0.30	23
Image005	0.13	0.25	0.20	30
Image007	0.14	0.15	0.14	20
Image015	0.14	0.42	0.31	27
Image016	0.18	0.26	0.22	24
Image017	0.18	0.18	0.18	27
Image018	0.14	0.15	0.15	23
Image019	0.14	0.19	0.17	27
Image020	0.19	0.26	0.23	27
Image021	0.12	0.13	0.13	20

Total Residuals (RMS) x	y	xy	Sigma0	Degrees of Freedom	Observations	Parameters	Constraints
0.18	0.26	0.22	0.549	461	596	233	98

Standard Errors From Limiting Error and Total Error Propogation (XYZ are in m)

Label	Limiting Sigma Estimates sX	sY	sZ	Total Sigma Estimates sX	sY	sZ	RMS	# Rays	List 11111111112222222223 12345678901234567890123456789 0
A101	0.0003	0.0003	0.0009	0.0026	0.0025	0.0033	0.2	5	NNNYYNNNNYYY
A103	0.0003	0.0003	0.0009	0.0022	0.0022	0.0030	0.1	5	NNNYYNNNNYYY

A106	0.0002	0.0002	0.0005	0.0018	0.0017	0.0026	0.2	7	NYNYYNNYNYYY
A108	0.0002	0.0002	0.0005	0.0017	0.0016	0.0026	0.2	9	NYYYYNNYYYYY
A111	0.0002	0.0002	0.0006	0.0016	0.0015	0.0026	0.2	8	NYYYNY*YYYYN
A113	0.0002	0.0002	0.0007	0.0017	0.0015	0.0026	0.2	8	YYYYNYYYYNNN
A116	0.0002	0.0002	0.0007	0.0018	0.0018	0.0026	0.2	7	YYYNNYYYYNNN
A118	0.0003	0.0003	0.0007	0.0020	0.0020	0.0028	0.2	5	YNYNNYYNYNNN
A121	0.0004	0.0003	0.0012	0.0026	0.0025	0.0034	0.2	3	YNNNNYYNNNNN
B101	0.0003	0.0003	0.0009	0.0026	0.0025	0.0028	0.3	5	NNNYYNNNNYYY
B103	0.0003	0.0003	0.0009	0.0022	0.0022	0.0025	0.2	5	NNNYYNNNNYYY
B106	0.0002	0.0002	0.0005	0.0018	0.0017	0.0020	0.2	7	NYNYYNNYNYYY
B108	0.0002	0.0002	0.0005	0.0017	0.0016	0.0019	0.2	9	NYYYYNNYYYYY
B111	0.0002	0.0002	0.0005	0.0016	0.0015	0.0020	0.3	9	NYYYNYYYYYYN
B113	0.0002	0.0002	0.0007	0.0016	0.0015	0.0020	0.2	8	YYYYNYYYYNNN
B116	0.0002	0.0002	0.0007	0.0018	0.0017	0.0020	0.2	7	YYYNNYYYYNNN
B118	0.0003	0.0003	0.0007	0.0020	0.0020	0.0023	0.2	5	YNYNNYYNYNNN
B121	0.0004	0.0003	0.0012	0.0026	0.0025	0.0029	0.2	3	YNNNNYYNNNNN
C101	0.0003	0.0003	0.0010	0.0026	0.0025	0.0033	0.1	5	NNNYYNNNNYYY
C103	0.0003	0.0003	0.0009	0.0022	0.0022	0.0030	0.2	5	NNNYYNNNNYYY
C106	0.0002	0.0002	0.0005	0.0018	0.0017	0.0027	0.1	7	NYNYYNNYNYYY
C108	0.0002	0.0002	0.0005	0.0017	0.0016	0.0026	0.2	9	NYYYYNNYYYYY
C111	0.0002	0.0002	0.0005	0.0016	0.0015	0.0027	0.2	9	NYYYNYYYYYYN
C113	0.0002	0.0002	0.0007	0.0017	0.0015	0.0027	0.2	8	YYYYNYYYYNNN
C116	0.0002	0.0002	0.0007	0.0018	0.0018	0.0027	0.1	7	YYYNNYYYYNNN
C118	0.0003	0.0003	0.0007	0.0020	0.0020	0.0028	0.1	5	YNYNNYYNYNNN
C121	0.0004	0.0003	0.0012	0.0026	0.0025	0.0033	0.3	3	YNNNNYYNNNNN
D101	0.0003	0.0003	0.0010	0.0026	0.0026	0.0044	0.2	5	NNNYYNNNNYYY
D106	0.0002	0.0002	0.0005	0.0019	0.0019	0.0039	0.1	7	NYNYYNNYNYYY
D111	0.0002	0.0002	0.0005	0.0017	0.0017	0.0039	0.1	10	YYYYNYYYYYYN
D116	0.0002	0.0002	0.0008	0.0019	0.0019	0.0039	0.3	7	YYYNNYYYYNNN
D121	0.0004	0.0003	0.0013	0.0026	0.0026	0.0044	0.1	3	YNNNNYYNNNNN
E101	0.0003	0.0003	0.0010	0.0027	0.0027	0.0058	0.2	5	NNNYYNNNNYYY
E106	0.0002	0.0002	0.0005	0.0020	0.0019	0.0055	0.2	7	NYNYYNNYNYYY
E111	0.0002	0.0002	0.0005	0.0018	0.0017	0.0054	0.4	10	YYYYNYYYYYYN
E116	0.0002	0.0002	0.0008	0.0020	0.0019	0.0054	0.6	6	YYYNNY*YYNNN
E121	0.0004	0.0003	0.0013	0.0027	0.0026	0.0058	0.1	3	YNNNNYYNNNNN
F101	0.0003	0.0003	0.0010	0.0028	0.0027	0.0073	0.1	5	NNNYYNNNNYYY
F106	0.0002	0.0002	0.0005	0.0021	0.0020	0.0071	0.2	7	NYNYYNNYNYYY
F111	0.0002	0.0002	0.0005	0.0019	0.0018	0.0070	0.2	10	YYYYNYYYYYYN
F116	0.0003	0.0003	0.0008	0.0021	0.0020	0.0071	0.3	5	*YYNNY*YYNNN
F121	0.0004	0.0003	0.0013	0.0028	0.0027	0.0073	0.1	3	YNNNNYYNNNNN
G101	0.0003	0.0003	0.0010	0.0029	0.0028	0.0089	0.2	5	NNNYYNNNNYYY
G106	0.0002	0.0002	0.0005	0.0022	0.0020	0.0087	0.1	7	NYNYYNNYNYYY
G111	0.0002	0.0002	0.0005	0.0021	0.0019	0.0087	0.2	10	YYYYNYYYYYYN
G116	0.0002	0.0002	0.0008	0.0023	0.0020	0.0087	0.3	7	YYYNNYYYYNNN
G121	0.0004	0.0004	0.0013	0.0029	0.0028	0.0089	0.2	3	YNNNNYYNNNNN

	Summary of Limiting STD Error Estimates			Summary of Total STD Error Estimates		
	X	Y	Z	X	Y	Z
RMS is	0.0003	0.0002	0.0008	0.0022	0.0021	0.0048
Minimum is	0.0002	0.0002	0.0005	0.0016	0.0015	0.0019
at point	D111	D111	A108	B111	B111	B108
Maximum is	0.0004	0.0004	0.0013	0.0029	0.0028	0.0089
at point	G121	G121	G121	G121	G101	G101

Triangulated Object Space Coordinates (XYZ are in m)

					Sightings #	List	1111111111222222222223
Label	X	Y	Z	RMS	Rays	1234567890123456789012345678901	
A101	341.6193	481.6008	699.2029	0.2	5	NNNYYNNNNYYY	
A103	342.4046	481.5650	699.3099	0.1	5	NNNYYNNNNYYY	
A106	343.8973	481.5161	699.5170	0.2	7	NYNYYNNYNYYY	
A108	344.6784	481.4879	699.6225	0.2	9	NYYYYNNYYYYY	
A111	345.9788	481.4503	699.8005	0.2	8	NYYYNY*YYYYN	
A113	346.7577	481.4249	699.9092	0.2	8	YYYYNYYYYNNN	

A116	348.1989	481.3862	700.1127	0.2	7	YYYNNYYYYNNN
A118	348.9755	481.3644	700.2172	0.2	5	YNYNNYYNYNNN
A121	350.4312	481.3514	700.4193	0.2	3	YNNNNYYNNNNN
B101	341.6170	481.3486	699.2005	0.3	5	NNNYYNNNNYYY
B103	342.3984	481.3122	699.3053	0.2	5	NNNYYNNNNYYY
B106	343.8987	481.2654	699.5144	0.2	7	NYNYYNNYNYYY
B108	344.6780	481.2334	699.6195	0.2	9	NYYYYNNYYYYY
B111	345.9791	481.1954	699.7980	0.3	9	NYYYNYYYYYYN
B113	346.7542	481.1747	699.9051	0.2	8	YYYYNYYYYNNN
B116	348.2005	481.1391	700.1061	0.2	7	YYYNNYYYYNNN
B118	348.9700	481.1227	700.2124	0.2	5	YNYNNYYNYNNN
B121	350.4361	481.0964	700.4169	0.2	3	YNNNNYYNNNNN
C101	341.6100	481.0921	699.1973	0.1	5	NNNYYNNNNYYY
C103	342.3915	481.0670	699.3017	0.2	5	NNNYYNNNNYYY
C106	343.8964	480.9931	699.5109	0.1	7	NYNYYNNYNYYY
C108	344.6764	480.9797	699.6156	0.2	9	NYYYYNNYYYYY
C111	345.9798	480.9289	699.7949	0.2	9	NYYYNYYYYYYN
C113	346.7534	480.9207	699.9021	0.2	8	YYYYNYYYYNNN
C116	348.2007	480.8779	700.0991	0.1	7	YYYNNYYYYNNN
C118	348.9776	480.8694	700.2092	0.1	5	YNYNNYYNYNNN
C121	350.4342	480.8443	700.4134	0.3	3	YNNNNYYNNNNN
D101	341.6235	480.8571	699.0803	0.2	5	NNNYYNNNNYYY
D106	343.8978	480.7704	699.4222	0.1	7	NYNYYNNYNYYY
D111	345.9963	480.7127	699.6766	0.1	10	YYYYNYYYYYYN
D116	348.2059	480.6543	700.0064	0.3	7	YYYNNYYYYNNN
D121	350.4470	480.6291	700.3175	0.1	3	YNNNNYYNNNNN
E101	341.6228	480.6075	699.0764	0.2	5	NNNYYNNNNYYY
E106	343.9018	480.5122	699.4127	0.2	7	NYNYYNNYNYYY
E111	345.9959	480.4620	699.6712	0.4	10	YYYYNYYYYYYN
E116	348.2183	480.3997	699.9990	0.6	6	YYYNNY*YYNNN
E121	350.4521	480.3671	700.3105	0.1	3	YNNNNYYNNNNN
F101	341.6239	480.3541	699.0693	0.1	5	NNNYYNNNNYYY
F106	343.8969	480.2629	699.4016	0.2	7	NYNYYNNYNYYY
F111	345.9896	480.2038	699.6672	0.2	10	YYYYNYYYYYYN
F116	348.2168	480.1444	699.9940	0.3	5	*YYNNY*YYNNN
F121	350.4554	480.1228	700.3029	0.1	3	YNNNNYYNNNNN
G101	341.6218	480.0988	699.0624	0.2	5	NNNYYNNNNYYY
G106	343.8949	480.0151	699.3954	0.1	7	NYNYYNNYNYYY
G111	346.0018	479.9505	699.6600	0.2	10	YYYYNYYYYYYN
G116	348.2166	479.8945	699.9914	0.3	7	YYYNNYYYYNNN
G121	350.4587	479.8675	700.2968	0.2	3	YNNNNYYNNNNN

Image Coordinate Rejections

Image Number Image002
F116
Image Number Image003

Image Number Image004

Image Number Image005

Image Number Image007

Image Number Image015

Image Number Image016
A111 E116 F116
Image Number Image017

Image Number Image018

Image Number Image019

Image Number Image020

Image Number Image021

Total Rejections 4

Australis Bundle Adjustment Results File: Bundle.txt

12 September, 2011 21:25:40

Quick Summary
Project: C:\Documents and Settings\pdlento\Desktop\Australis 2\Retro infrared\Retro infrared.aus
Adjustment: Preferred control points specified
Simulated Network: No
Folding Method: Standard
Scaling: N/A
Units: m
Number of Points: 47
Number of Images: 14
Number of Scale Bars: 1
Number of Iterations: 3
Elapsed CPU Time: 0.109 seconds

Adjusted Exterior Orientation Parameters (angles are decimal degrees, XYZ are m)

Results for Station Image001 FileName Camera 1 East 1 NIR.tif Camera NIR 1 Lens

Station Variable	Initial Value	Total Adjustment	Final Value	Initial Standard Error	Final Standard Error
X	352.1132	0.0013	352.1145	1.0000E+003	1.7692E-002
Y	481.0619	-0.0026	481.0593	1.0000E+003	6.1779E-002
Z	706.8830	0.0053	706.8883	1.0000E+003	2.4704E-002
AZ	105.3289	0.0969	105.4258	1.0000E+003	1.1101E+000
EL	-65.3152	0.0052	-65.3100	1.0000E+003	1.9528E-001
ROLL	-102.4525	-0.0709	-102.5234	1.0000E+003	1.3000E+000

Results for Station Image002 FileName Camera 1 Mideast 1 NIR.tif Camera NIR 1 Lens

Station Variable	Initial Value	Total Adjustment	Final Value	Initial Standard Error	Final Standard Error
X	348.6798	-0.0050	348.6748	1.0000E+003	9.8992E-003
Y	480.6363	-0.0108	480.6255	1.0000E+003	5.9415E-002
Z	706.1164	0.0041	706.1205	1.0000E+003	2.4210E-002
AZ	173.1415	0.2407	173.3822	1.0000E+003	1.4166E+000
EL	-86.4982	0.0073	-86.4909	1.0000E+003	5.6628E-001
ROLL	-173.8373	-0.2225	-174.0597	1.0000E+003	1.4593E+000

Results for Station Image003 FileName Camera 1 Mideast 2 NIR.tif Camera NIR 1 Lens

Station Variable	Initial Value	Total Adjustment	Final Value	Initial Standard Error	Final Standard Error
X	348.6696	0.0035	348.6731	1.0000E+003	1.1672E-002
Y	480.6218	-0.0013	480.6205	1.0000E+003	5.8857E-002
Z	706.1361	0.0015	706.1376	1.0000E+003	2.2887E-002
AZ	99.4154	0.0911	99.5065	1.0000E+003	1.3275E+000
EL	-68.2729	0.0393	-68.2336	1.0000E+003	1.4740E-001
ROLL	-100.1784	-0.0732	-100.2516	1.0000E+003	1.5061E+000

Results for Station Image004 FileName Camera 1 Midwest 1 NIR.tif Camera NIR 1 Lens

Station Variable	Initial Value	Total Adjustment	Final Value	Initial Standard Error	Final Standard Error
X	345.6012	-0.0087	345.5925	1.0000E+003	1.6620E-002
Y	480.6173	-0.0037	480.6136	1.0000E+003	6.1188E-002
Z	705.8414	-0.0015	705.8399	1.0000E+003	2.1159E-002

AZ	-96.4085	-0.0781	-96.4866	1.0000E+003	2.5425E+000
EL	-76.9661	0.0932	-76.8728	1.0000E+003	9.4323E-002
ROLL	95.3897	0.0694	95.4591	1.0000E+003	2.5288E+000

Results for Station Image005 FileName Camera 1 Midwest 2 NIR.tif Camera NIR 1 Lens

Station Variable	Initial Value	Total Adjustment	Final Value	Initial Standard Error	Final Standard Error
X	345.5716	0.0021	345.5738	1.0000E+003	8.7335E-003
Y	480.6206	0.0074	480.6280	1.0000E+003	6.0592E-002
Z	705.8668	0.0041	705.8709	1.0000E+003	2.3191E-002
AZ	99.4205	0.5452	99.9657	1.0000E+003	2.6286E+000
EL	-78.3300	0.0430	-78.2870	1.0000E+003	1.5380E-001
ROLL	-99.2811	-0.5451	-99.8262	1.0000E+003	2.7601E+000

Results for Station Image006 FileName Camera 1 West 1 NIR.tif Camera NIR 1 Lens

Station Variable	Initial Value	Total Adjustment	Final Value	Initial Standard Error	Final Standard Error
X	341.7043	0.0039	341.7082	1.0000E+003	1.7771E-002
Y	480.7558	-0.0056	480.7501	1.0000E+003	6.0085E-002
Z	705.1726	0.0020	705.1746	1.0000E+003	1.7569E-002
AZ	-96.0120	-0.0489	-96.0610	1.0000E+003	1.8924E+000
EL	-72.4023	0.0612	-72.3411	1.0000E+003	1.1264E-001
ROLL	94.2303	0.0389	94.2692	1.0000E+003	1.8996E+000

Results for Station Image007 FileName Camera 1 West 2 NIR.tif Camera NIR 1 Lens

Station Variable	Initial Value	Total Adjustment	Final Value	Initial Standard Error	Final Standard Error
X	341.6743	0.0085	341.6828	1.0000E+003	1.5616E-002
Y	480.7739	-0.0061	480.7678	1.0000E+003	6.0460E-002
Z	705.1685	0.0053	705.1738	1.0000E+003	2.1120E-002
AZ	-107.5925	-0.1622	-107.7547	1.0000E+003	5.3597E+000
EL	-84.0757	0.0994	-83.9763	1.0000E+003	2.0802E-001
ROLL	107.7787	0.1696	107.9483	1.0000E+003	5.3089E+000

Results for Station Image015 FileName Camera 2 East 1 NIR.tif Camera NIR 2 Lens

Station Variable	Initial Value	Total Adjustment	Final Value	Initial Standard Error	Final Standard Error
X	351.6694	-0.0004	351.6689	1.0000E+003	1.6906E-002
Y	481.0694	-0.0003	481.0690	1.0000E+003	6.2287E-002
Z	706.8904	0.0016	706.8920	1.0000E+003	2.2536E-002
AZ	98.2244	0.0347	98.2591	1.0000E+003	1.0167E+000
EL	-62.7924	0.0165	-62.7759	1.0000E+003	1.4072E-001
ROLL	-96.6785	-0.0191	-96.6976	1.0000E+003	1.2225E+000

Results for Station Image016 FileName Camera 2 Mideast 1 NIR.tif Camera NIR 2 Lens

Station Variable	Initial Value	Total Adjustment	Final Value	Initial Standard Error	Final Standard Error
X	348.2265	-0.0063	348.2202	1.0000E+003	1.3111E-002
Y	480.6222	-0.0034	480.6189	1.0000E+003	6.0151E-002
Z	706.0524	0.0006	706.0530	1.0000E+003	2.2485E-002
AZ	-118.6349	0.1444	-118.4906	1.0000E+003	5.0879E+000
EL	-84.1461	0.0317	-84.1144	1.0000E+003	2.6885E-001
ROLL	119.1791	-0.1374	119.0418	1.0000E+003	5.0366E+000

Results for Station Image017 FileName Camera 2 Mideast 2 NIR.tif Camera NIR 2 Lens

Station Variable	Initial Value	Total Adjustment	Final Value	Initial Standard Error	Final Standard Error
X	348.2290	0.0007	348.2297	1.0000E+003	9.8400E-003
Y	480.6130	0.0005	480.6136	1.0000E+003	5.8894E-002
Z	706.0815	-0.0005	706.0809	1.0000E+003	2.1961E-002
AZ	99.3324	-0.0591	99.2733	1.0000E+003	1.5844E+000
EL	-71.4094	0.0587	-71.3507	1.0000E+003	1.4252E-001
ROLL	-98.6011	0.0655	-98.5355	1.0000E+003	1.7484E+000

Results for Station Image018 FileName Camera 2 Midwest 1 NIR.tif Camera NIR 2 Lens

Station Variable	Initial Value	Total Adjustment	Final Value	Initial Standard Error	Final Standard Error
X	345.1408	-0.0052	345.1356	1.0000E+003	1.6185E-002
Y	480.6173	-0.0016	480.6156	1.0000E+003	6.1552E-002
Z	705.8286	-0.0063	705.8224	1.0000E+003	1.9863E-002
AZ	-90.4702	-0.1412	-90.6114	1.0000E+003	2.3827E+000
EL	-76.0135	0.0572	-75.9564	1.0000E+003	8.0207E-002
ROLL	90.6441	0.1299	90.7740	1.0000E+003	2.3736E+000

Results for Station Image019 FileName Camera 2 Midwest 2 NIR.tif Camera NIR 2 Lens

Station Variable	Initial Value	Total Adjustment	Final Value	Initial Standard Error	Final Standard Error
X	345.1284	0.0016	345.1300	1.0000E+003	8.1377E-003
Y	480.6327	0.0068	480.6395	1.0000E+003	6.1067E-002
Z	705.8513	0.0001	705.8514	1.0000E+003	2.2234E-002
AZ	97.0002	0.2425	97.2427	1.0000E+003	3.3612E+000
EL	-80.7359	0.0771	-80.6589	1.0000E+003	1.3563E-001
ROLL	-97.2362	-0.2484	-97.4845	1.0000E+003	3.4823E+000

Results for Station Image020 FileName Camera 2 West 1 NIR.tif Camera NIR 2 Lens

Station Variable	Initial Value	Total Adjustment	Final Value	Initial Standard Error	Final Standard Error
X	341.2973	0.0023	341.2997	1.0000E+003	1.6526E-002
Y	480.7680	-0.0031	480.7649	1.0000E+003	5.8401E-002
Z	705.0295	0.0018	705.0313	1.0000E+003	1.6556E-002
AZ	-92.6307	0.0107	-92.6200	1.0000E+003	1.8050E+000
EL	-71.6964	-0.0054	-71.7018	1.0000E+003	1.0341E-001
ROLL	91.1264	-0.0124	91.1140	1.0000E+003	1.8162E+000

Results for Station Image021 FileName Camera 2 West 2 NIR.tif Camera NIR 2 Lens

Station Variable	Initial Value	Total Adjustment	Final Value	Initial Standard Error	Final Standard Error
X	341.2665	0.0050	341.2715	1.0000E+003	1.5775E-002
Y	480.7929	-0.0067	480.7862	1.0000E+003	5.9668E-002
Z	705.0410	0.0041	705.0451	1.0000E+003	1.9617E-002
AZ	-95.6250	0.1163	-95.5087	1.0000E+003	3.7510E+000
EL	-81.0419	-0.0272	-81.0691	1.0000E+003	1.4437E-001
ROLL	95.7476	-0.1091	95.6385	1.0000E+003	3.7152E+000

Summary of Image Coordinate Residuals (units are micrometres)

Sta #	RMS of Image Residuals x	y	xy	Number of non-rejected points
Image001	0.19	0.22	0.21	27

Image002	0.25	0.57	0.44	24
Image003	0.25	0.24	0.25	26
Image004	0.38	0.67	0.54	23
Image005	0.37	0.33	0.35	29
Image006	0.40	0.35	0.38	23
Image007	0.51	0.20	0.38	20
Image015	0.41	0.56	0.49	34
Image016	0.22	0.28	0.25	20
Image017	0.23	0.36	0.30	30
Image018	0.28	0.28	0.28	23
Image019	0.28	0.24	0.26	27
Image020	0.22	0.21	0.22	27
Image021	0.29	0.26	0.27	20

Total Residuals (RMS)				Degrees of			
x	y	xy	Sigma0	Freedom	Observations	Parameters	Constraints
0.32	0.37	0.35	0.799	559	706	245	98

Standard Errors From Limiting Error and Total Error Propogation (XYZ are in m)

	Limiting Sigma Estimates			Total Sigma Estimates				Sightings #	List	
Label	sX	sY	sZ	sX	sY	sZ	RMS	Rays	1234567890123456789012345678901	
A101	0.0003	0.0004	0.0013	0.0038	0.0036	0.0048	0.3	6	NNNNYYYNNNNYYY	
A103	0.0003	0.0003	0.0010	0.0032	0.0032	0.0043	0.4	7	NNNNYYYNNYNYYY	
A106	0.0003	0.0003	0.0007	0.0026	0.0025	0.0037	0.2	8	NNYNYYYNNYNYYY	
A108	0.0003	0.0003	0.0006	0.0025	0.0023	0.0036	0.5	11	NNYYYYYYNYYYYY	
A111	0.0003	0.0003	0.0006	0.0023	0.0021	0.0036	0.5	10	YNYYYYNYNYYYYN	
A113	0.0003	0.0003	0.0009	0.0024	0.0022	0.0036	0.5	9	YYYYYNNYYYYNNN	
A116	0.0003	0.0003	0.0009	0.0026	0.0025	0.0037	0.2	8	YYYYNNNYYYYNNN	
A118	0.0004	0.0003	0.0009	0.0029	0.0029	0.0040	0.2	6	YYNYNNNYYNYNNN	
A121	0.0004	0.0004	0.0013	0.0038	0.0036	0.0048	0.3	4	YYNNNNNYYNNNNN	
B101	0.0003	0.0003	0.0014	0.0037	0.0036	0.0040	0.3	6	NNNNYYYNNNNYYY	
B103	0.0003	0.0003	0.0010	0.0032	0.0032	0.0034	0.3	7	NNNNYYYNNYNYYY	
B106	0.0003	0.0003	0.0007	0.0026	0.0025	0.0028	0.3	8	NNYNYYYNNYNYYY	
B108	0.0003	0.0003	0.0006	0.0024	0.0023	0.0027	0.4	11	NNYYYYYYNYYYYY	
B111	0.0003	0.0003	0.0006	0.0023	0.0021	0.0026	0.2	10	YNYYYYNYNYYYYN	
B113	0.0003	0.0003	0.0009	0.0023	0.0022	0.0027	0.4	9	YYYYYNNYYYYNNN	
B116	0.0003	0.0003	0.0009	0.0026	0.0025	0.0029	0.3	8	YYYYNNNYYYYNNN	
B118	0.0004	0.0003	0.0009	0.0029	0.0029	0.0032	0.3	6	YYNYNNNYYNYNNN	
B121	0.0004	0.0004	0.0013	0.0037	0.0036	0.0040	0.3	4	YYNNNNNYYNNNNN	
C101	0.0004	0.0003	0.0014	0.0037	0.0036	0.0047	0.2	6	NNNNYYYNNNNYYY	
C103	0.0003	0.0003	0.0010	0.0032	0.0032	0.0042	0.3	7	NNNNYYYNNYNYYY	
C106	0.0003	0.0003	0.0007	0.0026	0.0025	0.0038	0.2	8	NNYNYYYNNYNYYY	
C108	0.0003	0.0003	0.0006	0.0024	0.0023	0.0037	0.5	11	NNYYYYYYNYYYYY	
C111	0.0003	0.0003	0.0006	0.0024	0.0021	0.0037	0.4	10	YNYYYYNYNYYYYN	
C113	0.0004	0.0003	0.0010	0.0024	0.0022	0.0037	0.4	8	YYYY*NNYYYYNNN	
C116	0.0003	0.0003	0.0009	0.0026	0.0025	0.0038	0.3	8	YYYYNNNYYYYNNN	
C118	0.0004	0.0003	0.0009	0.0029	0.0029	0.0040	0.5	6	YYNYNNNYYNYNNN	
C121	0.0004	0.0004	0.0014	0.0038	0.0036	0.0047	0.3	4	YYNNNNNYYNNNNN	
D101	0.0004	0.0003	0.0014	0.0038	0.0038	0.0063	0.3	6	NNNNYYYNNNNYYY	
D106	0.0003	0.0003	0.0007	0.0027	0.0027	0.0056	0.3	9	NNYNYYYYNYNYYY	
D111	0.0003	0.0003	0.0007	0.0025	0.0025	0.0055	0.4	10	YYYYYNNYNYYYYN	
D116	0.0003	0.0003	0.0010	0.0027	0.0027	0.0056	0.3	8	YYYYNNNYYYYNNN	
D121	0.0004	0.0004	0.0014	0.0038	0.0038	0.0062	0.3	4	YYNNNNNYYNNNNN	
E101	0.0004	0.0003	0.0014	0.0039	0.0039	0.0083	0.2	6	NNNNYYYNNNNYYY	
E106	0.0003	0.0003	0.0007	0.0028	0.0028	0.0079	0.2	9	NNYNYYYYNYNYYY	
E111	0.0003	0.0003	0.0007	0.0026	0.0025	0.0077	0.3	10	YYYYYNNYNYYYYN	
E116	0.0003	0.0003	0.0010	0.0029	0.0028	0.0078	0.4	8	YYYYNNNYYYYNNN	
E121	0.0004	0.0004	0.0014	0.0039	0.0038	0.0083	0.3	4	YYNNNNNYYNNNNN	
F101	0.0004	0.0003	0.0014	0.0041	0.0040	0.0105	0.3	6	NNNNYYYNNNNYYY	
F106	0.0003	0.0003	0.0007	0.0030	0.0029	0.0102	0.3	9	NNYNYYYYNYNYYY	
F111	0.0003	0.0003	0.0007	0.0028	0.0026	0.0101	0.3	10	YYYYYNNYNYYYYN	
F116	0.0003	0.0003	0.0010	0.0030	0.0029	0.0102	0.4	8	YYYYNNNYYYYNNN	
F121	0.0004	0.0004	0.0014	0.0040	0.0039	0.0104	0.4	4	YYNNNNNYYNNNNN	
G101	0.0004	0.0004	0.0014	0.0042	0.0041	0.0129	0.5	6	NNNNYYYNNNNYYY	
G106	0.0003	0.0003	0.0007	0.0032	0.0030	0.0126	0.3	9	NNYNYYYYNYNYYY	
G111	0.0003	0.0003	0.0007	0.0030	0.0027	0.0125	0.2	10	YYYYYNNYNYYYYN	

G116	0.0003	0.0003	0.0010	0.0033	0.0029	0.0126	0.4	7	YYNYNNNYYYYNNN
G121	0.0004	0.0005	0.0014	0.0042	0.0040	0.0128	0.3	4	YYNNNNNYYNNNNN

	Summary of Limiting STD Error Estimates			Summary of Total STD Error Estimates		
	X	Y	Z	X	Y	Z
RMS is	0.0003	0.0003	0.0010	0.0031	0.0030	0.0069
Minimum is	0.0003	0.0003	0.0006	0.0023	0.0021	0.0026
at point	A108	C108	A108	B111	B111	B111
Maximum is	0.0004	0.0005	0.0014	0.0042	0.0041	0.0129
at point	G121	G121	G121	G101	G101	G101

Triangulated Object Space Coordinates (XYZ are in m)

				Sightings #	List	1111111111222222222223
Label	X	Y	Z	RMS	Rays	12345678901234567890123456789O
A101	341.6211	481.5989	699.2045	0.3	6	NNNNYYYNNNNYYY
A103	342.4045	481.5627	699.3115	0.4	7	NNNNYYYNNYNYYY
A106	343.8962	481.5160	699.5177	0.2	8	NNYNYYYNNYNYYY
A108	344.6770	481.4882	699.6232	0.5	11	NNYYYYYYNYYYYY
A111	345.9763	481.4516	699.8003	0.5	10	YNYYYYNYNYYYYN
A113	346.7544	481.4265	699.9090	0.5	9	YYYYYNNYYYYNNN
A116	348.1972	481.3877	700.1104	0.2	8	YYYYNNNYYYYNNN
A118	348.9754	481.3649	700.2155	0.2	6	YYNYNNNYYNYNNN
A121	350.4344	481.3501	700.4199	0.3	4	YYNNNNNYYNNNNN
B101	341.6193	481.3471	699.2000	0.3	6	NNNNYYYNNNNYYY
B103	342.3987	481.3106	699.3067	0.3	7	NNNNYYYNNYNYYY
B106	343.8980	481.2658	699.5142	0.3	8	NNYNYYYNNYNYYY
B108	344.6770	481.2341	699.6199	0.4	11	NNYYYYYYNYYYYY
B111	345.9770	481.1964	699.7993	0.2	10	YNYYYYNYNYYYYN
B113	346.7510	481.1761	699.9054	0.4	9	YYYYYNNYYYYNNN
B116	348.1989	481.1407	700.1038	0.3	8	YYYYNNNYYYYNNN
B118	348.9691	481.1238	700.2099	0.3	6	YYNYNNNYYNYNNN
B121	350.4386	481.0949	700.4181	0.3	4	YYNNNNNYYNNNNN
C101	341.6118	481.0918	699.1949	0.2	6	NNNNYYYNNNNYYY
C103	342.3926	481.0663	699.3021	0.3	7	NNNNYYYNNYNYYY
C106	343.8962	480.9938	699.5120	0.2	8	NNYNYYYNNYNYYY
C108	344.6756	480.9807	699.6166	0.5	11	NNYYYYYYNYYYYY
C111	345.9781	480.9303	699.7975	0.4	10	YNYYYYNYNYYYYN
C113	346.7509	480.9225	699.9016	0.4	8	YYYY*NNYYYYNNN
C116	348.1989	480.8789	700.0971	0.3	8	YYYYNNNYYYYNNN
C118	348.9767	480.8698	700.2077	0.5	6	YYNYNNNYYNYNNN
C121	350.4360	480.8420	700.4143	0.3	4	YYNNNNNYYNNNNN
D101	341.6262	480.8562	699.0796	0.3	6	NNNNYYYNNNNYYY
D106	343.8984	480.7705	699.4241	0.3	9	NNYNYYYYNYNYYY
D111	345.9947	480.7141	699.6792	0.4	10	YYYYYNNYNYYYYN
D116	348.2039	480.6555	700.0066	0.3	8	YYYYNNNYYYYNNN
D121	350.4498	480.6262	700.3159	0.3	4	YYNNNNNYYNNNNN
E101	341.6244	480.6066	699.0731	0.2	6	NNNNYYYNNNNYYY
E106	343.9025	480.5129	699.4149	0.2	9	NNYNYYYYNYNYYY
E111	345.9947	480.4640	699.6750	0.3	10	YYYYYNNYNYYYYN
E116	348.2158	480.4011	700.0004	0.4	8	YYYYNNNYYYYNNN
E121	350.4538	480.3632	700.3086	0.3	4	YYNNNNNYYNNNNN
F101	341.6266	480.3530	699.0657	0.3	6	NNNNYYYNNNNYYY
F106	343.8978	480.2638	699.4056	0.3	9	NNYNYYYYNYNYYY
F111	345.9885	480.2053	699.6710	0.3	10	YYYYYNNYNYYYYN
F116	348.2144	480.1447	699.9970	0.4	8	YYYYNNNYYYYNNN
F121	350.4559	480.1189	700.3059	0.4	4	YYNNNNNYYNNNNN
G101	341.6251	480.0987	699.0586	0.5	6	NNNNYYYNNNNYYY
G106	343.8962	480.0161	699.3990	0.3	9	NNYNYYYYNYNYYY
G111	346.0005	479.9527	699.6648	0.2	10	YYYYYNNYNYYYYN
G116	348.2142	479.8943	699.9938	0.4	7	YYNYNNNYYYYNNN
G121	350.4589	479.8623	700.2979	0.3	4	YYNNNNNYYNNNNN

Image Coordinate Rejections

Image Number Image001

Image Number Image002

Image Number Image003

Image Number Image004

Image Number Image005
C113
Image Number Image006

Image Number Image007

Image Number Image015

Image Number Image016

Image Number Image017

Image Number Image018

Image Number Image019

Image Number Image020

Image Number Image021

Total Rejections 1